

AD-780 531

HIGH CHAMBER PRESSURE BLAST TUBE  
AND NOZZLE MATERIAL EVALUATION.  
VOLUME I

Wendell A. Stephen

United Technology Center

Prepared for:

Air Force Rocket Propulsion Laboratory

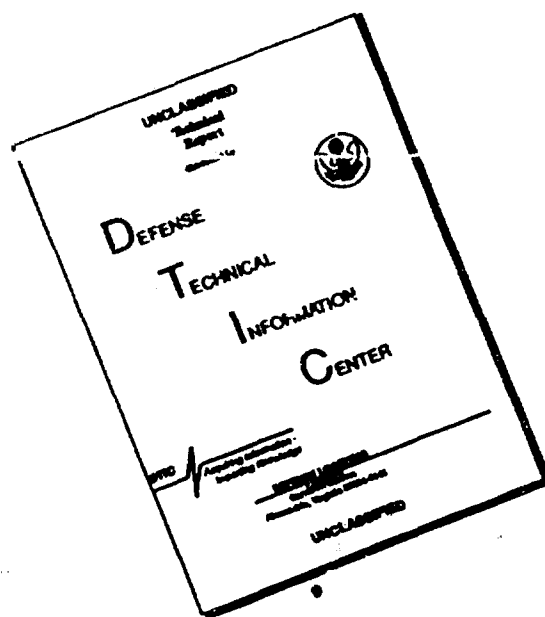
17 June 1974

DISTRIBUTED BY:

**NTIS**

National Technical Information Service  
U. S. DEPARTMENT OF COMMERCE  
5285 Port Royal Road, Springfield Va. 22151

# DISCLAIMER NOTICE



THIS DOCUMENT IS BEST QUALITY AVAILABLE. THE COPY FURNISHED TO DTIC CONTAINED A SIGNIFICANT NUMBER OF PAGES WHICH DO NOT REPRODUCE LEGIBLY.

Unclassified  
Security Classification

AD780 531

DOCUMENT CONTROL DATA - R & D

(Security classification of title, body of abstract and indexing annotation must be entered when the overall report is classified)

1. ORIGINATING ACTIVITY (Corporate author) <b>United Technology Center</b>		2a. REPORT SECURITY CLASSIFICATION <b>Unclassified</b>	
		2b. GROUP -	
3. REPORT TITLE <b>High Chamber Pressure Blast Tube and Nozzle Material Evaluation</b>			
4. DESCRIPTIVE NOTES (Type of report and inclusive dates) <b>Final report covering the period of April 1971 to July 1973</b>			
5. AUTHOR(S) (First name, middle initial, last name) <b>Wendell A. Stephen</b>			
6. REPORT DATE <b>June 17, 1974</b>		7a. TOTAL NO OF PAGES <b>162 179</b>	7b. NO. OF REFS <b>7</b>
9a. CONTRACT OR GRANT NO <b>F04611-71-C-0051</b>		9a. ORIGINATOR'S REPORT NUMBER(S) <b>UTC 2410-FR</b>	
b. PROJECT NO. <b>Project 3059</b>			
c.		9b. OTHER REPORT NO(S) (Any other numbers that may be assigned this report) <b>AFRPL-TR-73-60</b>	
d. BPSN 623059			
10. DISTRIBUTION STATEMENT <b>Approved for public release; distribution unlimited</b>			
11. SUPPLEMENTARY NOTES		12. SPONSORING MILITARY ACTIVITY <b>AFRPL/MKCC Edwards, CA 93523</b>	
13. ABSTRACT <p>The contract objectives were to evaluate the effects of propellant corrosivity and blast tube contraction ratio on candidate nozzle materials in high chamber pressure rocket motor environments (3,000 and 3,500 psia). The baseline hotside nozzle materials were selected based on contract No. F04611-69-C-0065 results. A total of 16 lightweight aft closures and nozzles were designed, fabricated, and test fired. High velocity (Mach numbers of .31 and .53) blast tubes with contraction ratios of 2.0 and 1.3, respectively, were used on all nozzles, except for one assembly which was a conventional configuration without a blast tube. The effects of propellant flame temperature and corrosivity were evaluated by testing with both 18% and 5% aluminized, 88% solids loaded CTPB propellants. The effects of both cylindrical and keyhole port grain configurations also were evaluated. Conventional state-of-the-art phenolic, elastomeric, and graphite materials were used. In addition, two advanced carbon-carbon composites were tested as blast tube liners. Both pyrolytic graphite washers and wire-wound tungsten were used for the throat insert. Based on these tests, the material capability, design configuration, and analytical models were proven for this application. This report describes the various program activities from initial material and configuration selection to final test firing demonstration and analysis of test results.</p> <p>Reproduced by NATIONAL TECHNICAL INFORMATION SERVICE U S Department of Commerce Springfield VA 22151</p>			

DD FORM 1473  
1 NOV 65

Unclassified  
Security Classification

14. KEY WORDS	LINK A		LINK B		LINK C	
	ROLE	WT	ROLE	WT	ROLE	WT
Blast tube materials performance High pressure materials evaluation Exit nozzles for tactical missiles						

1a

# **HIGH CHAMBER PRESSURE BLAST TUBE AND NOZZLE MATERIAL EVALUATION**

**VOLUME I**

**W. A. Stephen**

**T. E. Frakes**

**T. V. O'Hara**

**APPROVED FOR PUBLIC RELEASE; DISTRIBUTION UNLIMITED**

*ib*

UTC 2410-FR

## FOREWORD

This technical report summarizes work performed under contract No. F04611-71-C-0051 by UTC, Sunnyvale, California, for AFRPL, Edwards, California. This contract resulted from UTC Proposal 70-71, "Nozzles for Tactical Air Launch Motor Regimes," issued in response to Air Force RFP No. F04611-71-Q-0008.

The work reported herein was performed under the technical direction of Mr. J. Wanchek, AFRPL. The UTC program manager was Mr. W. A. Stephan and the project engineer was Mr. T. E. Frakes.

Special recognition should be given to Mr. R. Owen, Mr. P. O'Driscoll, Mr. R. Sihner, Mr. P. Henderson, Mr. D. Agbayani, and Aerotherm Division of Acurex Corporation for their technical contribution.

This technical report has been reviewed and is approved.

James Wanchek  
Project Engineer

## CONTENTS

Section		Page
I	INTRODUCTION	1
II	SUMMARY	2
III	CONTRACT OBJECTIVES	7
IV	ACCOMPLISHMENTS	8
V	PHASE I - PROGRAM DEFINITION	10
	1. Design Constraints	10
	2. Propellant	10
	3. Materials Test Matrix	13
VI	PHASE II - NOZZLE DESIGN AND FABRICATION	20
	1. Nozzle Design	20
	2. Nozzle Analysis	24
	a. Basic 3,000-Psi Blast Tube Design	24
	b. 3,500-Psi Blast Tube Design	26
	3. Instrumentation	38
	4. Nozzle Fabrication	40
	5. Nondestructive Testing	43
VII	PHASE III - ROCKET MOTOR TESTING	45
	1. Processing of Propellant Cartridges	45
	2. Test Description	48
	a. Nozzle S/N 01	48
	b. Nozzle S/N 02	49
	c. Nozzle S/N 03	49
	d. Nozzle S/N 04	49
	e. Nozzle S/N 05	52
	f. Nozzle S/N 06	52
	g. Nozzle S/N 07	54
	h. Nozzle S/N 08	54
	i. Nozzle S/N 09	54
	j. Nozzle S/N 10	54
	k. Nozzle S/N 11	57
	l. Nozzle S/N 12	57
	m. Nozzle S/N 13	59
	n. Nozzle S/N 14	59
	o. Nozzle S/N 15	59
	p. Nozzle S/N 16	62
VIII	PHASE IV - POSTTEST EVALUATION	64
	1. Nozzle Material Performance	64
	a. Blast Tube and Ablative Components	64
	b. Posttest Evaluation of Nozzle Insert Performance	80
	2. Comparison of Actual and Predicted Test Pressures	87

*Pages III and IV are Blank*

CONTENTS (Continued)

Section		Page
IX	MAINTAINABILITY AND RELIABILITY	88
X	CONCLUSIONS	89
XI	RECOMMENDATIONS	91
	REFERENCES	92
	APPENDIX I: Material Properties Data	93
	APPENDIX II: Thermal and Ablation Analysis of Nozzles S/N 14 and S/N 16	95
	APPENDIX III: Structural Analysis of Nozzle Throat Ejection Loads and Steel Shells (MEOP = 3,600 psi)	153

## ILLUSTRATIONS

Figure		Page
1	Blast Tube Nozzle Design	21
2	Wire-Wound Tungsten Test Configuration	23
3	Finite Element Grid for Graph-i-tite G-90 Blast Tube	27/28
4	Safety Factors for Critical Axial Stress in the Graph-i-tite G-90 Blast Tube	29
5	Predicted Isotherm of Tungsten Throat Package at 1 Sec	29
6	Predicted Isotherm of Tungsten Throat Package at 3 Sec	30
7	Predicted Isotherm of Tungsten Throat Package at 6 Sec	30
8	Predicted Isotherm of Tungsten Throat Package at 10 Sec	31
9	Revised Isotherms Due to Additional One-Dimensional Analyses at 10 Sec	31
10	Comparison of Actual and Predicted Surface Ablation for Nozzle S/N 14	32
11	Comparison of Actual and Predicted Surface Ablation for Nozzle S/N 16	32
12	Finite Element Grid for Tungsten Throat Insert	35/36
13	Instrumentation Design	39
14	Keyhole Port Grain Design	47
15	Pressure-Time Trace, Nozzle S/N 01	48
16	Pressure-Time Trace, Nozzle S/N 02	50
17	Axial Thrust-Time History, Nozzle S/N 02	50
18	Pressure-Time Trace, Nozzle S/N 03	51
19	Pressure-Time Trace, Nozzle S/N 04	51
20	Axial Thrust-Time History, Nozzle S/N 04	52
21	Pressure-Time Trace, Nozzle S/N 05	53
22	Pressure-Time Trace, Nozzle S/N 06	53
23	Pressure-Time Trace, Nozzle S/N 07	55
24	Pressure-Time Trace, Nozzle S/N 08	55

## ILLUSTRATIONS (Continued)

Figure		Page
25	Pressure-Time Trace, Nozzle S/N 09	56
26	Pressure-Time Trace, Nozzle S/N 10	56
27	Pressure-Time Trace, Nozzle S/N 11	58
28	Pressure-Time Trace, Nozzle S/N 12	58
29	Pressure-Time Trace, Nozzle S/N 13	60
30	Pressure-Time Trace, Nozzle S/N 14	60
31	Cross Section View of Test-Fired Nozzle S/N 14	61
32	Pressure-Time Trace, Nozzle S/N 15	62
33	Pressure-Time Trace, Nozzle S/N 16	63
34	Aft Closure Materials, Average Ablation from Test-to-Test	66
35	MXCE-280 Ablation vs Blast Tube Length	72
36	MXCE-280 Performance vs Blast Tube	73
37	Entrance View of Test-Fired Blast Tube S/N 13 (Keyhole Port Grain Effect)	75
38	Aft End View of Test-Fired Blast Tube S/N 13 (Keyhole Port Grain Effect)	76
39	Entrance View of Throat Package S/N 13 (Keyhole Port Grain Effect)	77
40	Aft Entrance Cap Average Performance of Graph-i-tite G-90 Material	79
41	Average Ablation Rates from Test-to-Test in Exit Cone	82
42	Pyrolytic Graphite Throat Erosion vs Chamber Pressure	84
43	Postfire View of Throat Insert S/N 14	85
44	Postfire View of Throat Insert S/N 16	86

## TABLES

Table		Page
I	Test Summary	3
II	UTP-11,475 Composition	11
III	Composition of UTP-13,615 Propellant	12
IV	Corrosivity Index of Propellant	13
V	Materials Test Matrix	14
VI	Test Material Description	15/16
VII	Tungsten Throat Package Ablation Analysis Summary	33
VIII	Factor of Safety Summary	38
IX	Candidate Phenolic Material Cured Density Summary	41/42
X	Propellant Cartridge Summary	46
XI	Erosion Data - Aft Closure	65
XII	Erosion Data - Forward Entrance Cap	68
XIII	Erosion Data - Blast Tube	69/70
XIV	Erosion Data - Aft Entrance Cap	78
XV	Erosion Data - Exit Cone	81
XVI	Summary of Pretest and Posttest Throat Diameters	83

## ABBREVIATIONS

AFRPL	Air Force Rocket Propulsion Laboratory
AP	ammonium perchlorate
CTPB	carboxy-terminated polybutadiene
EPDM	ethylene propylene diene monomer
HIPPO	high internal pressure producing orifice
HTC	heat transfer coefficient
MEOP	maximum expected operating pressure
NDT	nondestructive testing
PBAN	polybutadiene-acrylic acid-acrylonitrile
O/F	oxidizer to fuel
SRBDM	short range bomber defense missile
TDC	top dead center
UTC	United Technology Center
UTP	United Technology Center propellant prefix

## SECTION I

### INTRODUCTION

AFRPL and industry systems studies have shown that high chamber pressure offers significant gains in the performance of air-launched missiles that usually are limited in length and volume. By increasing the chamber pressure, the total impulse of a propulsion unit can be increased by as much as 25% due to increases in both specific impulse and propellant volumetric loading of the case. The chamber pressure for tactical motors frequently optimizes in the region of 2,000 to 3,000 psia with MEOPs as high as 3,500 psia.

The exit nozzle has always been one of the more vulnerable components in the severe environment imposed by the high pressure rocket motor. The exit nozzle can survive only if the hotside materials can withstand the high flame temperature and corrosive environment. This environment becomes ever more severe when backside envelope and soakout temperature constraints are imposed. Highly volumetric-limited systems such as the SRBDM often require packaging space around the exit nozzle for hydraulic power supplies and controls. This dictates use of a blast tube between the aft closure and nozzle throat plane. To maximize this packaging space, blast tubes with low contraction area ratios are used, resulting in high velocities and, therefore, an even more harsh operating environment for the materials.

AFRPL has funded several programs during the past 5 years to evaluate material performance in exit nozzles for high chamber pressure applications. These programs have proven that there are hotside materials that permit realization of the predicted gains of higher chamber pressure operation. However, this work has emphasized performance of high chamber pressure nozzle materials used in less-than-optimum configurations with lower performance propellant compositions (typical of booster motors rather than of the high performance formulations required for tactical air-launched missiles).

The purpose of this program was to extend the high chamber pressure materials evaluation to include the effects of propellant formulation variables on nozzle materials and to define more fully the utility of materials used with high velocity blast tube configurations. The propellants chosen represent both a high performance system for optimized tactical air-launched missiles and a lower performance, more corrosive formulation which would be required by such system constraints as radar attenuation or particle impingement on the launch aircraft. Blast tubes with contraction ratios of 1.3 to 2.0 were evaluated at maximum pressure levels of 3,000 and 3,400 psia.

This program was baselined using the most optimum hotside materials defined during contract No. F04611-69-C-0065<sup>(1)</sup>\* and evaluating the materials with these propellants, pressure levels, and flow environments.

\*References are listed on page 92.

## SECTION II

### SUMMARY

This report presents a summary of the results and conclusions made for contract No. F04611-71-C-0051, "Nozzles for Tactical Air Launch Motor Regimes." The contract period of performance was from April 1971 to July 1974. The program objectives were to evaluate the effects of propellant chemistry, solids loading, and blast tube configurations upon nozzle materials in high chamber pressure rocket motors operating in the pressure range of 2,500 to 3,500 psia. During this program, a total of 16 firings were conducted at AFRPL using the UTC HIPPO test motor. Table I presents a summary of these tests. Numerous candidate phenolic, graphite, carbon-carbon composite, and tungsten materials were evaluated for application to the blast tube and nozzle. This program demonstrated that off-the-shelf materials are available which will meet the performance requirements for a nozzle system typical of the current SRBDM concept.

The program was conducted in the following four phases:

- A. Phase I - Program Definition
- B. Phase II - Nozzle Design and Fabrication
- C. Phase III - Rocket Motor Testing
- D. Phase IV - Posttest Evaluation.

One major subcontractor, Aerotherm Division of Acurex Corp., was used during the program. This subcontractor primarily was responsible for conducting thermochemical analysis predictions of surface recession and in-depth thermal penetration for the candidate materials.

The initial objectives were directed toward evaluation of materials for high velocity blast tubes (i.e., contraction area ratios of 1.3 and 2.0) with respective Mach numbers of .53 and .31. During these initial firings, it was demonstrated that off-the-shelf phenolic materials performed adequately. The one anomalous area in these initial firings was the performance of the throat insert. The previous program, contract No. F04611-69-C-0065, demonstrated pyrolytic graphite washers provided a minimal eroding throat ( $\sim 3.0$  mils/sec) when operating at 3,000 psia chamber pressure for 20 sec. Higher rates were anticipated for this contract due to the change in propellant binder from PBAN to CTPB; however, the erosion experienced was up to five times that previously experienced even with the duration reduced to 10 sec. This result has not been explained and is not in agreement with kinetically controlled thermochemical predictions. Since these high erosion rates were encountered and it was desired to evaluate material performance at 3,500 psia, the throat material was changed to UTC's wire-wound tungsten (TECHMET<sup>®</sup>) for the last three firings. This material demonstrated an essentially noneroding throat contour.

TABLE I  
TEST SUMMARY  
(Sheet 1 of 2)

Test No.	Average Web Pressure psia	Web Duration sec	Maximum Pressure, psia	Blast Tube Contraction Ratio	Propellant Aluminum Content, percent	Throat Insert	Grain Configuration	Comments
1	---	---	2575	2.0	18	Pyrolytic graphite washers	Cylindrical port	Throat retention inadequate - ejected throat at 5 sec
2	2500	10.8	2800	2.0	18	Pyrolytic graphite washers	Cylindrical port	Test successful
3	2550	12.0	2700	1.3	18	Pyrolytic graphite washers	Cylindrical port	Test successful
4	2450	11.0	2850	2.0	5	Pyrolytic graphite washers	Cylindrical port	Test successful
5	2650	10.5	3025	1.3	5	Pyrolytic graphite washers	Cylindrical port	Test successful
6	---	---	2900	2.0	5	Pyrolytic graphite washer	Cylindrical port	Throat ejected at 7.5 sec due to excessive Pyrobond blast tube thermal expansion
7	---	---	3100	2.0	5	Pyrolytic graphite washer	Keyhole port	Failure at ignition due to gas leakage past thermocouple instrumentation port
8	2500	10.8	2800	1.3	18	Pyrolytic graphite washer	Cylindrical port	Test successful

TABLE I  
TEST SUMMARY  
(Sheet 2 of 2)

Test No.	Average Web Pressure, psia	Web Duration, sec	Maximum Pressure, psia	Blast Tube Contraction Ratio	Propellant		Throat Insert	Grain Configuration	Comments
					Aluminum Content, percent	Pyrolytic			
9	2525	10.3	2800	2.0	5	Pyrolytic graphite washers	Cylindrical port	Test successful	
10	---	---	2825	1.3	5	Pyrolytic graphite washers	Cylindrical port	Throat ejected at 9.5 sec; Pycobond blast tube appeared to fail structurally causing throat blockage.	
11	---	---	2725	2.0	5	Pyrolytic graphite washers	Cylindrical port	Throat ejected at 8.5 sec; Pyrostrand blast tube appeared to fail structurally causing throat blockage	
12	3000	6.9	3200	1.3	5	Pyrolytic graphite washers	Keyhole port	Test successful	
13	2450	11.5	3650	1.3	18	Pyrolytic graphite washers	Keyhole port	Test successful	
14	3200	10.6	3400	---	18	Wire-wound tungsten	Cylindrical port	Test successful; high erosion encountered downstream of tungsten insert	
15	---	---	3225	1.3	18	Wire-wound tungsten	Cylindrical port	Throat ejected at 9.5 sec; degraded throat retention system	
16	3250	10.7	3300	1.3	18	Wire-wound tungsten	Cylindrical port	Test successful; high erosion encountered downstream of tungsten insert	

Design constraints for the nozzle were established using the SRBDM system as the baseline. The test nozzles incorporated a 1.72-in.-diameter throat; therefore, all components such as blast tube material thicknesses, etc., were scaled to be representative of the larger SRBDM nozzle. All test nozzles (S/N 14 excepted) incorporated an 8.1-in.-long cylindrical blast tube with contraction ratios of 1.3 and 2.0. The exit expansion ratio was 7.15. Lightweight steel hardware was used to provide realistic material stress loading. Two propellant systems with two propellant configurations each were evaluated. Both propellant systems were 88% solids loaded CTPB formulations. One system was a high performance 18% aluminized system while the second system was a highly corrosive formulation with a 5% aluminum content. Both cylindrical bore and keyhole port grain configurations were tested with each propellant.

The blast tube materials evaluated were carbon, silica, and hybrid carbon-silica phenolics, carbon-carbon composites, and polycrystalline graphites. Low cost glass phenolics and elastomers were evaluated as aft closure insulation. Candidate materials were segmented axially in each test zone for approximately one-third of the test firings. One common material at each location was used as a baseline during each firing where the components were segmented. The baseline materials were: Durez 16771 (aft closure), MXCE-280 (blast tube), Graph-i-tite G-90 (aft entrance cap), and FM5055 (exit cone).

All graphitic components were inspected radiographically and ultrasonically. No defects were detected except for one lot of pyrolytic graphite washers which were severely delaminated. These were rejected; therefore, it was not possible to make an assessment of accept/reject criteria based on NDT detected defects and their effects on material performance.

Pretest and posttest predictions (for tests 2, 3, 5, 6, 9, and 13) were made of the thermochemical performance of selected candidate materials. These results were compared with the posttest measurements to verify the accuracy of the analytical model. These results are presented in volume II of this report and show that the analytical models are accurate within the  $\pm 25\%$  goal for all areas except for the pyrolytic graphite throat washers and for components tested with the keyhole port grain configuration.

Representative material performance data were obtained for 10 of the 16 test firings. The major contributor to the lack of success in the other firings was the lack of characterized material properties of carbon-carbon composites used as blast tube liners. All three tests using these materials resulted in a throat ejection. Most of the other candidate materials performed adequately. Five materials exhibited outstanding performance for the particular area of application. Low cost (<\$1.50/lb) glass phenolic (Durez 16771) and asbestos-loaded EPDM elastomer (R155) provided more than adequate erosion resistance as aft closure insulation. A fibrous carbon-phenolic with an elastomeric modifier (MXCE-280) performed exceptionally well as a molded blast tube liner material. A flat laminate of carbon-phenolic (MX4926) provided the necessary erosion resistance as an entrance cap to the blast tube. This material virtually eliminated the problem of gouging previously experienced with fibrous molded units. Wire-wound tungsten further demonstrated its ability to

provide a noneroding throat insert. With the higher erosion rates experienced on pyrolytic graphite plate, wire-wound tungsten is the only material that has demonstrated its ability to withstand this environment with minimal throat area change.

Based on these tests, the following materials are recommended for use in high chamber pressure nozzle design:

<u>Nozzle Location</u>	<u>Material</u>
Aft closure	Durez 16771 (Hooker Chemical Corp.) R-155 (Rocketdyne)
Forward entrance cap	Flat laminate MX4926 (Fiberite Corp.)
Blast tube	MXCE-280 (Fiberite Corp.)
Aft entrance cap	Graph-i-tite G-90 (Carborundum Corp.)
Throat insert	TECHMET (United Technology Center)
Exit cone	MX4926 (Fiberite Corp.) FM5055 (U.S. Polymeric, Inc.)

These test results demonstrated the sensitivity of material performance to circumferential gaps between adjoining materials in high velocity regions. The test nozzle is threaded into the aft closure, and a gap is left between the hotside materials to allow for thermal expansion. This gap was filled with zinc chromate putty. During contract No. F04611-69-C-0065, it was demonstrated that this gap could vary up to 0.070 to 0.090 in. before severe degradation of adjoining material. This effect became considerably more sensitive to gap width for the more corrosive, higher flame temperature propellants and the increased velocity blast tube configurations. Test results demonstrated that this gap should be maintained between 0.020 and 0.030 in.

### SECTION III

#### CONTRACT OBJECTIVES

The contract objectives were to evaluate the effects of propellant chemistry, solids loading, and blast tube contraction ratio upon nozzle materials in high chamber pressure rocket motor environments (2,500 to 3,500 psia). The specific objectives were:

- A. Demonstrate the effects of low (5%) and high (18%) aluminum content propellants on high chamber pressure nozzles and blast tube materials
- B. Demonstrate material performance for high velocity blast tubes at high chamber pressure
- C. Verify accuracy of previously developed analytical techniques to predict material performance within  $\pm 25\%$ .

SECTION IV  
ACCOMPLISHMENTS

A comparison of the expected and achieved accomplishments of this contract is summarized below:

<u>Expected</u>	<u>Achieved</u>
A. Verify material surface recession predictions for both low and highly oxidized propellant environments to within $\pm 25\%$	A. Thermochemical predictions were within the $\pm 25\%$ of test firing results for all materials except the pyrolytic graphite throat washers and for the aft closure materials behind the keyhole slot
B. Provide a lightweight low contraction ratio blast tube nozzle design for application to high chamber pressure, tactical, air-launched motor regimes	B. Blast tubes with contraction ratios of 1.3 and 2.0 exhibited satisfactory performance with MXCE-280 carbon-phenolic. Graphitized composites were not successfully demonstrated for blast tube liner applications. The use of MXCE-280 material results in blast tube diameters that are applicable to volumetric-limited systems such as SRBDM
C. Demonstrate minimal erosion (less than 3 mils/sec) for throat inserts during high chamber pressure tests in highly aluminized and highly oxidizing environments	C. Two throat insert materials were evaluated: pyrolytic graphite plate and wire-wound tungsten. The pyrolytic graphite plate eroded at $\sim 6$ to 15 mils/sec. Wire-wound tungsten has demonstrated a noneroding throat for the highly aluminized propellant but is not suitable for the highly oxidizing environments
D. Generate material performance data for low contraction ratio blast tube nozzles in high pressure, highly oxidizing environments	D. Acceptable performance data were obtained for various carbon- and silica-phenolic blast tube materials. Tests showed MXCE-280 was the best. Ablation rates at 2,600 psia (average) were up to 50 and 36 mils/sec for contraction ratios of 1.3 and 2.0, respectively. (Increasing the pressure by 600 psia increases the ablation by $\sim 15\%$ )

Expected

- E. Evaluate additional cost-effective materials for high chamber pressure applications, especially for the motor aft closure
- F. Establish initial assessments of accept/reject criteria for graphitic components based on NDT.

Achieved

- E. Low cost materials of glass phenolic (Durez 16771) and asbestos-loaded EPDM elastomer (R155) were proven to be adequate for the aft closure insulation
- F. All graphitic components were void-free with the exception of a few pyrolytic graphite washers which were too severely delaminated to be used; therefore, this goal was not attained.

## SECTION V

### PHASE I - PROGRAM DEFINITION

#### 1. DESIGN CONSTRAINTS

Design constraints were established which reflect representative system constraints of envelope, thermal environment, and duty cycles for advanced high acceleration tactical air-launched missiles. These design guidelines were essentially as presented in reference 1 except for the following modification. A single pulse of 10 sec for both 3,000 and 3,500 psia maximum was used for the duty cycle. The Martin-Marietta Co. propulsion specification for the SRBDM, No. 70-9061, dated March 1970, was selected as a baseline system. This specification represents a larger configuration than the test nozzles which incorporated a 1.72-in.-diameter throat. The material thicknesses which allowed for this larger configuration were used in the materials selection criteria. This is important for such system constraints as blast tube liner thickness where materials with high ablation and/or thermal conductivity are not acceptable. A backside steel temperature limitation of 300°F was also imposed as a design constraint. Lightweight steel shells were used which provide stress loadings of radial growth and flexing at the attach joint under pressurization. Safety factors of 1.5 were used in the designs.

#### 2. PROPELLANT

Two composite propellant formulations were used. Both formulations are 88% solids loaded with a CTPB binder which is representative for application to a high performance tactical propulsion unit. One of these systems is an 18% aluminized high performance formulation and is designated UTP-11,475. The composition, exhaust gas properties, and ballistic data are presented in table II.

The second propellant, UTP-13,615, is a derivative of UTP-11,475. The propellant was formulated with 5% aluminum and 83% AP for use in tactical propulsion systems when mission requirements such as radar attenuation and/or launch vehicle considerations dictate a low aluminum content. The propellant formulation, exhaust properties, and ballistic data are presented in table III.

The 5% aluminized formulation has a reduced flame temperature but is highly corrosive due to the additional oxidizer which replaced the reduction of aluminum content. The 18% aluminized formulation is less corrosive but has a considerably increased flame temperature.

These formulations provide an environment that is considerably more severe in chemical attack than the previously tested PBAN formulations. One of the accepted measures of propellant severity is the corrosivity index which is based on the oxygen available in the exhaust products for attack on the exposed nozzle component surfaces. This corrosivity index is defined as follows:

TABLE II

UTP-11,475 COMPOSITION

Ingredients

Binder (CTPB), wt-%	9.58
Curative, wt-%	0.62
Plasticizer, wt-%	1.80
Aluminum, wt-%	18.00
Oxidizer, wt-%	70.00

Ballistic Properties

Density, lb/in. <sup>3</sup>	0.065
O/F ratio	1.33
Chamber pressure, psia	1,000
Exhaust, psia	14.7

<u>Exhaust Gas Composition</u>	<u>Chamber Pressure, psia</u>	<u>Exhaust, psia</u>
Temperature, °K	3,594	2,315
Combustion products, moles/100 g		
AlCl	0.01914	0.0001
AlCl <sub>2</sub>	0.01645	0.0004
AlOCl	0.0085	0.0001
AlOH	0.0165	0.0001
CO	0.7694	0.7555
CO <sub>2</sub>	0.0564	0.07105
Cl	0.0535	0.0080
H	0.1568	0.01893
HCl	0.4791	0.5865
H <sub>2</sub>	0.9337	1.0076
H <sub>2</sub> O	0.5550	0.5273
NO	0.0039	0.0000
H <sub>2</sub>	0.2984	0.3004
O	0.0045	0.0000
OH	0.0460	0.0016
O <sub>2</sub>	0.0010	0.0000
Al <sub>2</sub> O <sub>3</sub> (liquid)	0.3020	0.1182
Al <sub>2</sub> O <sub>3</sub> (solid)	---	0.2150
Total moles of gas/100 g	3.422	3.278

TABLE III  
COMPOSITION OF UTP-13,615 PROPELLANT

<u>Ingredients</u>	
Binder, wt-%	9.58
Curative, wt-%	0.62
Plasticizer, wt-%	1.80
Aluminum, wt-%	5.0
Oxidizer, wt-%	83.0

<u>Ballistic Properties</u>	
Density, lb/in. <sup>3</sup>	0.0629
O/F ratio	2.59
Chamber pressure, psia	1,000
Exhaust, psia	14.7

<u>Exhaust Gas Composition</u>	<u>Chamber Pressure, psia</u>	<u>Exhaust, psia</u>
Temperature, °K	3,231	1,810
Combustion products, moles/100 g		
AlCl <sub>2</sub>	0.0020	0.0000
AlHO <sub>2</sub>	0.0015	0.0000
AlOCl	0.0020	0.0000
CO	0.5289	0.4168
CO <sub>2</sub>	0.2992	0.4115
Cl	0.0547	0.0007
H	0.0399	0.0004
HCl	0.6431	0.7037
H <sub>2</sub>	0.3174	0.3577
H <sub>2</sub> O	1.3665	1.3499
NO	0.0088	0.0000
N <sub>2</sub>	0.3512	0.3556
O	0.0051	0.0000
OH	0.0682	0.0001
O <sub>2</sub>	0.0089	0.0000
Al <sub>2</sub> O <sub>3</sub> (liquid)	0.0894	0.0000
Al <sub>2</sub> O <sub>3</sub> (solid)	0.0000	0.0926
Total moles of gas/100 g	3.700	3.598

$$\text{Corrosivity index} = \frac{\text{moles of } [\text{CO}_2 + \text{H}_2\text{O} + \text{O} + 2\text{O}_2 + \text{OH} + \text{NO}]}{\text{Total moles of gas}}$$

The values of this index for both the PBAN and CTPB propellants are presented in table IV.

Even though the corrosivity index for the 18% aluminum CTPB does not appear to be much greater than for the PBAN formulation, the resulting erosion is significantly increased for the CTPB propellant which has an increase in flame temperature of 6,010°F versus 5,700°F for PBAN.

### 3. MATERIALS TEST MATRIX

A materials test matrix was defined using the materials selection criteria defined in reference 1. This material selection criteria analytically rates the candidate materials for each nozzle test zone using as input the steady-state thermochemical screening analysis presented in volume II of this report. It also rates analytically the system constraints of envelope, backside temperature, compatibilities, etc., as defined by the design constraints, and other parameters such as cost effectiveness, availability, and previous experience. The final test matrix is presented in table V. These materials and their suppliers are defined in table VI. The majority of the material properties are presented in reference 2.\*

The thermochemical screening results showed that carbonaceous materials offered superior erosion resistance over silica-phenolic or glass-phenolic for the high aluminum propellant systems. For the more highly corrosive 5% aluminum formulations, either silica-phenolic or carbon-phenolic may perform best depending upon the application. Therefore, both carbon and silica materials were evaluated in the corrosive environment, with the carbon-based materials being the only ones evaluated for the higher flame temperature propellants. The carbon-based materials which were evaluated in both propellant systems were selected as the baseline for test firing segmented components.

TABLE IV  
CORROSIVITY INDEX OF PROPELLANT

<u>Propellant</u>	<u>Type</u>	<u>Binder, %</u>	<u>Oxidizer, %</u>	<u>Aluminum, %</u>	<u>Corrosivity Index at Throat</u>
UTP-3001	PBAN	16	68	16	0.130
UTP-11,475	CTPB	12	70	18	0.191
UTP-13,615	CTPB	12	83	5	0.481

\* Appendix I presents the available properties of R155 and Pycobond

The material selection criteria were weighted in favor of the low cost aft closure materials since previous testing under contract No. F04611-69-C-0065 showed the higher quality more costly materials were not required. Both the glass-phenolic and asbestos-loaded EPDM elastomer materials are very low cost and are also functional over the operating range of -65° to +165°F. The effect of fiber length (0.25 and 1 in.) was also evaluated for the glass-phenolic Durez materials.

The forward entrance cap was not segmented even though successful results on contract No. F04611-69-C-0065 demonstrated segmentation of this component could be achieved. The program required the entrance cap to turn the higher temperature (18% aluminum), more corrosive (5% aluminum) flow at considerably higher velocities than for the previous program; therefore, this component was not selected as a test zone. Posttest inspection of the low contraction area ratio entrance caps revealed severe gouging in the molded MXCE-280 components. The materials test matrix was modified to replace this MXCE-280 with a flat laminate molding fabricated from carbon-phenolic broadgoods (MX4926). This modification proved satisfactory and was used throughout the remainder of the tests.

Since primary interest was in the blast tube, materials were examined ranging from high cost, erosion resistant Graph-i-tite G-90 to lower cost, less erosion resistant silica-phenolic MX2625. Approximately half the blast tubes were segmented both axially and circumferentially. Based on previous testing at lower velocities, MXCE-280 carbon-phenolic was selected as the baseline material. Other candidate materials were flat laminate moldings of carbon-phenolic MX4926, molded silica-phenolic MX2625, molded hybrid carbon-silica MXSC-195, polycrystalline Graph-i-tite G-90 segmented into 1-in.-wide rings, and two carbon-carbon materials, Pycobond and Pyrostrand.

Based upon the results and recommendations from contract No. F04611-69-C-0065, the material selection for the aft entrance cap was limited to polycrystalline graphites. This previous testing showed Graph-i-tite G-90 to be the most erosion resistant material. This is logical due to its high density (>1.90 g/cc); therefore, this material was selected as the baseline. To get this density level and, hence, performance, Graph-i-tite G-90 must be cored and reimpregnated in multiple cycles. This extra processing increases the cost as well as requires longer leadtimes. Based on potentially lower costs and expeditious delivery, two other quality grades of polycrystalline graphite were evaluated, P03 and Speer 8882.

Based on the highly successful performance of pyrolytic graphite plate during the previous contract, this material initially was selected as the throat material for all test firings. Erosion rates several times that predicted by thermochemical analysis were encountered in the motor environment during this program. To ensure this firing performance was not unique to the single material supplier, additional material was purchased from an alternate source. No difference in erosion resistance was observed in two firings conducted on this material. Due to the poor performance of the pyrolytic graphite plate and a requirement for a pressure increase to 3,500 psia on the last three tests, UTC's wire-wound tungsten was selected for the throat insert.

TABLE V  
MATERIALS TEST MATRIX

ITEM	LOCATION	1	2	3	4	5	6	7	8	9	10	11	12	13	14	15	16
PROPELLANT GRAIN	-	CP	CP	CP	CP	CP	CP	KP	CP	CP	CP	CP	KP	KP	CP	CP	CP
ALUMINUM CONTENT, %	-	18	18	18	5	5	5	5	18	5	5	5	5	18	18	18	18
AFT CLOSURE	TDC	DUREZ 16771-1	DUREZ 16771-1	DUREZ 16771-1	DUREZ 16771-1	DUREZ 16771-1	MIX 2625	R-155	DUREZ 16771-1	DUREZ 16771-1	DUREZ 16771-1	R-155	DUREZ 16771-1	R-155	DUREZ 16771-1	R-155	DUREZ 16771-1
	BDC	R-155	R-155	MIX 2625	DUREZ 16771-1A	R-155	DUREZ 16771-1	DUREZ 16771-1A	DUREZ 16771-1	DUREZ 16771-1	DUREZ 16771-1						
FORWARD ENTRANCE	-	MIXCE 280	MIXCE 280	MIXCE 280	MIXCE 280	MIXCE 280	MIXCE 280	MIXCE 280	MIXCE 280	MIXCE 280	MIXCE 280	MIX 4926	MIX 4926	MIX 4926	MIX 4926	MIX 4926	MIX 4926
BLAST TUBE	TDC	MIXCE 280	MIXCE 280	MIXCE 280	MIXCE 280	MIXCE 280	MIXCE 280	MIXCE 280	MIXCE 280	MIXCE 280	MIXCE 280	MIXCE 280	MIXCE 280	MIXCE 280	MIXCE 280	MIXCE 280	MIXCE 280
	TDCA	MIXCE 280	MIXCE 280	G-90	MIX 2625	MIX 4926	PICOBOND	MIXCE 280	MIXCE 280	MIXCE 280	MIXCE 280	MIXCE 280	MIXCE 280	MIXCE 280	MIXCE 280	MIXCE 280	MIXCE 280
	BDCF	MIXSC 195	MIXSC 195	MIXCE 280	MIXCE 280	MIXCE 280	MIXCE 280	MIXCE 280	MIXCE 280	MIXCE 280	MIXCE 280	MIXCE 280	MIXCE 280	MIXCE 280	MIXCE 280	MIXCE 280	MIXCE 280
	BDCA	MIX 4926	MIX 4926	G-90	MIXCE 280	MIXCE 280	MIXCE 280	MIXCE 280	MIXCE 280	MIXCE 280	MIXCE 280	MIXCE 280	MIXCE 280	MIXCE 280	MIXCE 280	MIXCE 280	MIXCE 280
AFT ENTRANCE CAP	TDC	G-90	G-90	G-90	G-90	8882	G-90	G-90	G-90	G-90	G-90	G-90	G-90	G-90	G-90	G-90	G-90
	BDC	PO3	PO3	PO3	8882	G-90	G-90	G-90	G-90	G-90	G-90	G-90	G-90	G-90	G-90	G-90	G-90
THROAT	-	PG	PG	PG	PG	PG	PG	PG	PG*	PG†	PG	PG	PG	PG	W <sup>3</sup>	W <sup>3</sup>	W <sup>3</sup>
EXIT CORE	TDC	FM 5055	FM 5055	FM 5055	FM 5055	MIX 4926	FM 5055	FM 5055	FM 5055	MX 2600	MX 2600	MX 2600	MX 4926	FM 5055	FM 5055	FM 5055	FM 5055
	BDC	MX 2600	MX 2600	MX 2600	MX 2600	MX 2600	MX 2600	MX 2600	MX 2600	MX 2600	MX 2600	MX 2600	MX 2600	MX 2600	MX 2600	MX 2600	MX 2600
BLAST TUBE AREA RATIO	-	2.0	2.0	1.3	2.0	1.3	2.0	2.0	1.3	2.0	1.3	2.0	1.3	1.3	-	1.3	1.3

\* SUPERTEMP PYROLITIC GRAPHITE WASHERS. SECOND WASHER FROM AFT END WAS FROM PYROGENICS, INC.

† SUPERTEMP PYROLITIC GRAPHITE

TABLE V  
MATERIALS TEST MATRIX

ITEM	LOCATION	1	2	3	4	5	6	7	8	9
PROPELLANT GRAIN	—	CP	CP	CP	CP	CP	CP	KP	CP	CP
ALUMINUM CONTENT, %	—	18	18	18	5	5	5	5	18	5
AFT CLOSURE	TDC	DUREZ 16771-1	DUREZ 16771-1	DUREZ 16771-1	DUREZ 16771-1	DUREZ 16771-1	MX 2625	R-155	DUREZ 16771-1	DUREZ 16771-1
	BDC	R-155	R-155	MX 2625	DUREZ 16771-1/4	R-155	DUREZ 16771-1		DUREZ 16771-1/4	
FORWARD ENTRANCE	—	MXCE 280	MXCE 280	MXCE 280	MXCE 280	MXCE 280	MXCE 280	MXCE 280	MXCE 280	MXCE 280
BLAST TUBE	TDCF	MXCE 280	MXCE 280	MXCE 280	MXSE 280	MXSE 280	PYCOBOND	MXCE 280	MXCE 280	MXCE 280
	TDCA			G-90	MX 2625	MX 4926				
	BDCF	MXSC 195	MXSC 195	MXCE 280	MXSE 280	MXCE 280				
	BDCA	MX 4926	MX 4926	G-90						
AFT ENTRANCE CAP	TDC	G-90	G-90	G-90	G-90	8882	G-90	G-90	G-90	G-90
	BDC	PO3	PO3	PO3	8882	G-90				
THROAT	—	PG	PG	PG	PG	PG	PG	PG	PG*	PG†
EXIT CONE	TDC	FM 5055	FM 5055	FM 5055	FM 5055	MX 4926	FM 5055	FM 5055	FM 5055	FM 5055
	BDC				MX 2600	MX 2600				
BLAST TUBE AREA RATIO	—	2.0	2.0	1.3	2.0	1.3	2.0	2.0	1.3	2.0

\* SUPERTEMP PYROLITIC GRAPHITE WASHERS. SECOND WASHER FROM AFT END WAS FROM PYRC  
† SUPERTEMP PYROLITIC GRAPHITE

TABLE V  
 TEST MATRIX

6	7	8	9	10	11	12	13	14	15	16	
CP	KP	CP	CP	CP	CP	KP	KP	CP	CP	CP	
5	5	18	5	5	5	5	18	18	18	18	
MX 2625 DUREZ 16771-1	R-155	DUREZ 16771-1 DUREZ 16771-1/4	DUREZ 16771-1	DUREZ 16771-1	R-155	DUREZ 16771-1	R-155	DUREZ 16771-1	R-155	DUREZ 16771-1	
MXCE 280	MXCE 280	MXCE 280	MXCE 280	MXCE 280	MX 4926	MX 4926	MX 4926	MX 4926	MX 4926	MX 4926	
BOBOND	MXCE 280	MXCE 280	MXCE 280	MXCE 280	MXCE 280 SUPERTEMP PYCOBOND	MXCE 280 ARC PYROSTRAND	MXCE 280	MXCE 280	-	MXCE 280	MXCE 280
					MXCE 280 SUPERTEMP PYCOBOND	MXCE 280 ARC PYROSTRAND					
G-90	G-90	G-90	G-90	G-90	G-90	G-90	G-90	G-90	G-90	G-90	
PG	PG	PG*	PG†	PG	PG	PG	PG	W <sup>3</sup>	W <sup>3</sup>	W <sup>3</sup>	
FM 5055	FM 5055	FM 5055	MX 2600	MX 2600	MX 2600	MX 4926	FM 5055	FM 5055	FM 5055	FM 5055	
2.0	2.0	1.3	2.0	1.3	2.0	1.3	1.3	-	1.3	1.3	

WASHER FROM AFT END WAS FROM PYROGENICS, INC.

TABLE VI  
 TEST MATERIAL DESCRIPTION  
 (Sheet 1 of 2)

Material	Material Type	Manufacturer	Fabrication Technique	Comments
Durez 16771	Glass phenolic molding compound	Hooker Chemical Co.	Molded at 2,000 psi minimum	This product is now manufactured by Fiberite as MX16771 - mods 1/4 and -1 designate the fiber length
R155	Asbestos filled rubber (EPDM) compound	Rocketdyne Division North American Rockwell Corp.	Molded at 200 psi minimum	Easily fabricated by molding
MXCE-280	Elastomeric modified carbon phenolic (fibrous compound)	Fiberite Corp.	Molded at 2,000 psi minimum	---
MXSE-280	Elastomeric modified silica-phenolic (fibrous compound)	Fiberite Corp.	Molded at 2,000 psi minimum	---
MX4926	Carbon-phenolic tape or broadgoods	Fiberite Corp.	Flat laminate molded at 1,000 psi for forward entrance cap, blast tube, and throat retaining ring tapewrapped parallel to centerline for exit cone	Considered interchangeable with FM5055 based on previous high pressure test results
MXSC-195	Hybrid carbon/silica-phenolic broadgoods	Fiberite Corp.	Molded flat laminate at 1,000 psi for blast tube	Production reportedly ceased.
MX2625	Silica-phenolic chopped squares molding compound	Fiberite Corp.	Molded at 2,000 psi	
MX2600	Silica-phenolic tape or broadgoods	Fiberite Corp.	Tapewrapped for exit cone parallel to centerline	---

TABLE VI  
TEST MATERIAL DESCRIPTION  
(Sheet 2 of 2)

Material	Material Type	Manufacturer	Fabrication Technique	Comments
FM5055	Carbon-phenolic tape or broadgoods	U.S. Polymeric, Inc.	Flat laminate molded at 1,000 psia for forward entrance cap tapwrapped parallel to centerline for exit cone	Based on previous high pressure test results, this material is considered interchangeable with MX4926
Graph-i-tite G-90	Polycrystalline graphite	Carborundum Co.	Extruded grade	This material was only used in the cored and reimpregnated condition, density = 1.90 g/cc
P03	Polycrystalline graphite	Pure Carbon	Molded grade	Used as purchased in bulk form, 1.85 g/cc
Speer 8882	Polycrystalline graphite	Airco Speer, Division, Air Reduction Co., Inc.	Molded grade	Used as purchased in bulk form, 1.79 g/cc
Pyrolytic Graphite	Pyrolytic	Pyrogenics Inc.	Vapor deposited	Used on firings 1 through 7 and 10 through 13, Density $\geq$ 2.20 g/cc
Plate	---	Supertemp, Inc.	---	Used on firings 8 and 9, density = 2.185 to 2.196 g/cc
Techmet	Wire-wound tungsten	United Technology Center	Plasma spray tungsten matrix with wire-reinforcement	Material is approximately 80% $\gamma$ 85% as dense as forged tungsten
Pycobond	Carbon-Carbon Composite	Supertemp, Inc.	Carbon Graphite flat laminate cloth is bonded by infiltrating and carbon vapor deposition	Density = 1.65 g/cc
Pyrostrand	Carbon-Carbon composite	Atlantic Research Corp.	Vapor deposited graphite filament reinforced composite	---

Both silica-phenolic and carbon-phenolic were evaluated in the exit cone for the lower aluminum content propellant. Carbon-phenolic (FM5055) was selected as the baseline material since it is applicable to both propellant systems.

## SECTION VI

### PHASE II - NOZZLE DESIGN AND FABRICATION

#### 1. NOZZLE DESIGN

Two basic nozzles (conventional and blast tube) were designed. Figure 1 shows the blast tube design. The conventional design was used on only one nozzle (S/N 14) and is identical to the blast tube design except that the 8-in.-diameter section (blast tube) between the entrance cap and throat package was removed. The throat diameter was held constant at 1.72 in. An  $8^{\circ}30'$  half-angle exit cone with an expansion ratio of 7.15 and lightweight steel hardware was used. This provided a more accurate evaluation of candidate materials than heavyweight hardware, since the materials were exposed to the actual stress fields resulting from membrane deflections and joint rotation. All structural components were steel. The aft closure was 4340 steel forging heat-treated from 200 to 220 ksi. The nozzle shell and throat retaining ring were 4130 steel with a minimum yield strength of 70,000 psi. The aft closure was a flat conical shell with a  $64.5^{\circ}$  insulated surface. The closure was mounted in the large HIPPO aft closure which then attached to the motor barrel. The nozzle shell had a nominal thickness of 0.28 in. and adapted to the lightweight aft closure by a threaded joint. O-rings were used at all interfaces to seal against gas flow.

Materials evaluation was performed for six regions in the test nozzle: aft closure, forward entrance cap, blast tube, aft entrance cap, throat insert, and exit cone. Candidate materials were segmented axially within these test regions except for the throat insert and forward entrance cap.

The aft closure insulation consisted of a sandwich construction of a candidate material facing backed by a 0.4-in. thick glass-phenolic (Durez 16771) molded component. This backup insulator was a redundant feature to provide full protection for the test duty cycle in case either the candidate material failed or channeling was encountered in the segmentation bondline.

The entrance cap was divided into a forward and aft component. The forward entrance cap provided a transition zone from the steep aft closure into the blast tube, or the throat section, of the conventional nozzle (S/N 14). This forward section also provided protection for the leading edge of the blast tube. The forward entrance cap was bonded to the aft closure insulator and was backed by the same insulator as used on the aft closure.

The blast tube liner was a cylinder 8.105-in. long with a contraction ratio of 1.3 or 2.0. The candidate materials varied from 1.49 in. to 0.53 in. thick and were backed by MX2600 silica-phenolic tapewrapped parallel to the centerline which provided both thermal insulation and a redundant backup in case of candidate material or bondline failure.

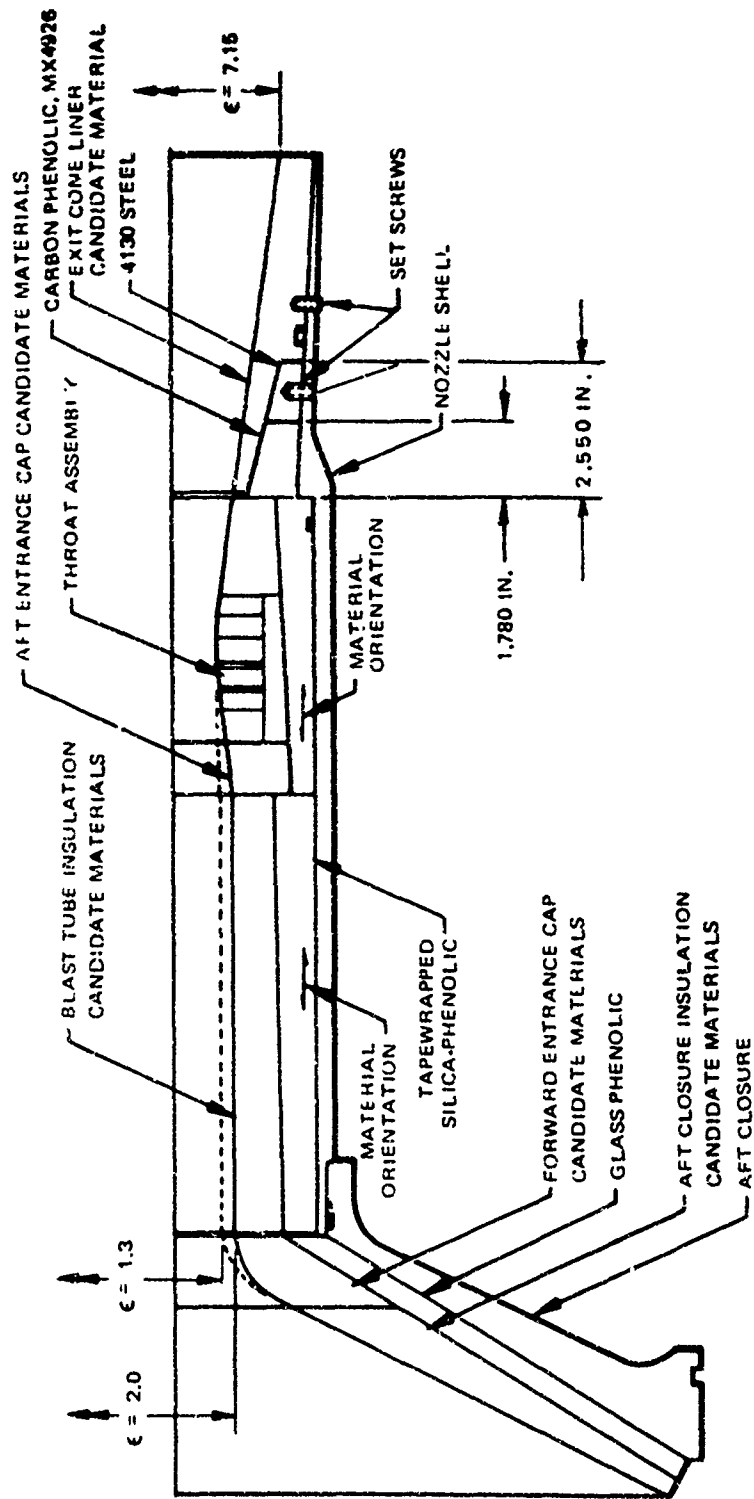


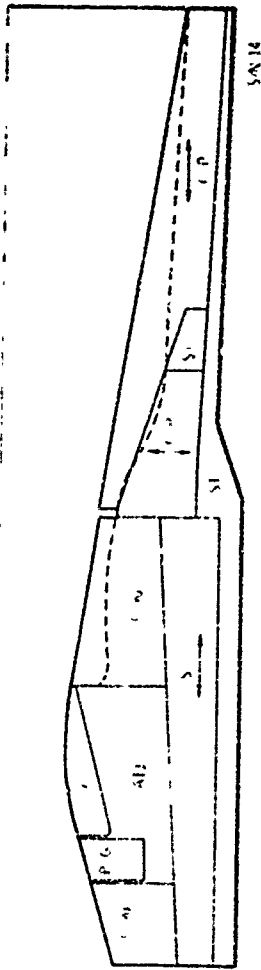
Figure 1. Blast Tube Nozzle Design

The aft entrance cap provided protection for the leading edge of the throat insert and was included as part of the overall throat package. Two throat insert materials were used, pyrolytic graphite and wire-wound tungsten. The initial design of the throat package hotside consisted of the aft entrance cap, six 0.50-in. thick edge-grain-oriented pyrolytic-graphite washers, and a carbon-phenolic throat retaining ring. After the first test, the retaining ring material was changed to Graph-i-tite G-90. The throat washers were supported on a noncharring cylinder of ATJ-graphite which allowed axial movement without radial interference. No bond was used between the throat washers and graphite backup. Initially, on contract No. F04611-69-C-0065, the washers were bonded to the graphite backup; however, this restricted axial movement was due to thermal expansion and resulted in the washers cracking. Polyethylene spacers were placed on both sides of the throat of washer No. 3 to allow for axial expansion. Upon expansion, the polyethylene was squeezed out of the annulus, permitting unrestricted axial growth.

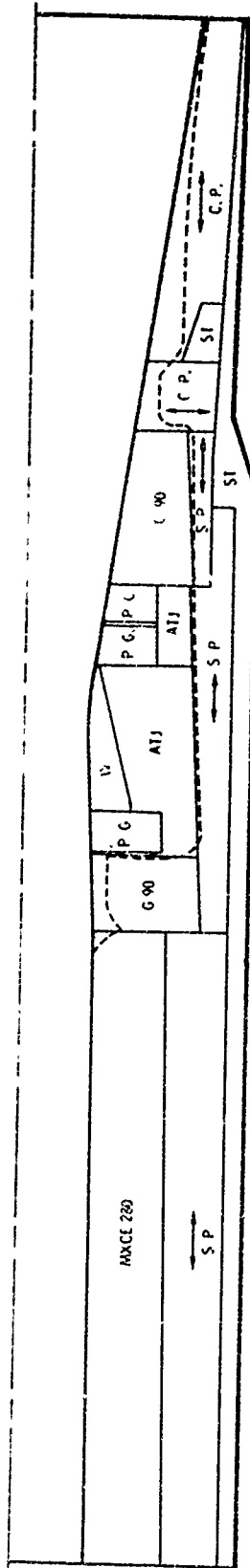
A silica-phenolic sleeve encircled the entire throat package. The sleeve was an FM5504 component, tapwrapped parallel to the centerline, which provided both radial support and thermal protection for the steel shell. A conical interface was used to facilitate bonding between the silica insulator and the adjoining entrance cap, the ATJ-graphite backup sleeve, and the Graph-i-tite G-90 retaining ring. This bond was used primarily for handling and machining since the bondline strength degraded within 6 sec following ignition due to the high thermal conductivity of the graphite components. A block of Graph-i-tite G-90 was used immediately aft of the pyrolytic-graphite washers. This polycrystalline graphite was used as a smooth bearing surface to transmit the throat ejection load into the retention system. It also provided sufficient ablation resistance so that its use at low area ratios was feasible.

A carbon-phenolic block was used for the first test to transmit the throat ejection loads into the steel shell. This component's ablation resistance and structural integrity were not sufficient to provide uniform and adequate axial support for the pyrolytic graphite washers. After the first firing, a steel throat retention ring was added with a carbon-phenolic retaining ring between the Graph-i-tite G-90 and the exit cone. The retention system was located under the exit cone liner for thermal protection. This retention system is the configuration proven under contract No. F04611-69-C-0065 and discussed in reference 2. A double row of 0.25-in. screws provided the primary method of retention with the epoxy bond between the exit cone liner and shell to provide a secondary method of retention.

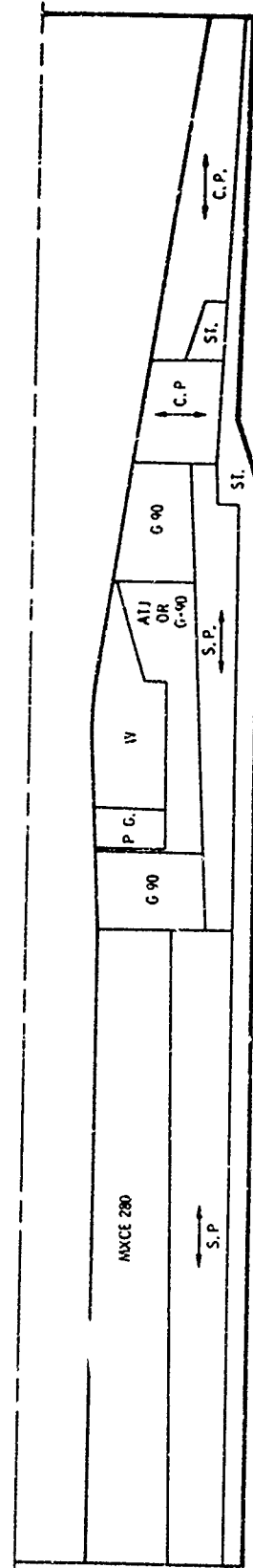
Wire-wound tungsten designs were used for the throat package in the final three tests. These designs are shown schematically in figure 2. All designs used graphite as a heat sink to back the wire-wound tungsten. Graph-i-tite G-90 was still used aft of the insert except for the second nozzle (S/N 15). In an attempt to improve the ablation resistance for this nozzle, two 0.5-in. pyrolytic-graphite washers were used immediately aft of the tungsten throat insert. An 0.5-in. pyrolytic-graphite washer was used immediately ahead of all three inserts to avoid undercutting the throat materials. The tungsten on the third insert was extended downstream to an area ratio of 1.76 instead of 1.22 as previously used.



S/N 14



S/N 15



S/N 16

Figure 2. Wire-Wound Tungsten Test Configuration

The exit cone liners were tapewrapped with parallel-to-centerline orientation using carbon-phenolic or silica-phenolic materials with the exception of nozzle S/N 16 which incorporated a helical tapewrap to provide better ply resistance to mechanical erosion at the forward end of the exit cone which protects the steel retention ring.

The nozzle was threaded to the insulated aft closure and rotated into the closure until the parts were in contact. The gap between the blast tube and forward entrance cap was measured and the nozzle was removed. The blast tube face was machined to allow a step joint of approximately 0.75 in. below the hotside surface. A ring was bonded to the forward entrance cap to complete the step joint which prevents a direct flame path to the steel housing. The step joint width was machined for a nominal 0.025-in. clearance. A layer of zinc chromate putty was used to fill the joint; then the nozzle was reassembled.

## 2. NOZZLE ANALYSIS

The test nozzle was analyzed thermally and structurally. The thermal analysis for the initial 13 tests conducted at a nominal pressure of 3,000 psia was done by Aerotherm and is summarized in volume II of this report. UTC conducted additional thermal analysis for support of specialized structural analysis such as the design of the 3,500-psia blast tube configuration and the redesign of test nozzle S/N 16.

The results of the thermal analysis conducted by both Aerotherm and UTC were used as input for the temperature-dependent structural analysis conducted by UTC. The nozzles were analyzed structurally for the combined pressure and thermal gradient stress fields. Temperature-dependent material properties were used. Most of the structural analysis was devoted to the throat package and graphite components, i.e., Graph-i-tite G-90 blast tube. The nozzle hotside materials were analyzed structurally using simple one-dimensional calculations using the indepth thermal profile provided by Aerotherm. Previous UTC-managed nozzle development programs have proved these simple one-dimensional calculations are a cost-effective approach.

The contract was separated into two main areas for the purpose of analysis: (1) the basic 3,000-psi blast tube design with pyrolytic graphite throat insert and (2) the 3,500-psi blast tube design with wire-wound tungsten throat insert. The following discussion presents these analyses.

### a. Basic 3,000 Psi Blast Tube Design

The basic design configuration utilized in the initial 13 tests was very similar to that previously test fired and reported in reference 2. Since this configuration had been analyzed and verified during actual test for the same pressure but for more severe durations, the analyses were restricted to those areas where modifications were made. These areas are the high velocity blast tubes and the lower cost aft closure insulation materials.

Analysis of the high velocity blast tubes and aft closure insulation was primarily surface recession and indepth heating. These results are summarized in volume II, section VI. In addition to these thermochemical and penetration analyses, a thermal structural analysis was conducted for the Graph-i-tite G-90 blast tube used in nozzle S/N 03. This analysis was conducted in three steps. Initially, a two-dimensional finite element analysis was made for a nonsegmented, 8-in.-long Graph-i-tite G-90 blast tube. The model included a nominal 0.5-in. graphite liner backed with a silica-phenolic insulator and a lightweight steel shell. The finite element grid for this configuration is presented in figure 3. This configuration was analyzed two times during the firing (1 and 5 sec after ignition). These two times are representative of the high thermal stresses early in firing where an integral bond is anticipated and the loss of the backside axial support due to bonding degradation. The critical hoop and axial stresses along with the resulting factors of safety are summarized below.

Time, sec	Element Grid No.	Hoop Stress, psi	Hoop Safety Factor	Axial Stress, psi	Axial Safety Factor
1	94	1,330	1.96	4,420	0.72
5	83	-11,700	1.11	4,120	0.94

The results confirmed that axial stresses are critical, and the remaining analyses were conducted to obtain positive safety factor margins by segmenting the Graph-i-tite G-90 into rings.

The second phase of the analysis involved a tradeoff of the thickness and the length of the rings. Individual ring thicknesses from 0.35 to 0.5 in. and lengths from 1 to 2 in. were evaluated. The resulting safety factors as a function of these parameters are shown in figure 4. As predicted, the length of the rings has the largest effect upon the axial stress safety factor; the effect of the ring web thickness is of lesser significance. The thermochemical analysis predicted approximately 0.2-in. material ablation. An initial liner thickness of 0.57 in. (0.35 in. after ablation) was selected with an individual ring length of 1 in. This configuration showed a safety factor greater than 2.0 at the critical time of 5 sec after ignition.

The analysis was then finalized for this configuration by evaluating the hoop stresses in the blast tube for five discrete times during the firing. The analytical model assumed a fixed backside restraint where no radial displacement of the Graph-i-tite G-90 was allowed. The analysis was checked at two discrete times for a flexible backside condition which accounts for the radial growth of the silica-phenolic and steel shell. These results are:

Time, sec	Maximum Hoop Stress Using Flexible Backside Model, psi		Maximum Hoop Stress Using Flexible Backside Model, psi	
	Hotside Surface	Graph-i-tite G-90 to Silica Interface	Hotside Surface	Graph-i-tite G-90 to Silica Interface
0.5	---	---	-9,290	250
1.0	-10,000	1,330	-11,200	1,096
1.5	---	---	-12,400	-1,330
5.0	-11,700	-3,860	-12,750	-4,960
11.0	---	---	-10,600	-11,000

The backup structure of the silica-phenolic and the steel shell is sufficiently rigid so that the hoop stresses are essentially the same for both fixed and flexible backside restraints. Due to the high conductivity of the graphite, a shallow gradient exists at later times (11 sec) resulting in essentially a uniform compressive load throughout the web thickness.

These analyses all assumed the bondline provided radial support even in a charred state which occurs at approximately 1.5 sec.

b. 3,500-psi Blast Tube Design

The last three nozzles (S/Ns 14, 15, and 16) were designed for operation at 3,500 psia for a 10-sec duration. A wire-wound tungsten throat insert replaced the pyrolytic graphite component previously used. The analysis was restricted to evaluation of the throat package and the nozzle and aft closure steel housings.

The thermal analysis of the throat package as a function of time was performed by UTC. This analysis consisted of defining the indepth profiles and predicting the ablation of the Graph-i-tite G-90 throat retention block located immediately downstream of the tungsten insert.

The indepth profiles of thermal penetration for the S/N 16 nozzle throat package are shown in figures 5 through 8. These profiles were generated from one-dimensional heat conduction runs at five locations and account for the increase in heating downstream of the tungsten throat insert due to the step effect. Subsequently, one more one-dimensional heat conduction run was made in the thin, downstream tungsten region to define the temperature distribution more accurately at the end of firing (10 sec). This revised isotherm drawing is shown in figure 9.

Most of the thermal analysis conducted by UTC involved predicting the high ablation on the Graph-i-tite G-90 throat retention ring which is increased due to the noneroding tungsten throat insert. Detailed results of this analysis are presented in appendix II.

The objective of the analysis was to develop a model which allowed prediction of the severe ablation of the Graph-i-tite G-90 and carbon-phenolic exit cone regions using nozzle S/N 14 test firing as a basis for defining the unknown coefficients. This model was then used to modify the design for nozzle S/N 16 in an attempt to reduce the ablation on the critical throat retention block. The results of the analysis compared to the test results for the two nozzles are shown in figures 10 and 11. Table VII summarizes these results for the analysis stations identified on figures 10 and 11.

The reason for the high ablation downstream of the tungsten throat insert is debatable. One theory, which appears most probable, is that a

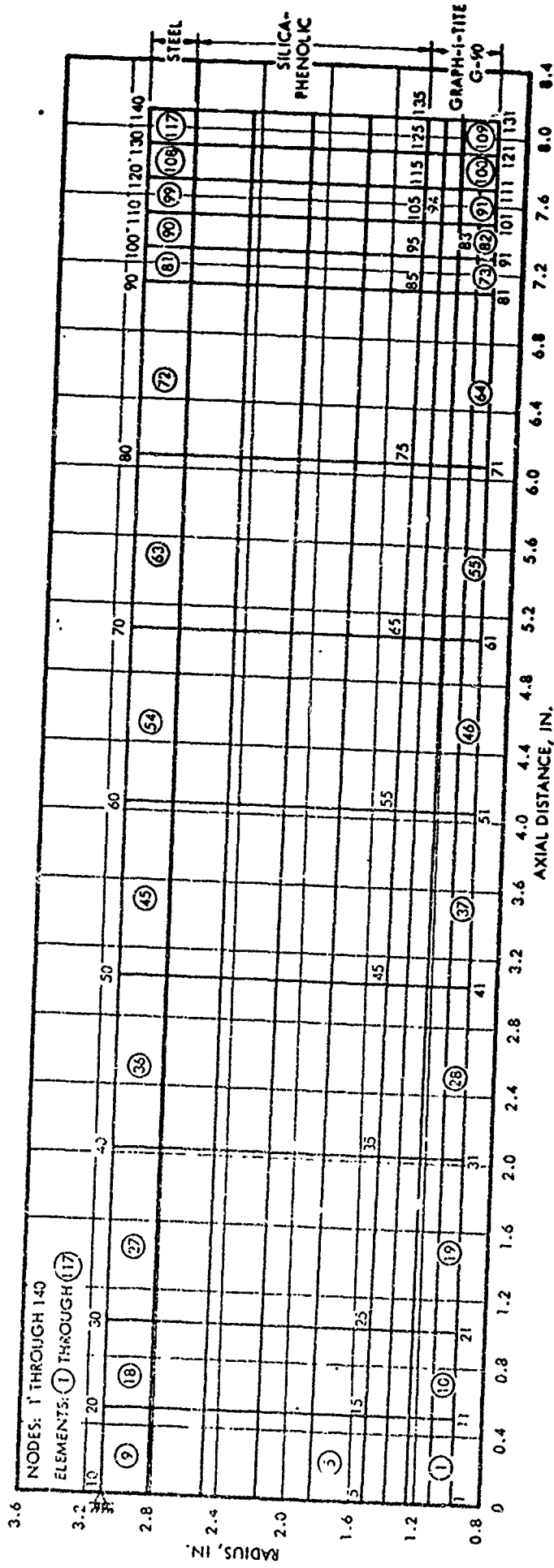
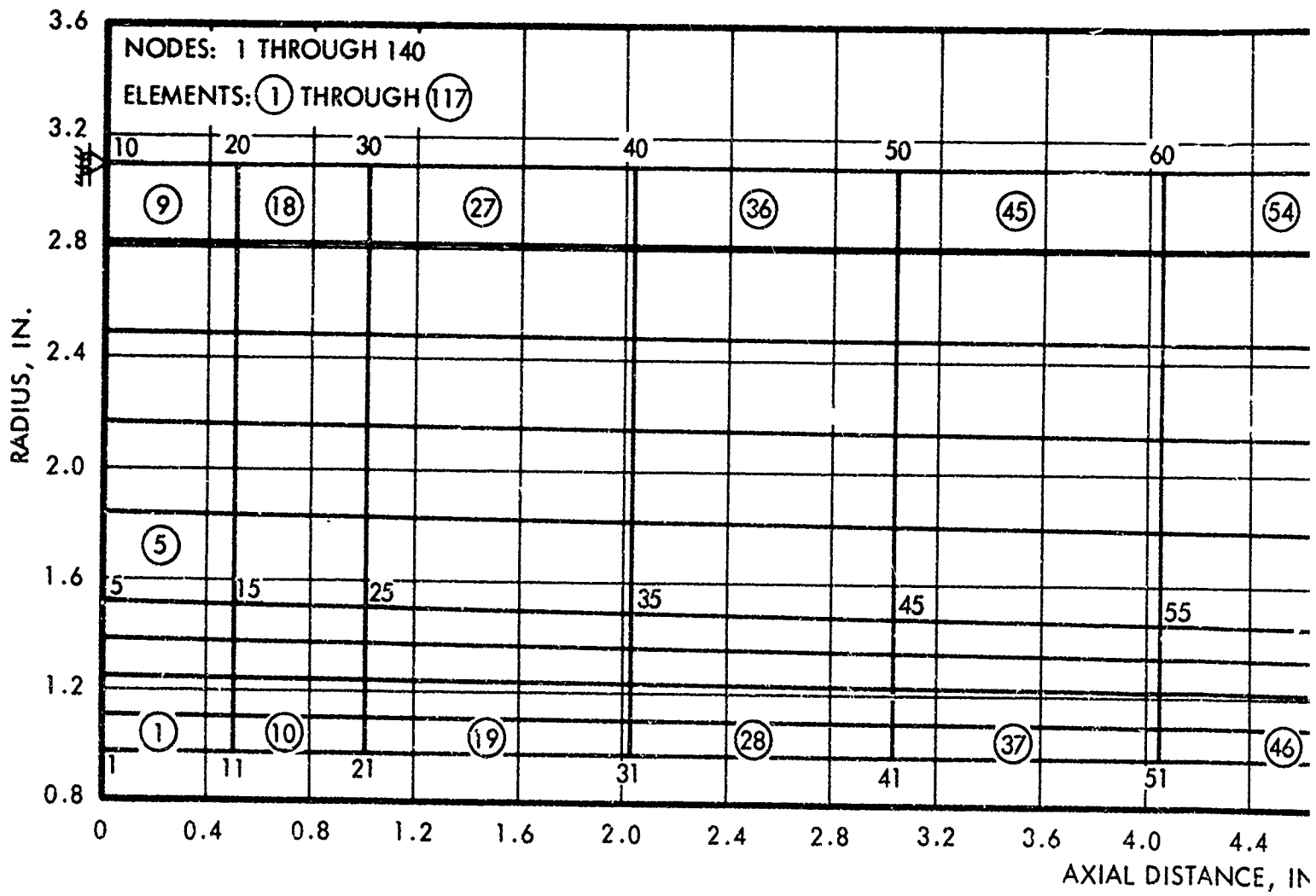


Figure 3. Finite Element Grid for Graph-ite G-90 Blast Tube



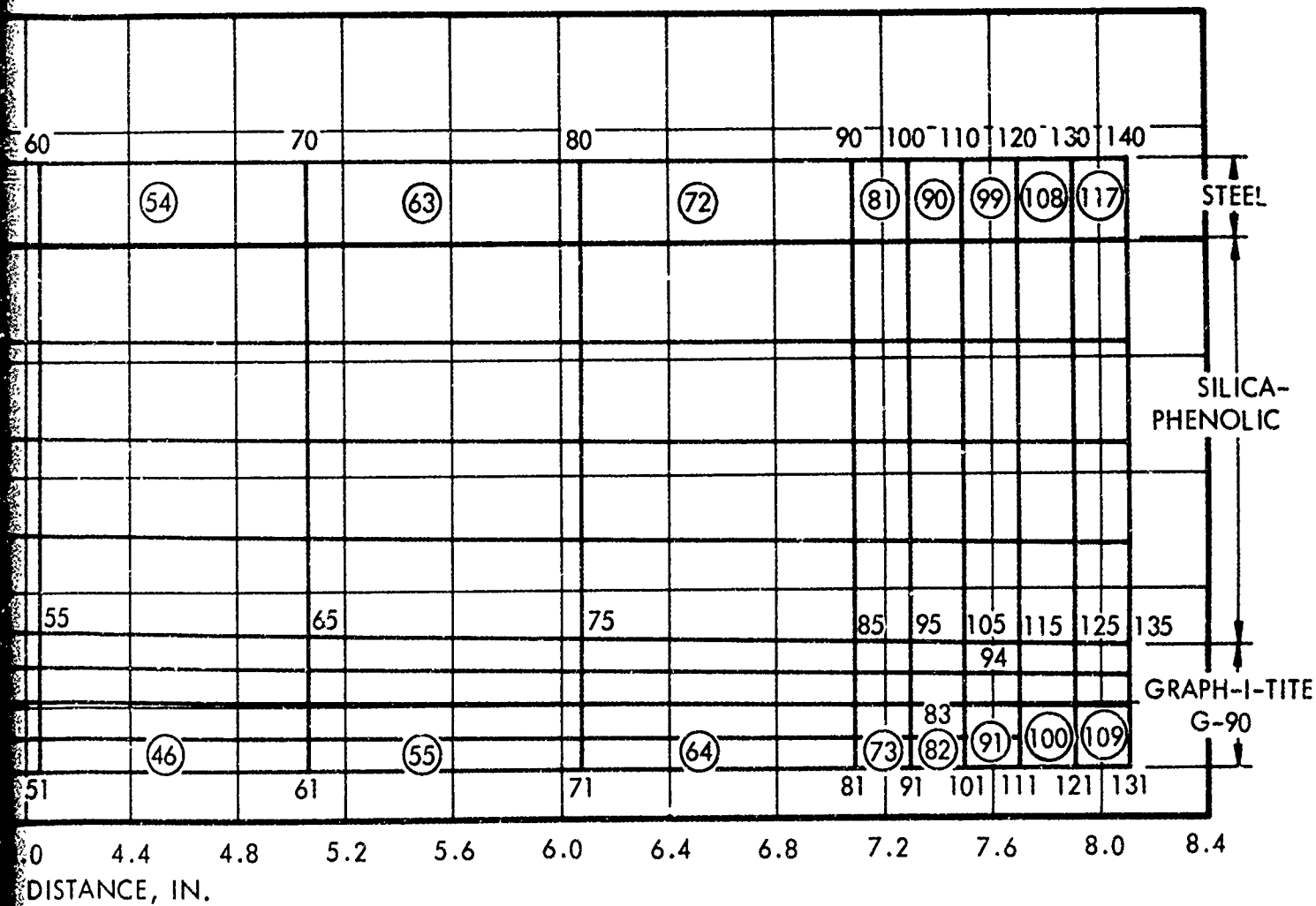


Figure 3. Finite Element Grid  
for Graph-i-tite G-90 Blast Tube

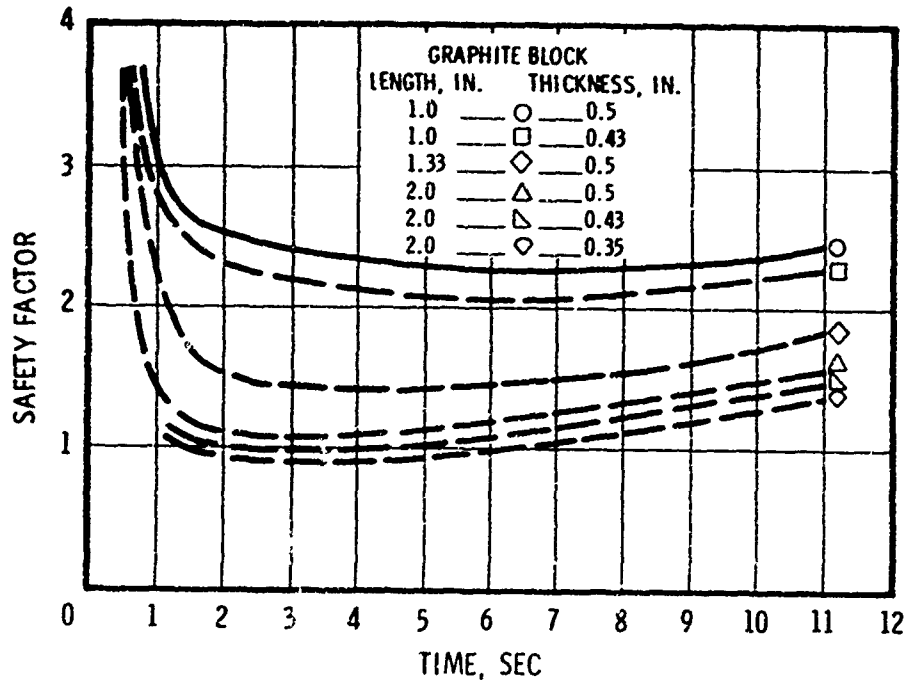


Figure 4. Safety Factors for Critical Axial Stress in the Graph-i-tite G-90 Blast Tube

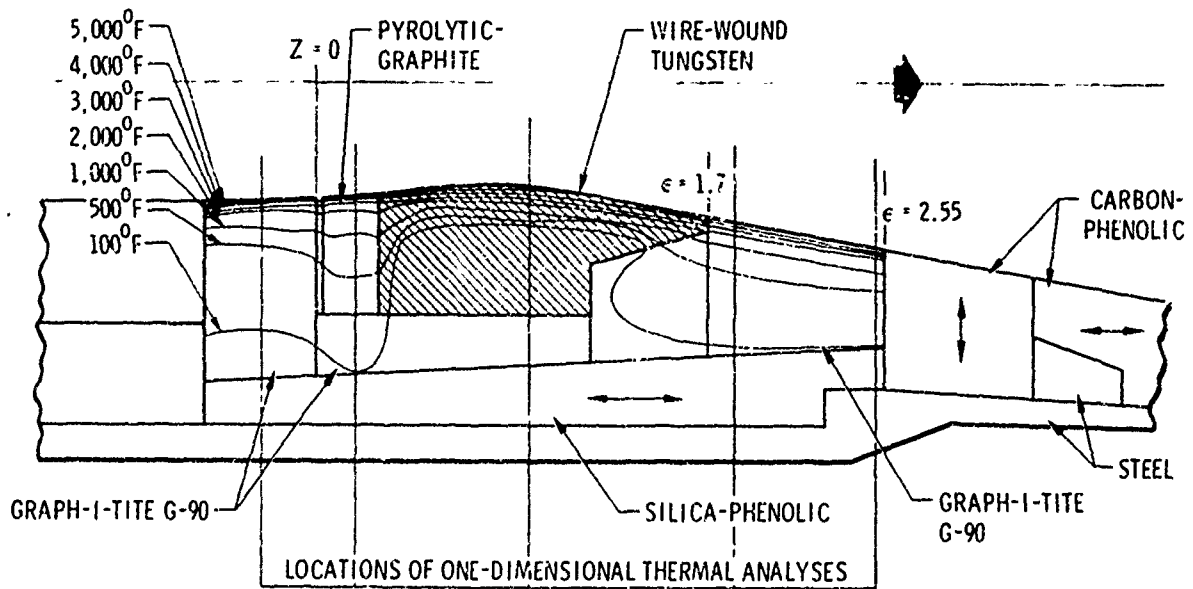


Figure 5. Predicted Isotherm of Tungsten Throat Package at 1 Sec (S/N 16 Nozzle)

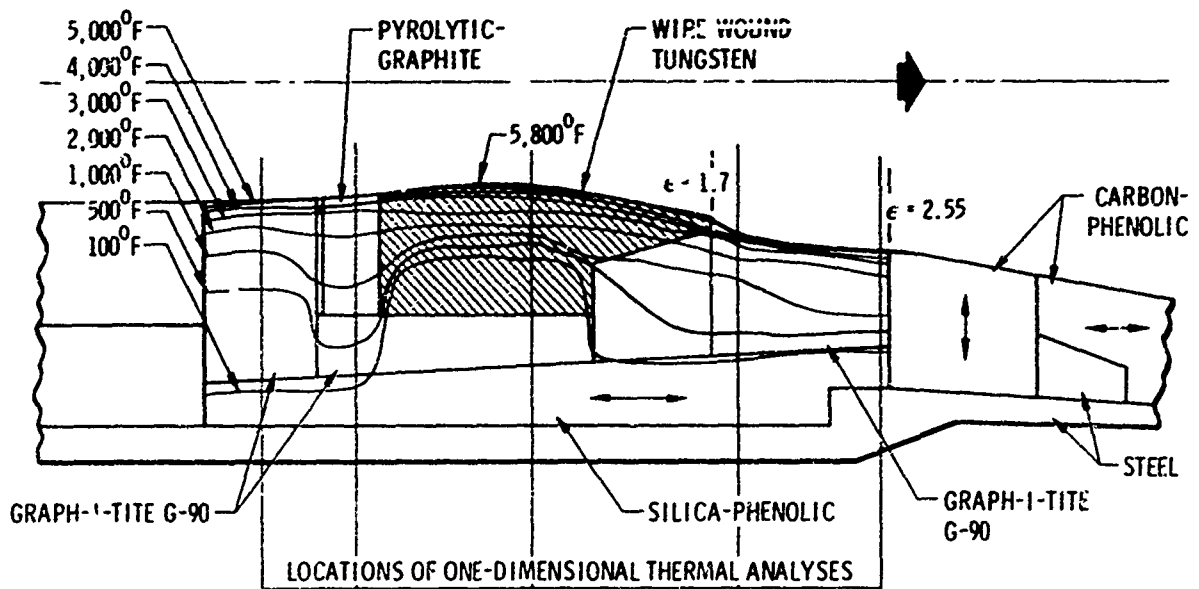


Figure 6. Predicted Isotherm of Tungsten Throat Package at 3 Sec (S/N 16 Nozzle)

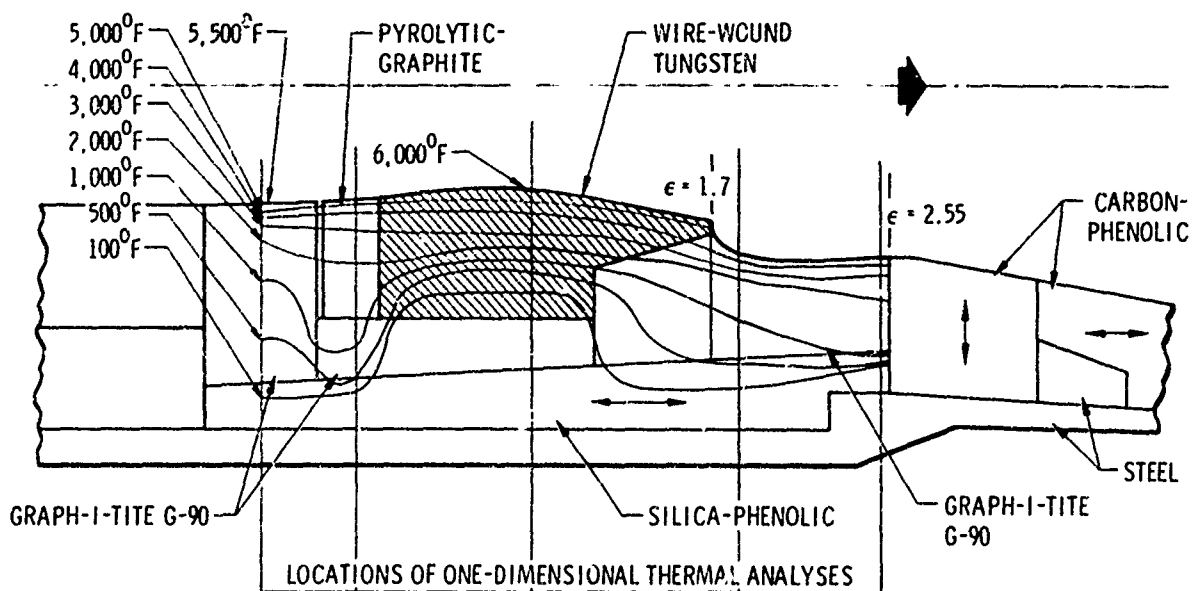


Figure 7. Predicted Isotherm of Tungsten Throat Package at 6 Sec (S/N 16 Nozzle)

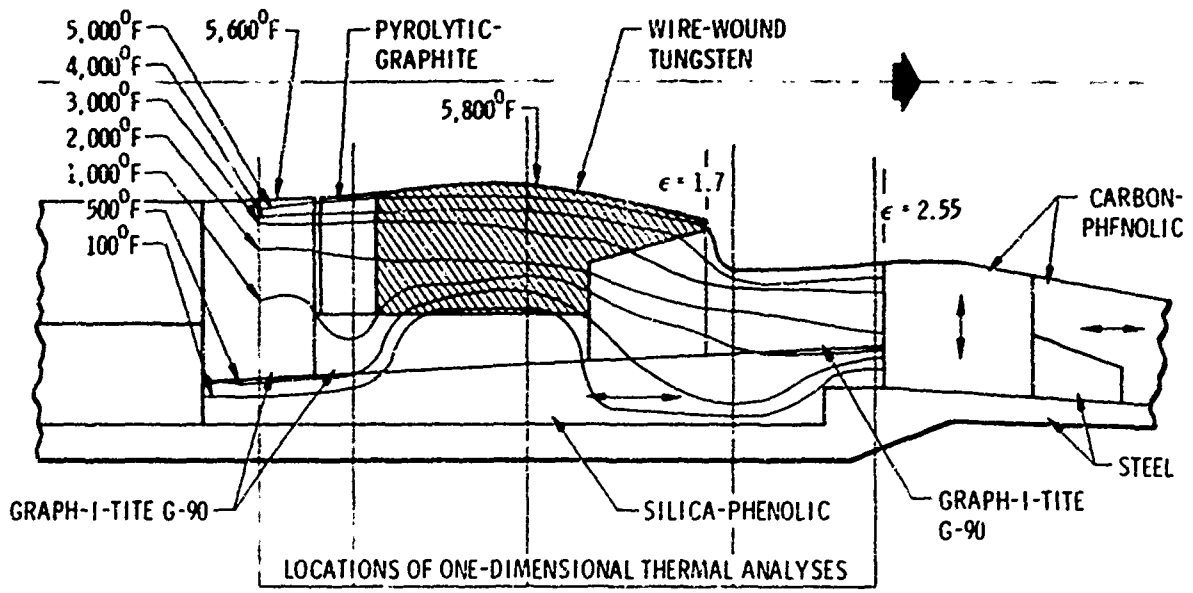


Figure 8. Predicted Isotherm of Tungsten Throat Package at 10 Sec (S/N 16 Nozzle)

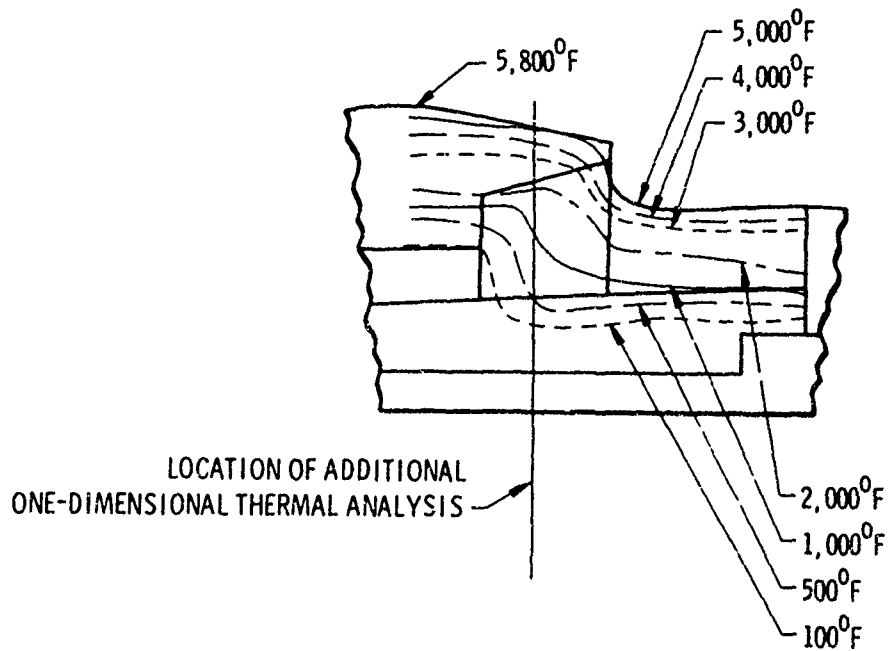


Figure 9. Revised Isotherm Due to Additional One-Dimensional Analyses at 10 Sec

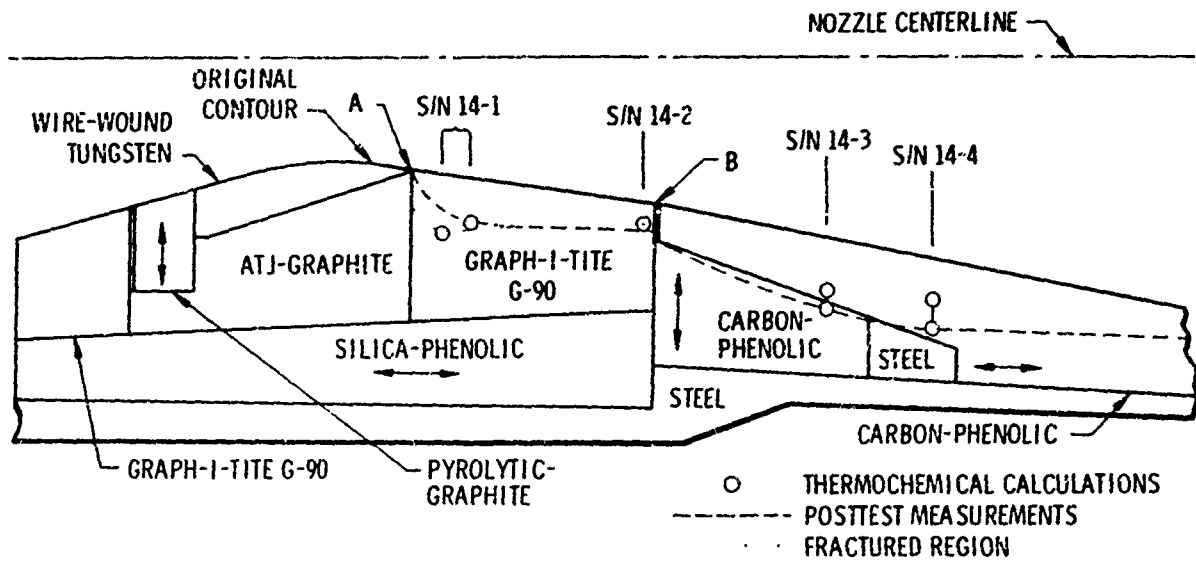


Figure 10. Comparison of Actual and Predicted Surface Ablation for Nozzle S/N 14

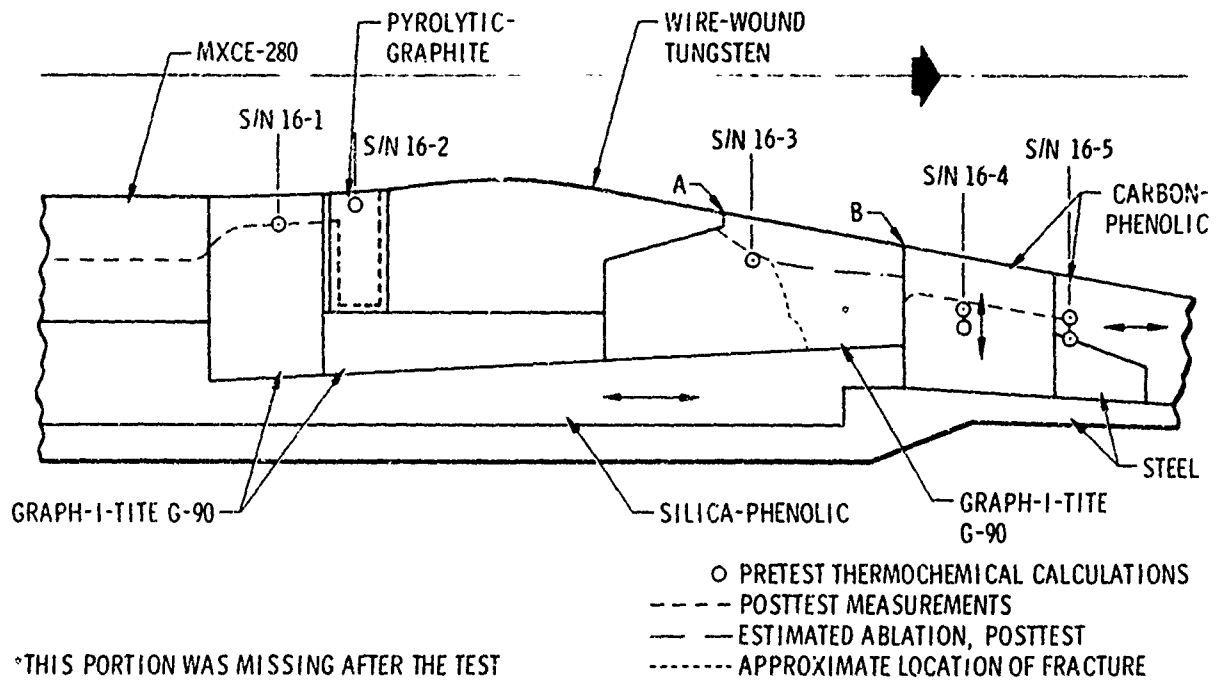


Figure 11. Comparison of Actual and Predicted Surface Ablation for Nozzle S/N 16

TABLE VII  
TUNGSTEN THROAT PACKAGE ABLATION ANALYSIS SUMMARY

Analysis Station*	Material Ablated		HTC/C <sub>pat</sub> 3,250 psia, lb/ft <sup>2</sup> -sec	HTC Multiplier†	Initial Station Radius, in.
	Predicted, in.	Measured, in.			
S/N 14-1	0.481	0.45‡	5.580	2.1	1.06
S/N 14-1	0.352	0.35	3.627	1.37	1.06
S/N 14-2	0.179	0.22	2.402	1.0	1.25
S/N 14-3	0.440	0.54	2.420	1.0	1.45
S/N 14-3	0.580	0.54	3.025	1.25	1.45
S/N 14-4	0.343	0.55	1.949	1.0	1.60
S/N 14-4	0.531	0.55	2.924	1.5	1.60
S/N 16-1	0.256	0.25	3.081	0.75	0.98
S/N 16-2	0.066	§	3.260	0.75	0.94
S/N 16-3	0.326	0.30	3.877	2.50	1.225
S/N 16-3	0.185	---	2.731	1.75	1.225
S/N 16-4	**	0.35	---	---	---
S/N 16-5	---	---	---	---	---

\* Analysis stations defined on figures 10 and 11.

† Based on boundary layer analyses.

‡ This measurement reflects the region where the graphite was chipped away, not ablated.

§ This pyrolytic-graphite piece was missing after the test.

|| This run had chemistry for no shock interaction and conventional flow gas dynamics.

\*\* Predictions for these stations are the same as for S/N 14-3 and S/N 14-4.

---

progressively larger rearward facing step is encountered as the graphite surface recedes which causes a region of flow separation. An increase in the localized heat transfer is encountered at the point of attachment of the resulting shock system, which results in increased ablation. Since this mechanism tends to "feed" itself, the effect on surface ablation becomes increasingly more severe. Limited research and experimental data are available. However, data presented in references 3 through 6 indicate

that the localized heat transfer coefficient may be increased on the order of 3 over the coefficient encountered in a uniform nonseparated flow environment. This multiplier undoubtedly is a strong effect of the Mach number (i.e., initial area ratio) where the rearward facing step occurs.

The value of this multiplier was selected using the test-fired hardware for nozzle S/N 14. To predict the measured results a value of approximately 1.4 times the heat transfer coefficient for nonseparated flow at the station of the upstream face of the step was used. By applying this factor to nozzle S/N 16 where the tungsten was extended to an area ratio of 1.76 (instead of an area ratio of 1.22 as for nozzle S/N 14), the ablation was approximately 63% less than predicted. To match the measured results for nozzle S/N 16, a prediction multiplier of 2.5 was required. The reasons for the range of multipliers is not clear at this time, but is encouraging that these required multipliers are within the range of experimental data as presented in references 3 through 6.

Subsequent studies are currently being conducted to clarify the difference. However, it may be necessary to take a significantly more sophisticated approach to predict the boundary layer and resultant separated region heat transfer than the one that has been taken in the present study. One approach would be to use a mass addition reacting boundary layer program for more precise boundary layer calculations and a laboratory testing program to measure the heating rates in the region of rearward facing steps in supersonic flow environments.

Multiaxial stresses in this throat package assembly were determined using a finite element stress analysis computer program (LI77ZZZ) which determines the displacements and stresses in axisymmetric solids with orthotropic, temperature-dependent properties. The finite element representation of the nozzle generated for this analysis is shown in figure 12. Adhesive bondlines were incorporated in the finite element model as shown.

The nozzle was analyzed for combined temperature and pressure distribution corresponding to motor firing times of 1, 3, 6, and 10 sec. The temperature distribution throughout the nozzle at each time was determined by thermal analysis (figures 5 through 9). Additional thermal analysis of the critical Graph-i-tite G-90 throat retention block was conducted for the revised temperature profiles for 10 sec duration (figure 10). The 10 sec example represented the maximum change experienced in the temperature profiles since maximum erosion is encountered at this time.

Many possible boundary conditions due to partial loss of bonds were investigated. As shown in figure 12, the throat insert was restrained axially at node points 191 through 195. A 0.002-in. radial displacement was assumed.

Wire-wound tungsten becomes ductile at relatively low temperatures and at room temperatures at high stress levels. To account for this non-linear character, an analysis of the plasticity was conducted to ensure that the modulus in any element was consistent with the temperature and stress level in that element. This was done by an iterative procedure

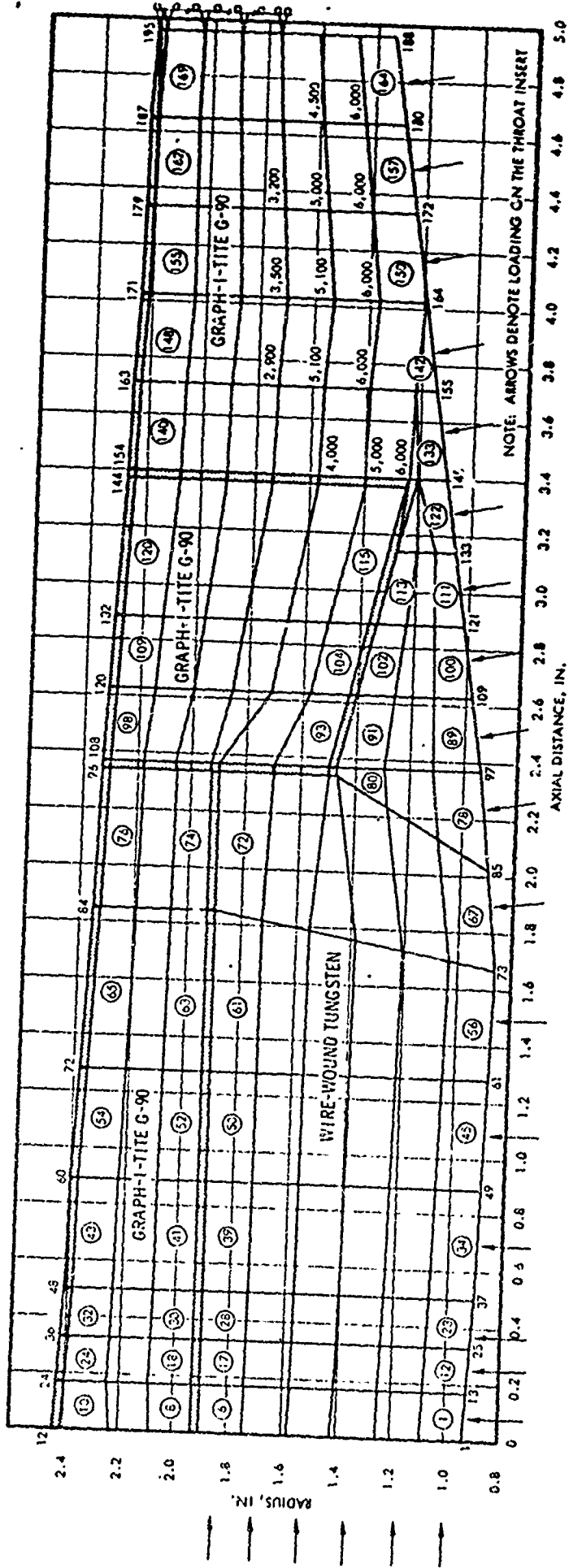


Figure 12. Finite Element Grid  
for Tungsten Throat Insert  
(S/N 16 Mossia)



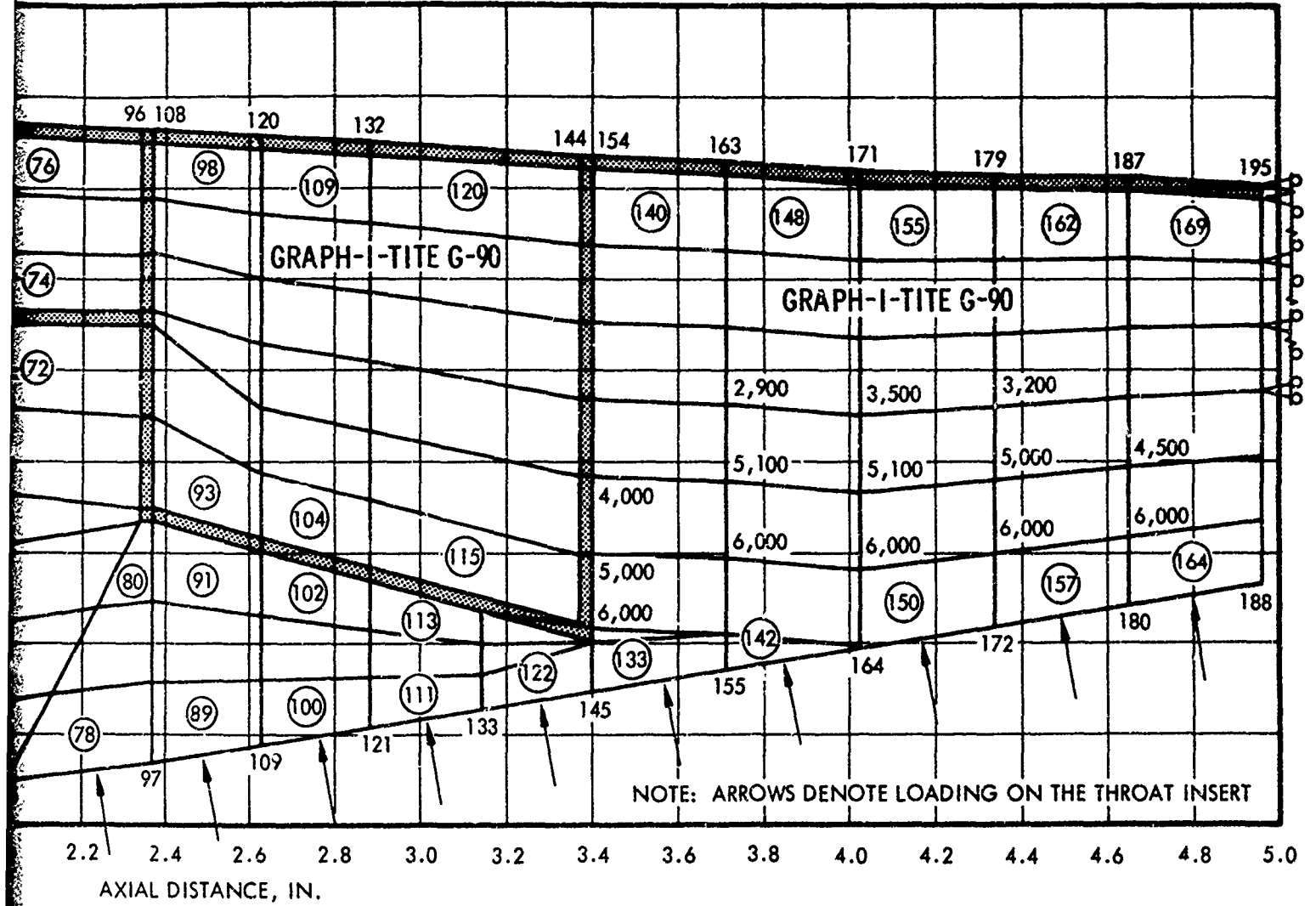


Figure 12. Finite Element Grid  
for Tungsten Throat Insert  
(S/N 16 Nozzle)

using the effective (von Mises) stress,  $\bar{\sigma}$ , in each element and the relationship

$$\frac{\bar{\sigma}}{\epsilon} = E$$

where  $\bar{\epsilon}$  is effective strain and E is the uniaxial modulus at effective strain.

Finally, the structural integrity of the nozzle was determined assuming all bonds were released (i.e., the bonds were all assumed to have negligible shear stiffness).

The uniaxial factors of safety were calculated for the combined pressure and thermoelastic stresses comparing maximum stresses with the corresponding temperature-dependent mechanical properties. The factor of safety is defined as

$$FS = \frac{F_{TU}(T_1)}{\sigma_1}$$

where  $F_{TU}(T_1)$  is the ultimate strength at operating temperature and  $\sigma_1$  is the operating stress in the element.

The critical stresses in the Graph-i-tite G-90 and wire-wound tungsten blocks were obtained assuming the Graph-i-tite G-90 under the tungsten ramp and the aft retention block were not segmented and all bonds released, i.e., had negligible shear stiffness. (A two-piece Graph-i-tite G-90 throat retention block does not produce significantly different stresses and the assumption of all bonds released results in more conservative results than actually expected with only some of the bonds being released with evaluated temperatures.) The resulting critical factors of safety are presented in table VIII.

The Graph-i-tite G-90 throat backup material experienced a critical hoop stress of 1,320 psi at 10 sec in finite element 63 to give a factor of safety of 1.97. The maximum axial stress gives a factor of safety of 4.40 at 6 sec in finite element 65 shown in figure 12.

The Graph-i-tite G-90 throat retention block experienced a maximum hoop stress of 900 psi at 10 sec in finite element 97 to give a factor of safety of 2.94. At 1 sec, a hoop stress of 1,170 psi was calculated giving a factor of safety of 2.22 but, for this case, all bonds were assumed to be intact. The critical axial stress of 2,340 psi at 10 sec in finite element 140 gives a factor of safety of 1.47.

The wire-wound tungsten throat experienced a maximum hoop stress of 1,164 psi in finite element 61 at 10 sec giving a factor of safety of 2.22 based on a plastic analysis. The factors of safety for the earlier times are lower than actually exists since they do not account for the plasticity of the wire-wound tungsten material. All axial stresses are compressive.

TABLE VIII  
FACTOR OF SAFETY SUMMARY

Part	Critical Stress	Time, sec			
		1	3	6	10
Wire-wound tungsten	Hoop stress	1.43*	1.57*	1.48*	2.22
	Axial stress	Compressive†	Compressive†	Compressive†	4.31 Compressive
Graph-i-tite G-90 throat backup	Hoop stress	2.71	2.37	2.30	1.97
	Axial stress	>10	9.0	4.40	4.49
Graph-i-tite G-90 throat retention	Hoop stress	1.67	2.05	2.07	2.94
	Axial stress	>10	8.3	4.17	1.47

\* Based on elastic analysis and not directly comparable to 10-sec result.

† Plastic redistribution analysis for wire-wound tungsten not performed.

The factors of safety reported are based exclusively on the comparison of maximum uniaxial stresses with design allowable uniaxial material strengths.

For orthotropic materials, stress components are compared to the appropriate directional strength. Temperature-degraded material strengths are used where applicable.

The throat insert ejection loads and hoop stress in the silica-phenolic were based on simplified hand calculations. These calculations and the resulting factors of safety are presented in appendix III. The factors of safety for the steel housings and throat retention system when operated at 3,600 psia MEOP, also are presented in appendix III.

### 3. INSTRUMENTATION

Special instrumentation was used to define the nozzle thermal environment and provide in-situ ablation measurements. This instrumentation consisted of two total heat flux sensors in the blast tubes for nozzles S/N 5 and 7 test firings. Figure 13 shows a schematic of the total heat flux sensors installed in a blast tube.

Basically, the total heat flux instrumentation consists of thermocouple instrumented ablative plugs fabricated of the same material as the candidate

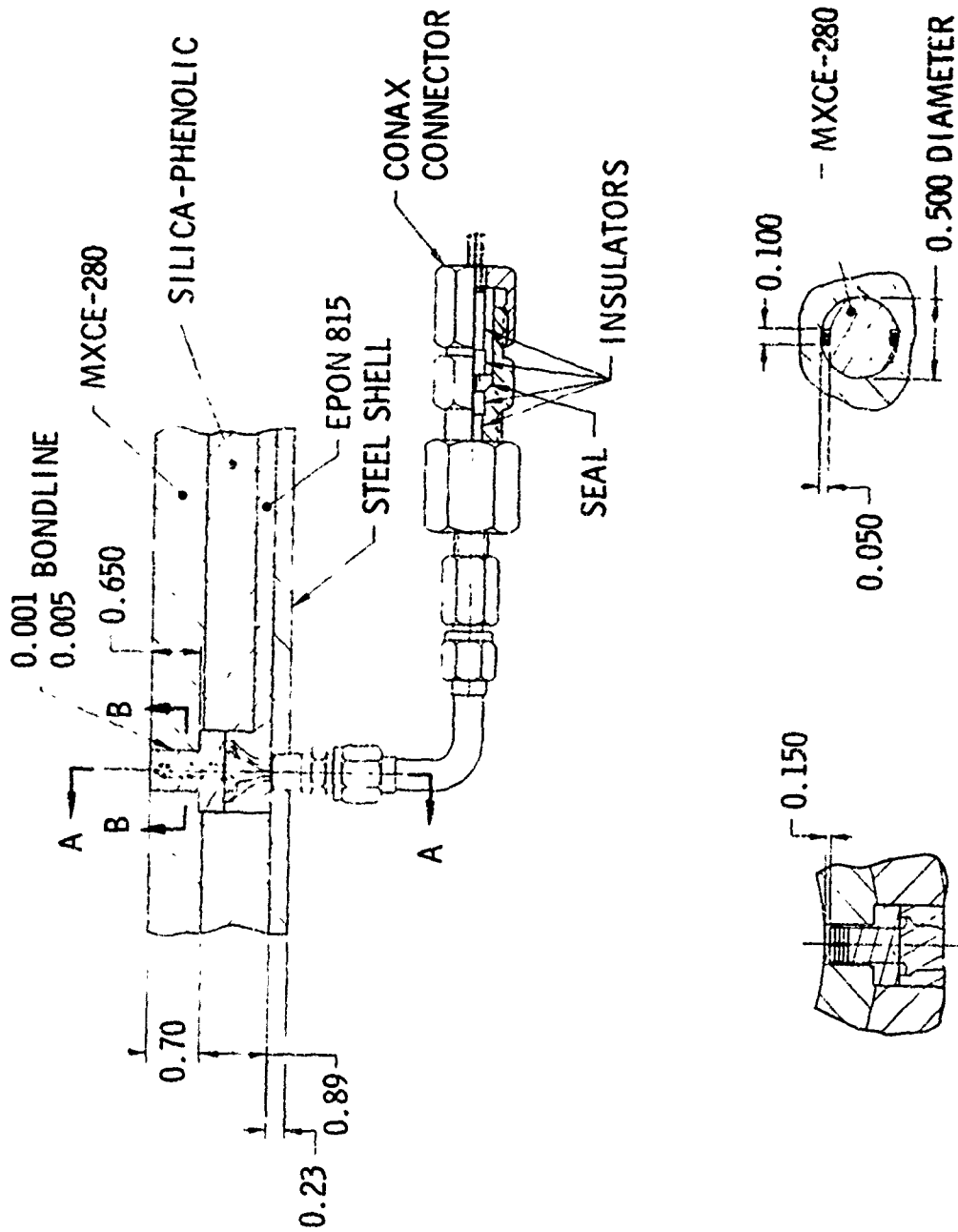


Figure 13. Instrumentation Design

component in which measurements are to be taken. The thermocouples are located at various depths which record the temperature profile as the surface and char layer recede. These measurements permit calculation of the total heat flux.

The heat flux sensor plugs were fabricated by Aerotherm using molded phenolic blocks of the MXCE-280 with the same fiber orientation as the component in which the instrumentation was installed. The plugs were rough-machined to approximate size, 0.010-in.-diameter holes were drilled, and the plug was final match-machined to the hole in the nozzle component to provide a maximum bondline of 0.005 in. Five  $W_5Re/W_{26}R_e$  thermocouples were installed.

Threaded ports were provided in the steel housings which allowed access to the thermocouple leadwires. Gas flow was sealed around the thermocouple leadwires by using pressure sealing Conax fittings.

#### 4. NOZZLE FABRICATION

All nozzle components were fabricated in the UTC engineering laboratories except for the steel hardware, aft closure insulators, carbon-carbon composite blast tubes of Pycobond and Pyrostrand, and the exit cone liner for nozzle S/N 16. All graphite components, except the carbon-carbon composites, were machined from bulk billet or washer stock. All Graph-i-tite G-90 was cored and reimpregnated to bring the billet density up to 1.90 g/cc or greater.

The plastic components were fabricated by molding or tapewrapping. Usually, the nozzle backup insulators and exit cone liners were tapewrapped parallel to centerline. The exit cone liner for nozzle S/N 16 was fabricated in two pieces by an outside vendor. The forward portion which covers the throat retention components was fabricated from a helical layup. Theoretically this would provide increased erosion resistance. The remainder of the exit cone was tapewrapped parallel to centerline. The aft closure insulators, forward entrance cap, and blast tube liners were molded from molding compound or flat laminates. The entrance cap and blast tube liners were molded into billets, and then cored and machined into the final contour. The fabrication method for each component and/or material is presented in table VI. The cured component density for each phenolic and elastomer is presented in table IX.

Fabrication and assembly procedures were basically the same as those described in reference 2. These procedures detail the fabrication process, provide for technician and quality control signoff, document the angular orientation of each component, detail the level of verification testing required, and document results i.e., tag end densities and tensile strengths. These procedures, along with materials certification, documentation of discrepancies, and a configuration summary, are included in a logbook for each test nozzle.

Detailed quality control was maintained throughout the fabrication and assembly cycle. All purchased raw materials or fabricated components, were accepted only after certification of conformance to applicable specifications or design drawings. The materials or components were stored in specific bonded areas until incorporation into the nozzle assembly. All phenolic and graphite components were inspected visually and by alcohol wipe after final machining. In addition, NDT was conducted on the graphitic components.

TABLE IX  
CANDIDATE PHENOLIC MATERIAL CURED DENSITY SUMMARY

Nozzle S/N	Aft Closure		Forward Ent...		Blast Tube		Exit Cone Liner		Throat Retaining Ring	
	Actual	Required	Actual	Required	Actual	Required	Actual	Required	Actual	Required
1	1.83	1.83	1.27	1.25	1.27	1.25	1.51	1.40	---	---
	1.278	1.26-1.28	---	---	1.55	1.55	---	---	---	---
	---	---	---	---	1.46	1.40	---	---	---	---
2	1.83	1.83	1.27	1.25	1.55	1.55	1.47	1.40	1.45	1.40
	1.278	1.26-1.28	---	---	1.27	1.25	---	---	---	---
3	1.83	1.83	1.27	1.25	1.27	1.25	1.47	1.40	1.45	1.40
	1.278	1.78	---	---	---	---	---	---	---	---
4	1.83	1.83	---	1.25	1.56	1.54	1.47	1.40	1.46	1.40
	1.83	1.83	---	---	1.74	1.78	1.77	1.68	---	---
	---	---	---	---	1.29	1.25	---	---	---	---
5	1.83	1.83	1.27	1.25	1.29	1.25	1.47	1.40	1.46	1.40
	1.276	1.26-1.28	---	---	1.47	1.40	---	---	---	---
	---	---	---	---	1.56	1.54	---	---	---	---
6	1.78	1.78	1.28	1.25	---	---	1.47	1.40	1.47	1.40
	1.84	1.83	---	---	---	---	---	---	---	---
7	1.276	1.26-1.28	1.29	1.25	1.29	1.25	1.47	1.40	1.47	1.40
	---	---	---	---	---	---	---	---	---	---
8	1.83	1.83	1.29	1.25	1.29	1.25	1.47	1.40	1.46	1.40
	1.83	1.83	---	---	---	---	---	---	---	---
9	1.83	1.83	1.29	1.25	1.29	1.25	1.76	1.68	1.47	1.40
	1.84	1.83	---	---	---	---	---	---	---	---
10	1.84	1.83	1.29	1.25	1.29	1.25	1.76	1.68	1.47	1.40
	1.276	1.26-1.28	1.46	1.40	1.29	1.25	1.72	1.68	1.50	1.40
11	1.84	1.83	1.47	1.40	1.29	1.25	1.45	1.40	1.46	1.40
	1.276	1.26-1.28	1.46	1.40	1.30	1.25	1.45	1.40	1.46	1.40
12	1.84	1.83	1.45	1.40	---	---	1.45	1.40	---	---
	1.276	1.26-1.28	1.49	1.40	1.30	1.25	1.44	1.40	1.46	1.40
13	1.84	1.83	1.43	1.40	1.30	1.25	1.46	1.40	1.42	1.40
	1.276	1.26-1.28	---	---	---	---	---	---	---	---
14	1.84	1.83	---	---	---	---	---	---	---	---
	1.276	1.26-1.28	---	---	---	---	---	---	---	---
15	1.84	1.83	---	---	---	---	---	---	---	---
	1.276	1.26-1.28	---	---	---	---	---	---	---	---
16	1.84	1.83	---	---	---	---	---	---	---	---
	1.276	1.26-1.28	---	---	---	---	---	---	---	---

TABLE IX

## CANDIDATE PHENOLIC MATERIAL CURED

Nozzle S/N	Aft Closure			Forward Entrance Cap			B
	Actual	Required	Material	Actual	Required	Material	R
1	1.83	1.83	Durez 16771-1	1.27	1.25	MXCE-280	1.27
	1.278	1.26-1.28	R155	---	---	---	1.55
	---	---	---	---	---	---	1.46
2	1.83	1.83	Durez 16771-1	1.27	1.25	MXCE-280	1.55
	1.278	1.26-1.28	R155	---	---	---	1.27
3	1.83	1.83	Durez 16771-1	1.27	1.25	MXCE-280	1.27
	1.278	1.78	MX2625	---	---	---	---
4	1.83	1.83	Durez 16771-1		1.25	MXCE-280	1.56
	1.83	1.83	Durez 16771-1A	---	---	---	1.74
	---	---	---	---	---	---	1.29
5	1.83	1.83	Durez 16771-1	1.27	1.25	MXCE-280	1.29
	---	1.26-1.28	R155	---	---	---	1.47
	1.276	---	---	---	---	---	1.56
6	1.78	1.78	MX2625	1.28	1.25	MXCE-280	---
	1.84	1.83	Durez 16771-1	---	---	---	---
7	1.276	1.26-1.28	R155	1.29	1.25	MXCE-280	1.29
8	1.83	1.83	Durez 1677-1	1.29	1.25	MXCE-280	1.29
	1.83	1.83	Durez 16771-1A	---	---	---	---
9	1.83	1.83	Durez 16771-1	1.29	1.25	MXCE-280	1.29
10	1.84	1.83	Durez 16771-1	1.29	1.25	MXCE-280	1.29
11	1.276	1.26-1.28	R155	1.46	1.40	MX4926	1.29
12	1.84	1.83	Durez 16771-1	1.47	1.40	MX4926	1.29
13	1.276	1.26-1.28	R155	1.46	1.40	MX4926	1.30
14	1.84	1.83	Durez 16771-1	1.45	1.40	MX4926	---
15	1.276	1.26-1.28	R155	1.49	1.40	MX4926	1.30
16	1.84	1.83	Durez 16771-1	1.43	1.40	MX4926	1.30

TABLE IX

## MATERIAL CURED DENSITY SUMMARY

Blast Tube			Exit Cone Liner			Throat Retaining Ring		
Actual	Required	Material	Actual	Required	Material	Actual	Required	Material
1.27	1.25	MXCE-280	1.51	1.40	FM5055	---	---	---
1.55	1.55	MXSC-195	---	---	---	---	---	---
1.46	1.40	MX4926	---	---	---	---	---	---
1.55	1.55	MXSC-195	1.47	1.40	FM5055	1.45	1.40	MX4926
1.27	1.25	MXCE-280	---	---	---	---	---	---
1.27	1.25	MXCE-280	1.47	1.40	FM5055	1.45	1.40	MX4926
---	---	---	---	---	---	---	---	---
1.56	1.54	MXSE-280	1.47	1.40	FM5055	1.46	1.40	MX4926
1.74	1.78	MX2625	1.77	1.68	MX2600	---	---	---
1.29	1.25	MXCE-280	---	---	---	---	---	---
1.29	1.25	MXCE-280	1.47	1.40	FM5055	1.46	1.40	MX4926
1.47	1.40	MX4926	---	---	---	---	---	---
1.56	1.54	MXSE-280	---	---	---	---	---	---
---	---	---	1.47	1.40	FM5055	1.47	1.40	MX4926
---	---	---	---	---	---	---	---	---
1.29	1.25	MXCE-280	1.47	1.40	FM5055	1.47	1.40	MX4926
1.29	1.25	MXCE-280	1.47	1.40	FM5055	1.46	1.40	MX4926
---	---	---	---	---	---	---	---	---
1.29	1.25	MXCE-280	1.76	1.68	MX2600	1.47	1.40	MX4926
1.29	1.25	MXCE-280	1.76	1.68	MX2600	1.47	1.40	MX4926
1.29	1.25	MXCE-280	1.72	1.68	MX2600	1.50	1.40	MX4926
1.29	1.25	MXCE-280	1.45	1.40	MX4926	1.46	1.40	MX4926
1.30	1.25	MXCE-280	1.45	1.40	FM5055	1.46	1.40	MX4926
---	---	---	1.45	1.40	FM5055	---	1.40	MX4926
1.30	1.25	MXCE-280	1.44	1.40	FM5055	1.46	1.40	MX4926
1.30	1.25	MXCE-280	1.46	1.40	FM5055	1.42	1.40	MX4926

Prior to bonding the insulators into the steel housings, the nozzle shell was mated to the aft closure and TDC was identified. The ablative components were oriented as specified in the material test matrix, table V. The bondlines were staggered between adjacent components to avoid a direct axial path for grooving in the bondline.

All bonding of components into the steel shell was done under pressure using UTC-fabricated bonding fixtures.

Only one material, the hybrid carbon-silica phenolic (MXSC-195) for the blast tube, was difficult to fabricate. However, production of this material supposedly has ceased and the advantages of the material in this application were essentially nil.

The components were segmented using the same techniques as defined in reference 2; namely, use of EA913 adhesive with simple butt joints having a thin bondline of 0.002 to 0.007 in. As shown during the previous contract, this technique allows evaluation of multiple materials for each firing by segmenting each component in axial or circumferential directions. No gouging was experienced which could be related to the bondlines.

## 5. NONDESTRUCTIVE TESTING

The purpose of NDT was to document and characterize defects to establish acceptance or rejection of components. It was planned to establish an initial assessment of the accept/reject criteria based on the correlation of test firing results with NDT evaluations. Because all components were essentially void-free, this anticipated goal was not attained.

NDT was included to document and characterize flaws or anomalies in the polycrystalline graphite aft entrance cap, pyrolytic graphite throat washers, and polycrystalline graphite Graph-i-tite G-90 throat retention blocks. These components were evaluated using radiography and ultrasonic velocity mapping in the as-received billet or doughnut form prior to machining. Radiography was used to detect voids, delaminations, cracks, and indications of low density. This technique satisfactorily indicates defects of 80 $\mu$ in. or wider in materials such as pyrolytic graphite plate. Ultrasonic velocity mapping was used to detect density variations by traversing the entire surface of the billets.

Because of the inherent nature of polycrystalline graphites, multiple small voids and inclusions are present even in high quality aerospace grade material. Minute density variations are also present in polycrystalline graphites as well as in pyrolytic graphite plate; therefore, limits were established for the size above which these anomalies should be documented. For polycrystalline graphites, voids or inclusion over 0.040 in. in any dimension were to be reported. For pyrolytic graphite, any delamination, void, inclusion, etc., and material crack or striation was to be documented. Density variations in excess of  $\pm 5\%$  of the average velocity measurement for the component were to be reported.

The three wire-wound tungsten throat inserts were evaluated using single-wall radiography and eddy current. Radiography was used for subsurface crack or

any other anomalous area detection. Since wire-wound tungsten inherently contains numerous minute voids in the plasma matrix (especially around the wires), no attempt was made to document these areas; only those voids in excess of 0.040 in. were documented. The eddy current technique shows the most potential for surface crack detection in wire-wound tungsten. This technique has been successfully used at UTC on previous wire-wound tungsten inserts.

In addition, alcohol wipe, dimensional, and visual inspections were performed on all nozzle components.

The NDT results showed that no defects were present in any of the graphite or tungsten nozzle components used. The only components which were rejected and not fired were those where major discrepancies such as delaminations, cracks, or low density areas obviously would sacrifice test nozzle reliability. The number of rejected components was extremely low, signifying that the quality control level during material formulation and component fabrication was good. The only instance for rejection of graphitic components was on one lot of pyrolytic graphite washers where six of 20 washers were severely delaminated. These components were rejected and replaced. All the polycrystalline graphite and wire-wound tungsten inserts were free of defects. All density variations of the graphitic materials were well within the  $\pm 5\%$  goal and usually fell within  $\pm 2\%$ .

## SECTION VII

### PHASE III - ROCKET MOTOR TESTING

The lightweight nozzle and aft closure assemblies were tested at high chamber pressure using the UTC HIPPO test motor located at AFRPL. Propellant grains, associated motor hardware, and test liaison personnel were furnished by UTC. AFRPL furnished all test tooling and stands, basic recording instrumentation, test personnel, photographic coverage, and data acquisition and reduction. The test motors were fired in a vertical position (nozzle up) on pads 1 and 2 of the AFRPL solid rocket test area. A total of 16 nozzle tests were conducted (table I). The specific nozzle and aft closure materials evaluated are shown in table V.

Thermocouples in the total heat flux sensors were recorded on standard AFRPL digital instrumentation.

The test motor assembly is shown in figure 8 of reference 2. A complete description of this test motor is included in reference 2. The test motor was instrumented with two 5,000-psi Taber pressure transducers. Axial thrust measurements were obtained using the AFRPL six-component stand; only axial thrust was recorded. The stand uses three Baldwin-Lima load cells rated at 10,000 lb each. The three load cell outputs are added together for the total thrust.

#### 1. PROCESSING OF PROPELLANT CARTRIDGES

The test motor contained cartridge loaded propellant grains. The two propellants used were 88% solids loaded CTPB systems having 18% and 5% aluminum content (UTP-11,475 and UTP-13,615). Three cylindrical and two keyhole port propellant grain configurations were used. The 5% aluminum cylindrical configuration had a port radius of 7.75 in., a web radius ratio of 1.6, and produced an average pressure of 2,800 psi. The 18% aluminum configuration had a port radius of 8.3 in., a web radius of 1.5, and produced an average pressure of 2,800 psi.

The average 3,200-psi configuration had a port radius of 8.3 in., which provides a web radius ratio of 1.5. The aft face and cylindrical bore was allowed to burn whereas the forward face was restricted. A summary of the overall dimensions and propellant weight for each propellant grain is presented in table X.

Two keyhole propellant grains using 5% and 18% aluminum content (UTP-13,615 and UTP-11,475) were tested. A typical keyhole port configuration is shown in figure 14. To evaluate the effects of the impingement of the high velocity combustion gases from the keyhole slot on the aft closure and nozzle materials, the grain aft face was configured to cantilever into the aft closure and to match the insulation contour. The grain aft face, which was restricted, was trimmed to the slot configuration to allow impingement on the candidate materials. The forward face of the grain was also restricted which allowed the grain to burn

**TABLE X**  
**PROPELLANT CARTRIDGE SUMMARY**

Tested with nozzle S/N	Configuration	Propellant weight, lb	Bore diameter, in.	Grain length, in.
01	Cylindrical	505	16.6	28.5
02	Cylindrical	505	16.6	28.5
03	Cylindrical	505	16.6	28.5
04	Cylindrical	443	15.5	23.75
05	Cylindrical	443	15.5	23.75
06	Cylindrical	443	15.5	23.75
07	Keyhole	435	3.2	35.1*
08	Cylindrical	505	16.6	28.5
09	Cylindrical	443	15.5	23.75
10	Cylindrical	443	15.5	23.75
11	Cylindrical	443	15.5	23.75
12	Keyhole	435	3.2	35.1*
13	Keyhole	508	3.2	35.1*
14	Cylindrical	529	16.6	29.94
15	Cylindrical	529	16.6	29.94
16	Cylindrical	529	16.6	29.94

\* Measured at bore diameter.

only in the keyhole port and slot. The keyhole slot extended to the cartridge wall. This configuration inherently possesses high stress/strain concentration factors at the slot tip. To reduce these loads to acceptable limits and prevent grain cracking or debonding, a flexible foot was fabricated from AL 60-9 potting compound. The foot is flexible and allows a large strain to be developed at the base of the slot without failure. The design and analysis of this flexible foot is presented in reference 2.

The grains were cast into both new and refurbished propellant cartridges. The Government-furnished propellant cartridges were refurbished by sandblasting the cartridge, bonding a layer of 0.080- to 0.100-in.-thick rubber insulation onto the existing cartridge insulation and replacing the forward end restrictor. The silica-loaded Buna-N rubber forward insulator was replaced with a 0.4-in.-thick air cast layer of AL 60 liner compound.

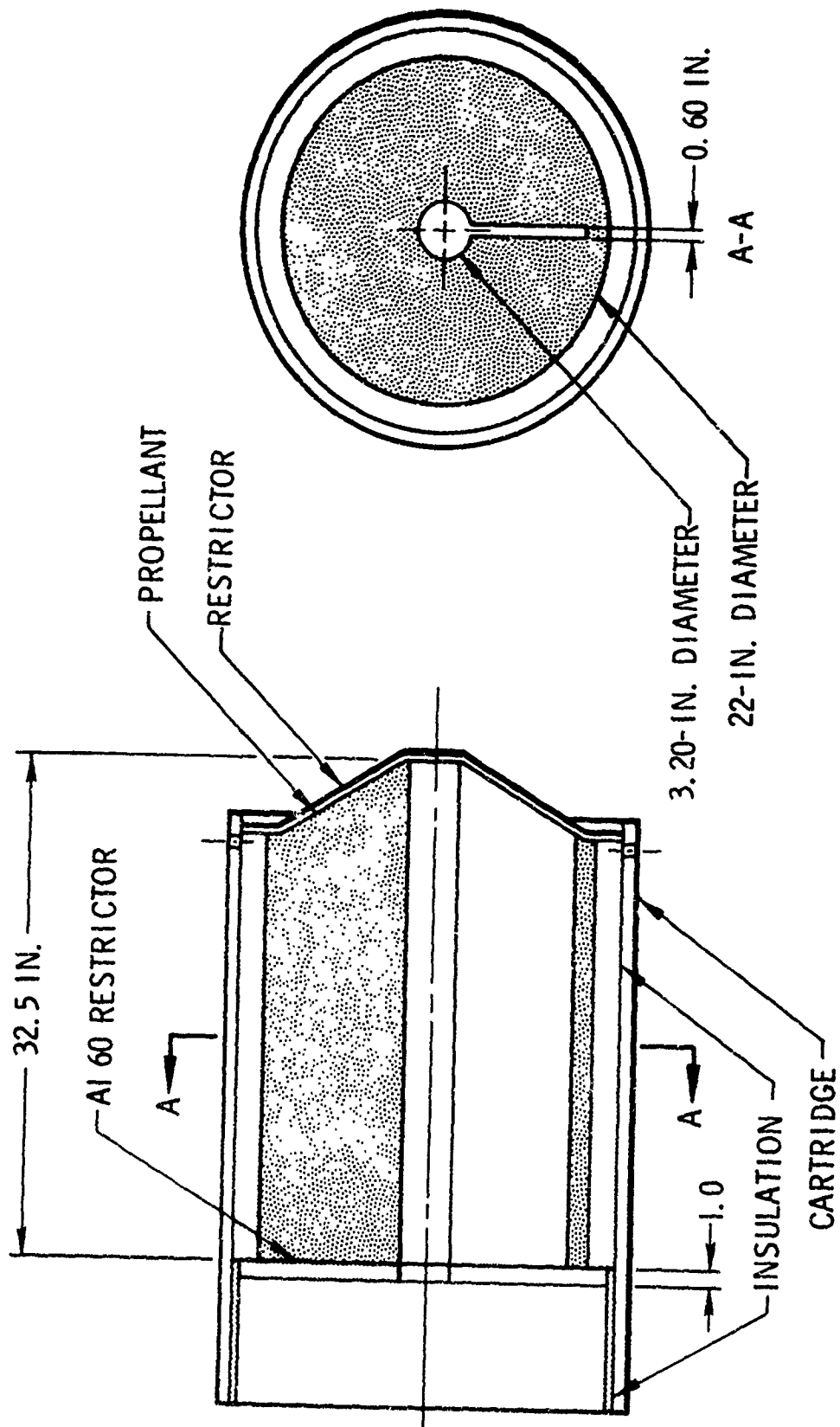


Figure 14. Keyhole Port Grain Design

The propellant was bayonet cast at ambient conditions and cured at either 140°F for 7 days or 160°F for 5 days. The casting mandrels were disposable cardboard Sonotubes for the cylindrical port and a reusable aluminum mandrel for the keyhole grain configuration.

## 2. TEST DESCRIPTION

### a. Nozzle S/N 01

The motor ignited and operated normally for approximately 5 sec. At that time, the chamber pressure dropped indicating loss of part of the throat. The test continued for approximately 3 sec at which time the pressure decreased further, indicating loss of the remaining throat insert. The remainder of the test firing was at a lower pressure corresponding to that predicted using the aft entrance cap as the throat restriction. The pressure-time trace is shown in figure 15. Postfire examination of the hardware shows that the pyrolytic graphite throat washers were missing. The aft entrance cap, the ATJ-graphite heat sink, and part of the carbon-phenolic retaining ring, which was severely eroded, were still in the nozzle. It appears that the throat retention system was inadequate even though the analysis showed positive margins of safety. Subsequent test firing results showed the CTPB propellant was considerably more severe on the throat retention system than originally anticipated, not necessarily in average erosion depth but in gouging and unevenness. Based on these

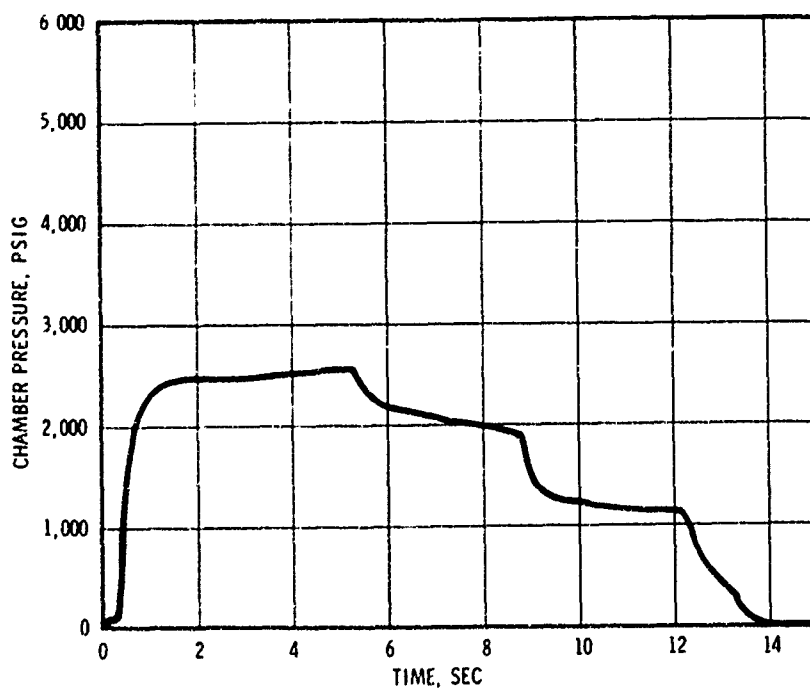


Figure 15. Pressure-Time Trace, Nozzle S/N 01

results, it appears the structural integrity of the carbon-phenolic ring was degraded due to gouging and high ablation. The pyrolytic graphite washers require an even and uniform axial support, which was not provided by the degraded ring.

b. Nozzle S/N 02

This test was the same as the test for nozzle S/N 01 which used the throat retention system verified under contract No. FO4611-69-C-0065 (reference 2). The test was conducted at a maximum chamber pressure of 2,800 psia with a web burning time of 10.8 sec (figure 16). Axial thrust is shown in figure 17. Visual observations indicated that the motor ignited, operated normally for 5.5 sec, and then chamber pressure decreased linearly to the end of the test. Posttest examination revealed that the pyrolytic graphite throat had ablated higher than predicted, and the Graph-i-tite G-90 retention ring had eroded unevenly and at a higher rate than predicted. The remaining nozzle components and aft closure were in good condition.

c. Nozzle S/N 03

This was the first test which used a blast tube with a contraction ratio of 1.3 and contained a segmented Graph-i-tite G-90 liner for the last half of the blast tube length. The test was conducted at a maximum chamber pressure of 2,700 psia with a web burning time of 12.0 sec (figure 18). Visual observations indicated that the motor ignited and operated the same as for nozzle S/N 02 but at a lower chamber pressure. Posttest examination revealed that the pyrolytic graphite throat ablation again was significantly higher than the predicted value of approximately 3 mil/sec. One of the Graph-i-tite G-90 rings in the blast tube was cracked; however, the remaining material in the nozzle except for the Graph-i-tite G-90 retaining ring eroded evenly, except for some gouging in the cracked area. The erosion pattern of the downstream Graph-i-tite G-90 throat retaining ring was similar to that experienced in nozzle S/N 02, except the erosion was greater for nozzle S/N 03.

d. Nozzle S/N 04

This was the first test using the 5% aluminized propellant grain. The test was conducted at a maximum chamber pressure of 2,850 psia with a web burning time of 11.0 sec (figure 19). The axial thrust is shown in figure 20. Visual observations indicated that the motor ignited and operated normally. Ablation of the pyrolytic graphite throat washers again was significantly higher than the predicted 1 mil/sec. The remainder of the nozzle appeared to perform as anticipated based on the previous two firings. The forward entrance cap was more severely eroded resulting in rounding off the leading edge of the blast tube. The surface of the entrance cap was also considerably more uneven, indicating severe chemical attack. Some localized heating was encountered on the nozzle shell to aft closure O-ring sealing area due to the direct line of sight path and wider (~0.040 in.) assembly gap.

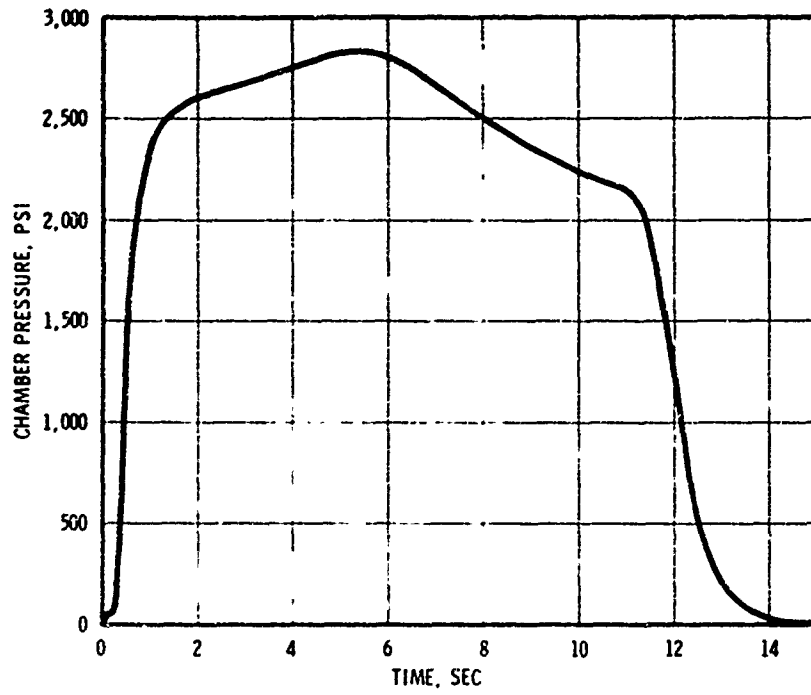


Figure 16. Pressure-Time Trace, Nozzle S/N 02

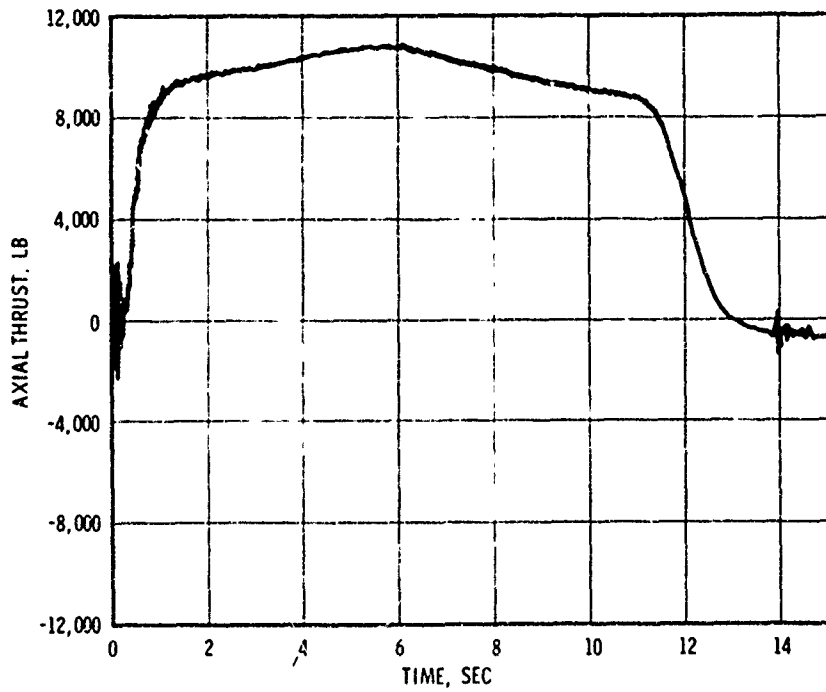


Figure 17. Axial Thrust-Time History, Nozzle S/N 02

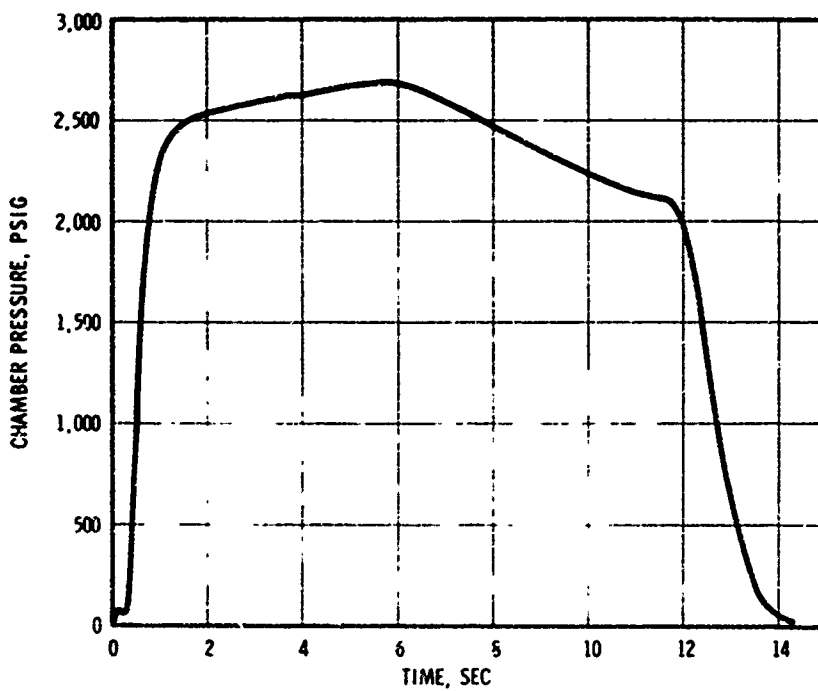


Figure 18. Pressure-Time Trace, Nozzle S/N 03

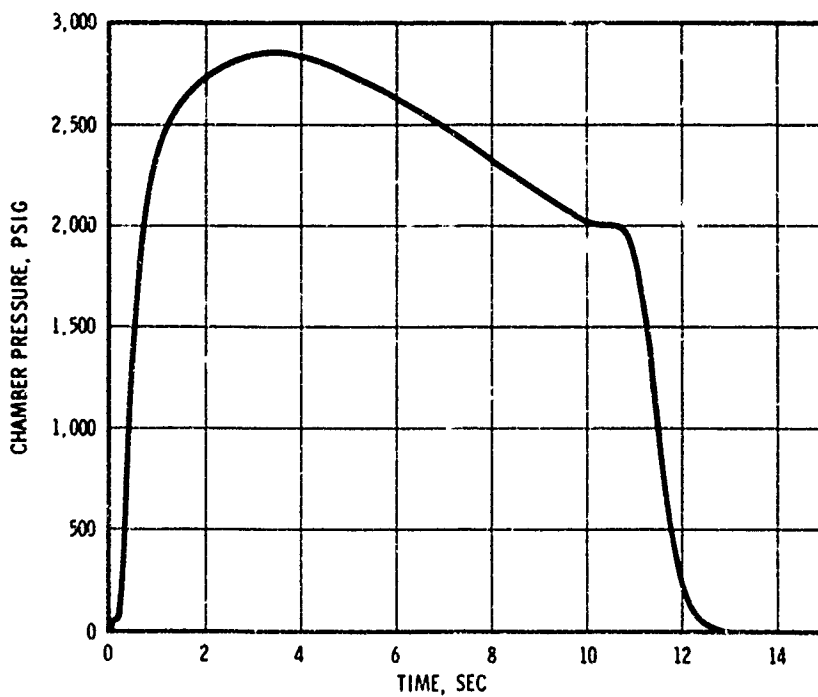


Figure 19. Pressure-Time Trace, Nozzle S/N 04

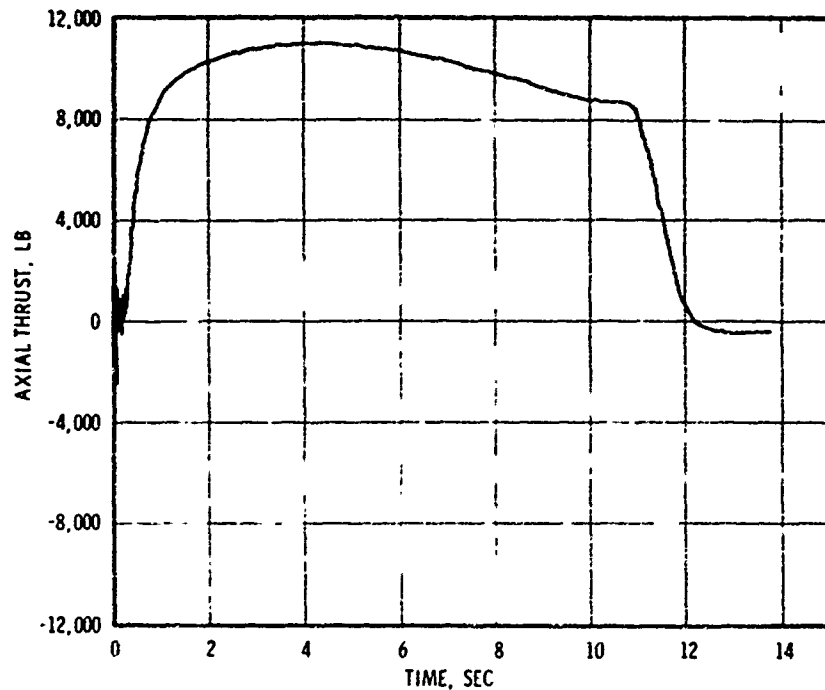


Figure 20. Axial Thrust-Time History, Nozzle S/N 04

e. Nozzle S/N 05

This test was conducted at a maximum chamber pressure of 3,025 psia with web burning time of 10.5 sec (figure 21). Visual observations indicated that the motor ignited and operated the same as for nozzle S/N 04. Data were obtained from seven of the eight thermocouples used on the test. Ablation rates of the blast tube materials in the forward portion were higher than expected due to local gouging in the MXCE-280 entrance cap. The gouging was increased due to insufficient clearance (0.006 in.) in the assembly gap between the blast tube liner and the forward entrance cap. During the firing, the blast tube liner and the forward entrance cap expanded and closed the assembly gap, exerting a compressive load on the parts. The stress was enough to crack the forward entrance cap resulting in gouging in two locations. The assembly gap was changed from 0.006 in. to 0.020 to 0.030 in. for all future assemblies. The gouging resulted in extremely uneven erosion in the blast tube.

f. Nozzle S/N 06

This nozzle was the initial unit to use a Pycobond blast tube. The motor ignited smoothly and reached a maximum pressure of 2,900 psia. The pressure began to decay, indicating high throat erosion. The throat was ejected at approximately 7.5 sec. The pressure-time trace is shown in figure 22. Posttest inspection showed that the throat insert was missing, and the Graph-i-tite G-90 aft entrance cap was sheared on a plane coincident

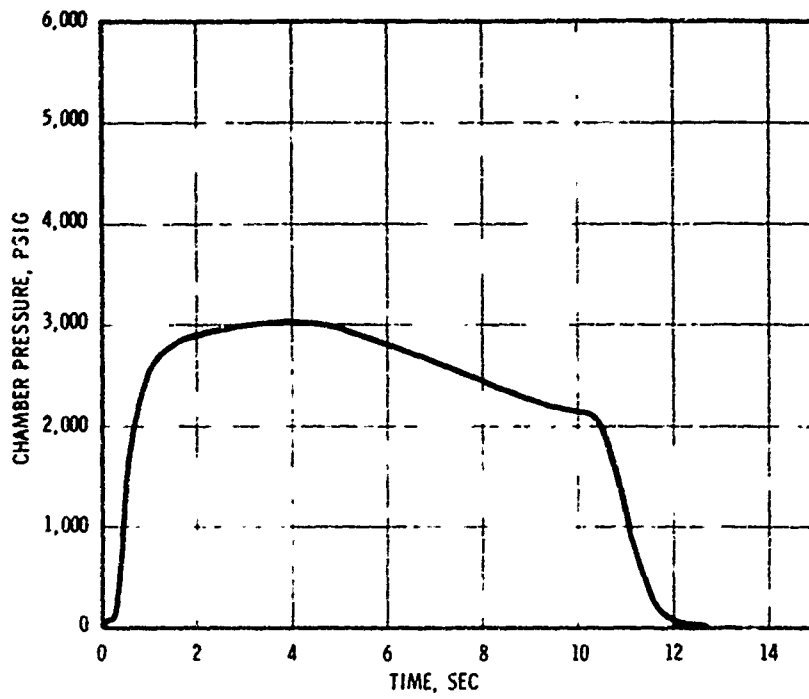


Figure 21. Pressure-Time Trace, Nozzle S/N 05

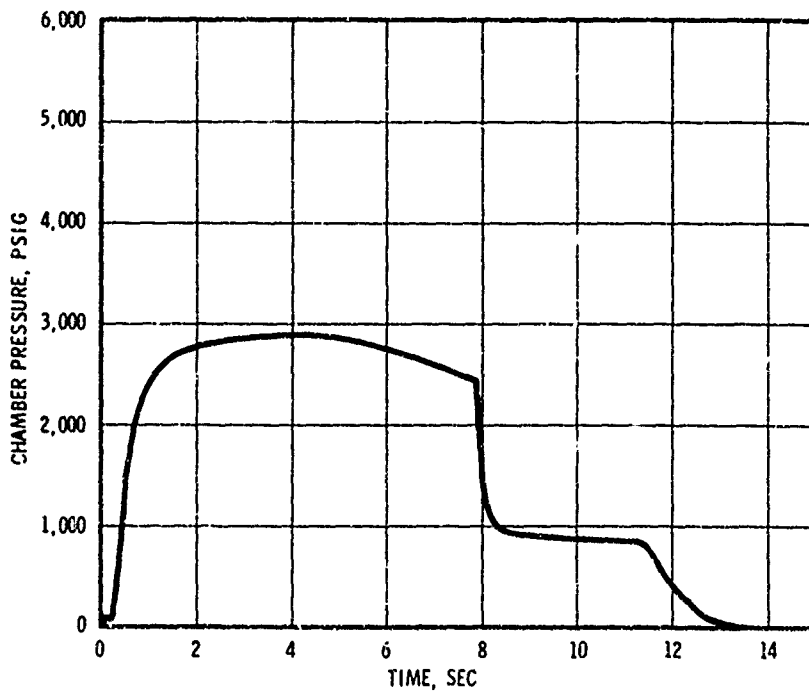


Figure 22. Pressure-Time Trace, Nozzle S/N 06

with the interface between the Pycobond blast tube and backup silica-phenolic insulator. The Pycobond blast tube liner had expanded considerably more than anticipated. New expansion data from Supertemp Corp. showed that the thermal expansion data at elevated temperatures were five times greater than originally provided.

g. Nozzle S/N 07

This test was the first 5% aluminized propellant firing with a keyhole port grain configuration. Upon ignition, the nozzle was engulfed in flames, indicating the loss of a pressure seal. The nozzle and blast tube liner were ejected at approximately 7.5 sec. The pressure-time trace is shown in figure 23. Improper bonding of the thermocouple plugs with EPON 915 allowed hot gases to flow around the thermocouple plugs. The Conax fittings also failed to seal, thereby allowing hot gases to vent through the steel shell causing the failure. This was documented from the high speed motion pictures. The inner aft closure was completely destroyed, and the heavy-weight aft closure was severely eroded on the inner diameter. The keyhole propellant grain performed as predicted and could not be linked to the failure.

h. Nozzle S/N 08

This test was conducted at a maximum chamber pressure of 2,800 psia with a web burning time of 10.8 sec (figure 24). The nozzle used a throat package of all pyrolytic graphite washers from Supertemp except for the second from the aft end which was from Pyrogenics. This change was made to determine if the high erosion rates that had been previously experienced on the pyrolytic graphite washers were a function of the material manufacturer. Visual observations indicated that the motor ignited and operated normally for the complete test. Postfire examination showed the hardware to be in excellent condition. Local gouging of the forward entrance cap was the only anomaly. The erosion rate of the Supertemp and pyrogenic throat material was essentially the same.

i. Nozzle S/N 09

This test was conducted at a maximum chamber pressure of 2,800 psia with a web burning time of 10.3 sec (figure 25). Visual and postfire observation indicated the test was completely successful without any localized gouging or uneven ablation. This throat insert also contained pyrolytic graphite washers from Supertemp.

j. Nozzle S/N 10

This test was conducted at a maximum chamber pressure of 2,825 psia. The pressure-time trace is shown in figure 26. Visual observations indicated that the motor ignited and operated normally for the first 5 sec, then decreased linearly until approximately 9.5 sec. The throat was ejected at that time. Postfire examination revealed:

- A. The forward section (MXCE-280) of the blast tube was intact, although it was eroded to the silica-phenolic at one location

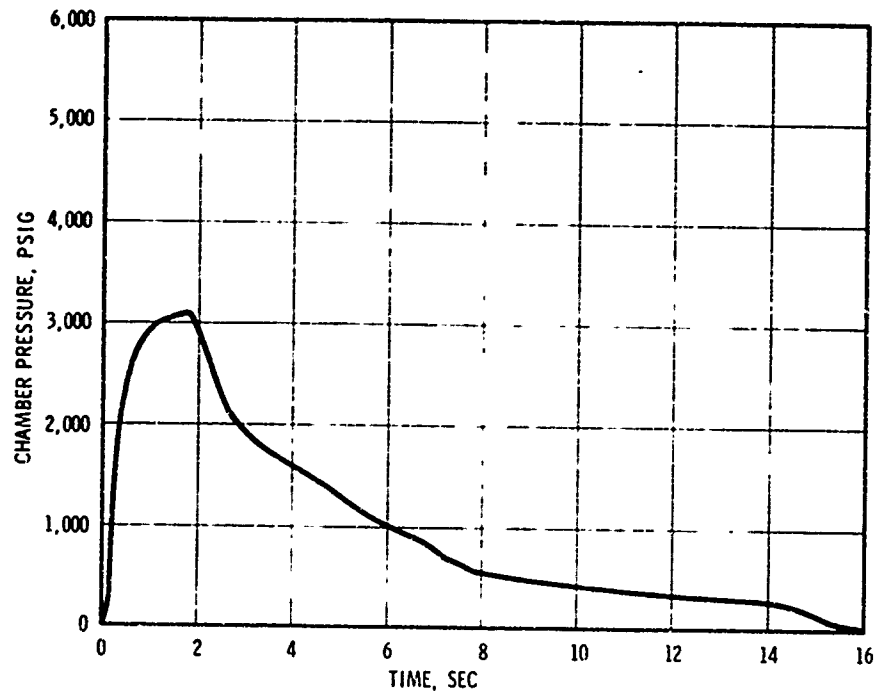


Figure 23. Pressure-Time Trace, Nozzle S/N 07

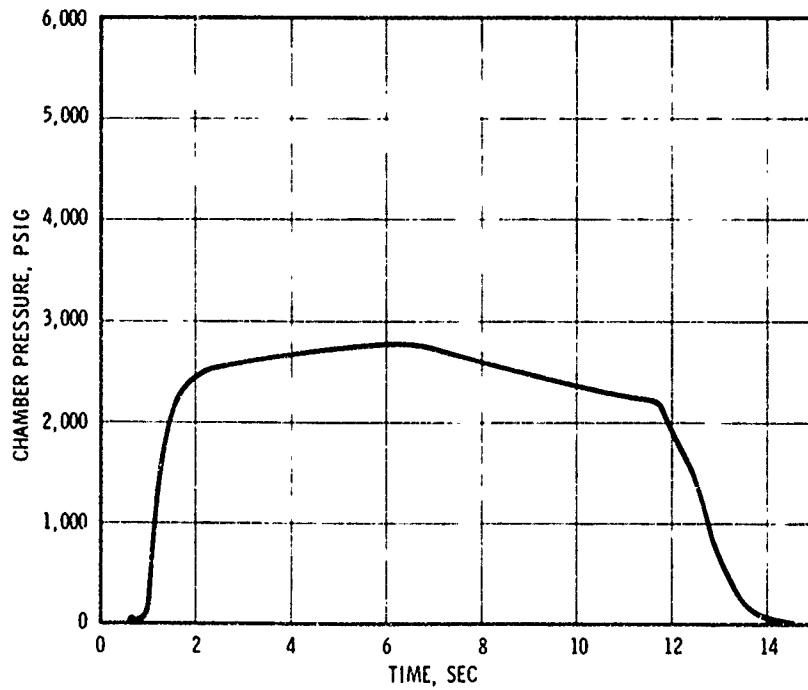


Figure 24. Pressure-Time Trace, Nozzle S/N 08

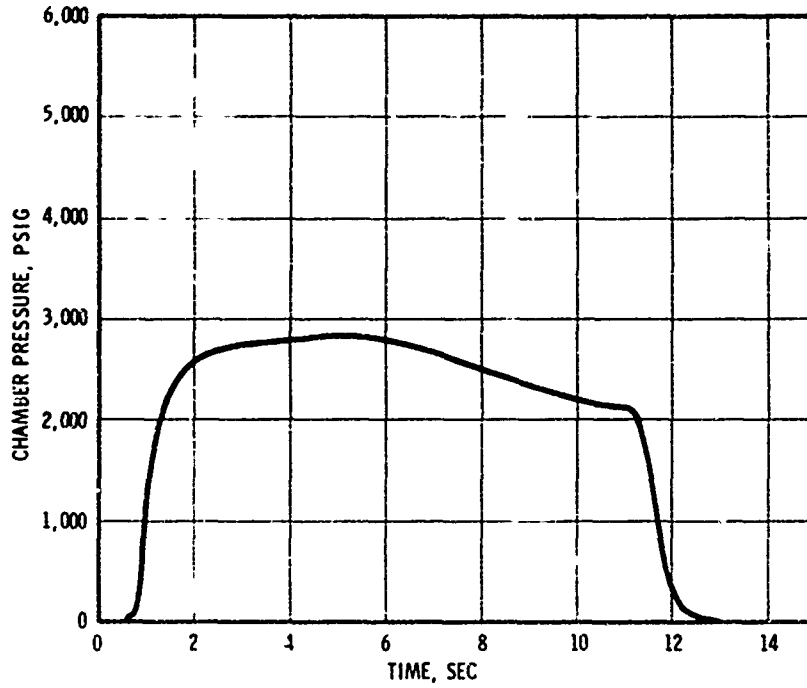


Figure 25. Pressure-Time Trace, Nozzle S/N 09

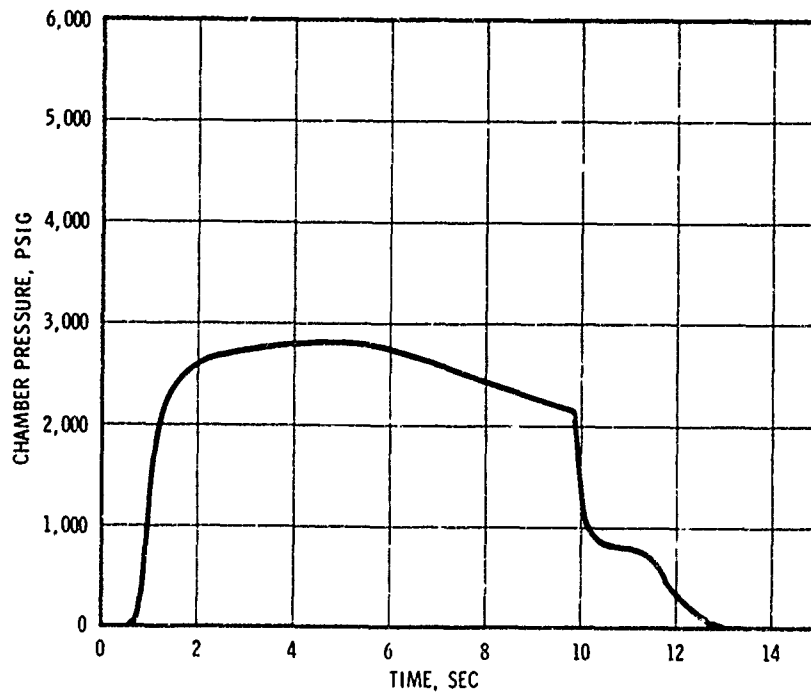


Figure 26. Pressure-Time Trace, Nozzle S/N 10

- B. The last half of the blast tube liner (Pycobond) was missing, along with the entire throat package, including the Graph-i-tite G-90 aft entrance cap which usually remains when the nozzle is ejected
- C. The entrance cap was severely gouged with some localized flow in the interface gap to the blast tube
- D. The leading edge of the exit cone was eroded evenly without any gouging. The exit cone appeared to be sheared at the radius of the retention ring indicating the throat failed by overload and not by thermal degradation of the retention system
- E. It appeared the reason for the throat ejection was due to the structural failure and breakup of the carbon-carbon composite blast tubes. Previous testing at these high pressure levels has shown that momentary blockage of the throat or any significant overload results in ejection of the throat insert.

k. Nozzle S/N 11

This test was conducted at a maximum chamber pressure of 2,725 psia, and the pressure-time trace is shown in figure 27. Visual observations indicated that the motor ignited and operated normally for the first 5 sec and then linearly decreased to approximately 8.5 sec at which time the throat was ejected. Postfire examination revealed:

- A. The forward section (MXCE-280) of the blast tube was intact and in good condition.
- B. The Pyrostrand was missing along with the throat package.
- C. Graph-i-tite G-90 cover washer to the Pyrostrand blast tube remained in the nozzle.
- D. Graph-i-tite G-90 aft entrance cap remained in the nozzle.
- E. The forward entrance cap was in good condition without any gouging. This was the first test where a flat laminate molding of MX4926 was used.
- F. The leading edge of the exit cone was eroded evenly without any gouging and sheared at the radius of the retention ring, indicating the throat failed by overload and not by thermal degradations of the retention system.

The failure of nozzles S/N 10 and 11 were similar. In both cases the carbon-carbon composite blast tube appeared to fail structurally resulting in throat blockage and ejection.

l. Nozzle S/N 12

This test used a 5% aluminum propellant with a keyhole port grain. The test was conducted at a maximum chamber pressure of 3,200 psia with a web burning time of 6.9 (figure 28). Visual observations indicated the motor

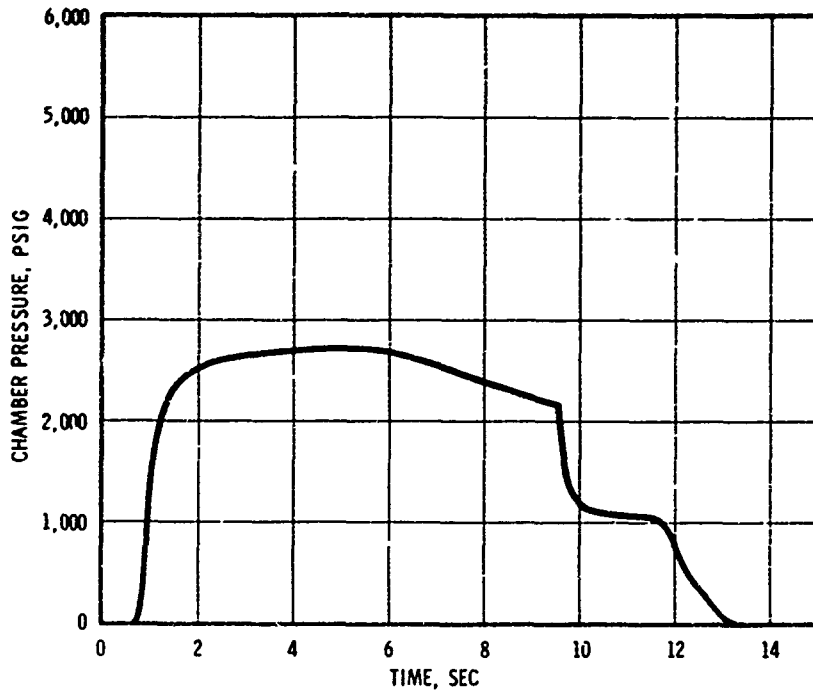


Figure 27. Pressure-Time Trace, Nozzle S/N 11

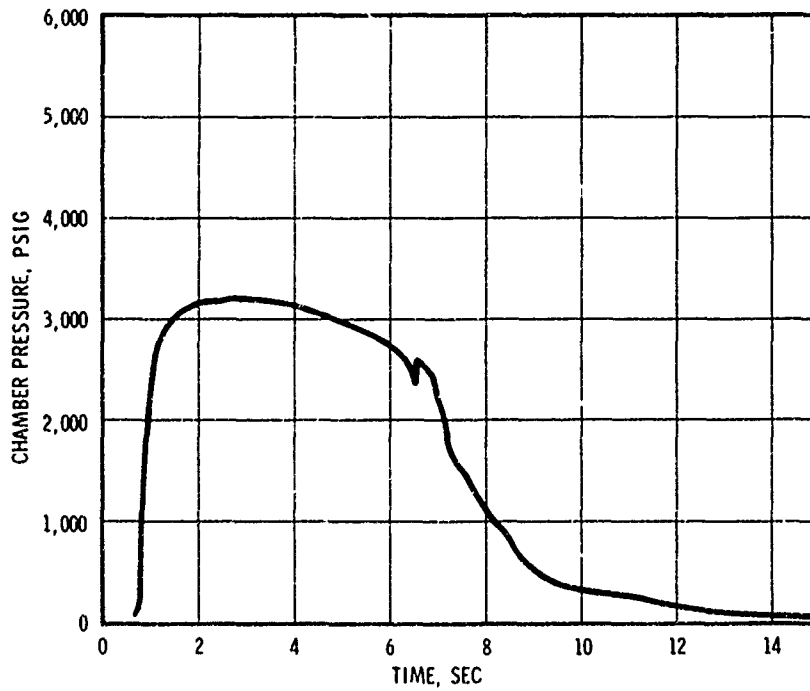


Figure 28. Pressure-Time Trace, Nozzle S/N 12

ignited and operated normally. There was an unexplained anomaly in the pressure trace at 7 sec. Postfire examination showed that the nozzle hardware was in excellent condition. No localized gouging was experienced on the MX4926 entrance cap. There was less erosion diametrically opposite the keyhole slot location than around the remainder of the circumference.

m. Nozzle S/N 13

This was the only 18% aluminized keyhole port grain configuration fired during this contract. A maximum pressure spike of 3,650 psia was encountered upon ignition, as shown in figure 29. This pressure spike is attributed to the plastic foam used to form a radial slot which is left in the grain. Since this firing, other configurations have been tested with this foam, resulting in high initial pressure spikes. The pressure immediately decayed to under 3,000 psia and regressed throughout the test firing. The web duration was 11.5 sec. Postfire inspection showed that the nozzle hardware was in excellent condition. No localized gouging in the entrance cap or blast tube was encountered. As experienced with the previous keyhole port test (nozzle S/N 12), less erosion was encountered diametrically opposite the keyhole slot than elsewhere on the inner circumference of the blast tube.

n. Nozzle S/N 14

This was the first test with the wire-wound tungsten throat insert. The test was conducted at a maximum pressure of 3,400 psia at a web burning time of 10.6 sec (figure 30). Visual observations indicated the motor ignited and operated normally. The sectioned nozzle is shown in figure 31. Postfire inspection revealed:

- A. The Graph-i-tite G-90 and pyrolytic graphite ring in front of the throat was in good condition.
- B. The tungsten throat inside diameter had decreased slightly and was in excellent condition without any signs of melting or surface defects. This small reduction in throat diameter is typical of previous firings where the tungsten insert is retained by a ramped interface with the backup material.
- C. The Graph-i-tite G-90 immediately downstream of the tungsten was eroded badly.
- D. The exit cone liner eroded to the steel retaining ring as a result of the high erosion of the Graph-i-tite G-90.
- E. The O-ring sealing area of the nozzle to aft closure interface was damaged locally; however, no gouging at the entrance cap was encountered.

o. Nozzle S/N 15

This was a repeat of the test for nozzle S/N 14 where two pyrolytic graphite washers were installed downstream of the tungsten throat insert in an attempt to reduce the localized gouging. This nozzle also incorporated

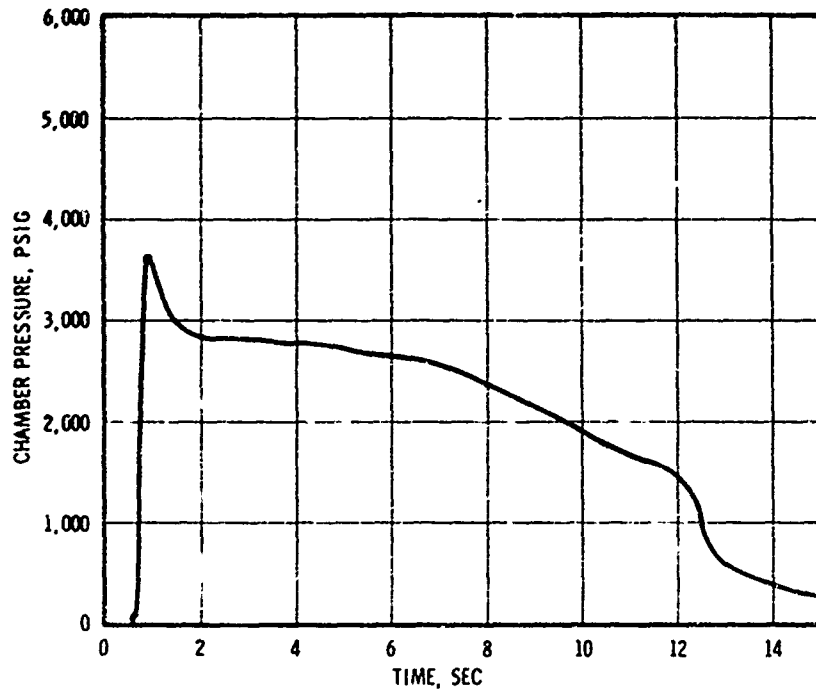


Figure 29. Pressure-Time Trace, Nozzle S/N 13

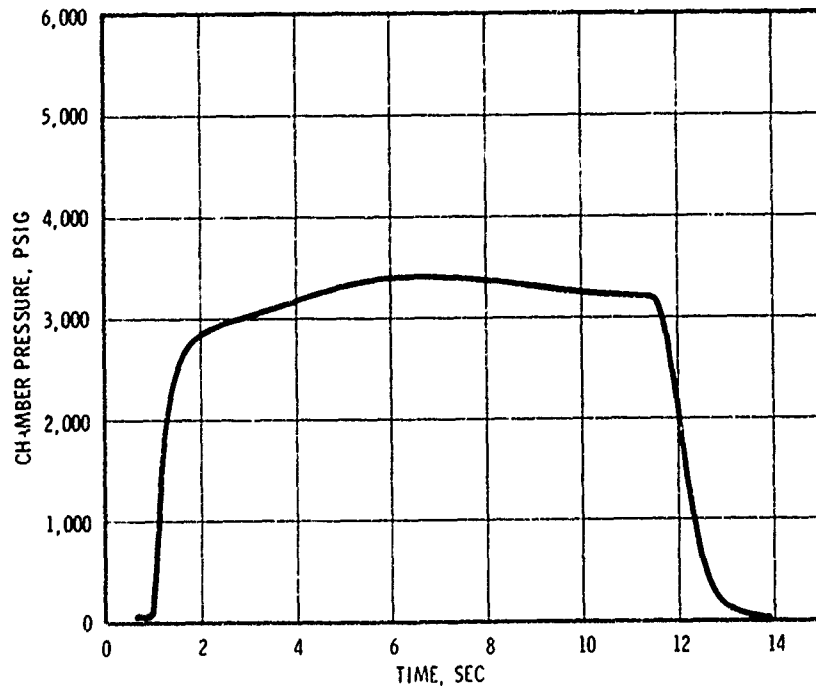


Figure 30. Pressure-Time Trace, Nozzle S/N 14

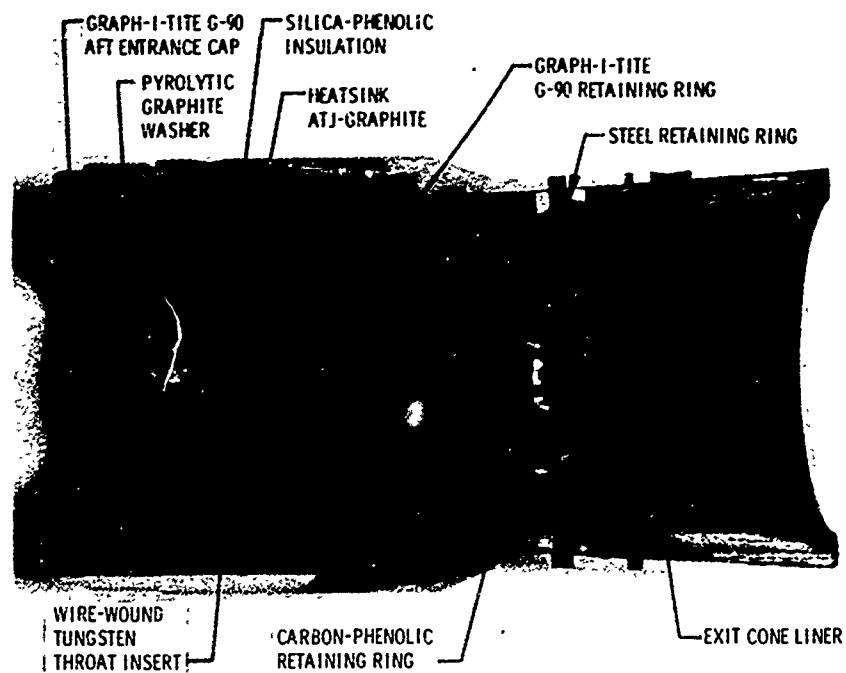


Figure 31. Cross Section View of Test-Fired Nozzle S/N 14

a 1.3 contraction area ratio blast tube. The test was conducted at a maximum chamber pressure of 3,225 psia, and the pressure-time trace is shown in figure 32. The motor ignited and operated at a slightly lower chamber pressure than for nozzle S/N 14 until approximately 9.5 sec. At that time, the pressure dropped to 1,000 psia indicating loss of the throat. Postfire examination revealed:

- A. The blast tube was in good condition.
- B. The throat package tungsten, forward Graph-i-tite G-90, aft Graph-i-tite G-90, three pyrolytic graphite washers, and ATJ-graphite were ejected and missing.
- C. The carbon-phenolic throat retention ring appeared to have eroded less than for nozzle S/N 14.

The exact reason for failure is not defined. It is theorized that the pyrolytic graphite washers were incapable of withstanding the severe flow environment and high heat flux aft of the throat. Pyrolytic graphite tends to delaminate and is susceptible to chunking in a turbulent environment. Assuming this material failed and the thin throat retention sleeve of ATJ-graphite was exposed, the material may be structurally degraded to the point that it can no longer support the throat load and fails allowing the insert to be ejected.

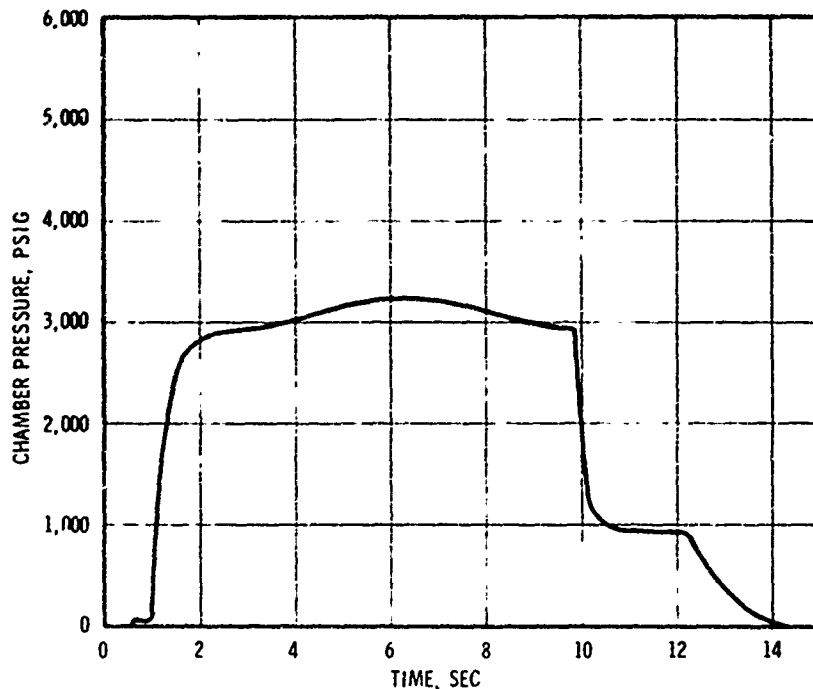


Figure 32. Pressure-Time Trace, Nozzle S/N 15

p. Nozzle S/N 16

This was a repeat of the test for nozzles S/N 14 and 15 with the tungsten extended aft to an area ratio of 1.7. The exit cone was a two-piece design (see section VI). The test was conducted at a maximum chamber pressure of 3,300 psia and a web burning time of 10.7 sec (see figure 33). Visual observation indicated the motor ignited and operated normally except for a slight rise in pressure at approximately 10 sec. Postfire inspection revealed:

- A. The blast tube was in excellent condition, no localized gouging was encountered on the entrance cap or blast tube.
- B. The Graph-i-tite G-90 in front of the throat was in good condition.
- C. The pyrolytic graphite entrance washer was ejected.
- D. The tungsten throat inside diameter had increased an average of 0.010 in. and was in excellent condition. The throat diameter is not reduced because the method of throat retention does not result in high radial compressive loads as in S/N 14 nozzle.
- E. The Graph-i-tite G-90 downstream of the tungsten was eroded severely with approximately the aft 0.625 in. missing, which allowed the throat insert to move aft.

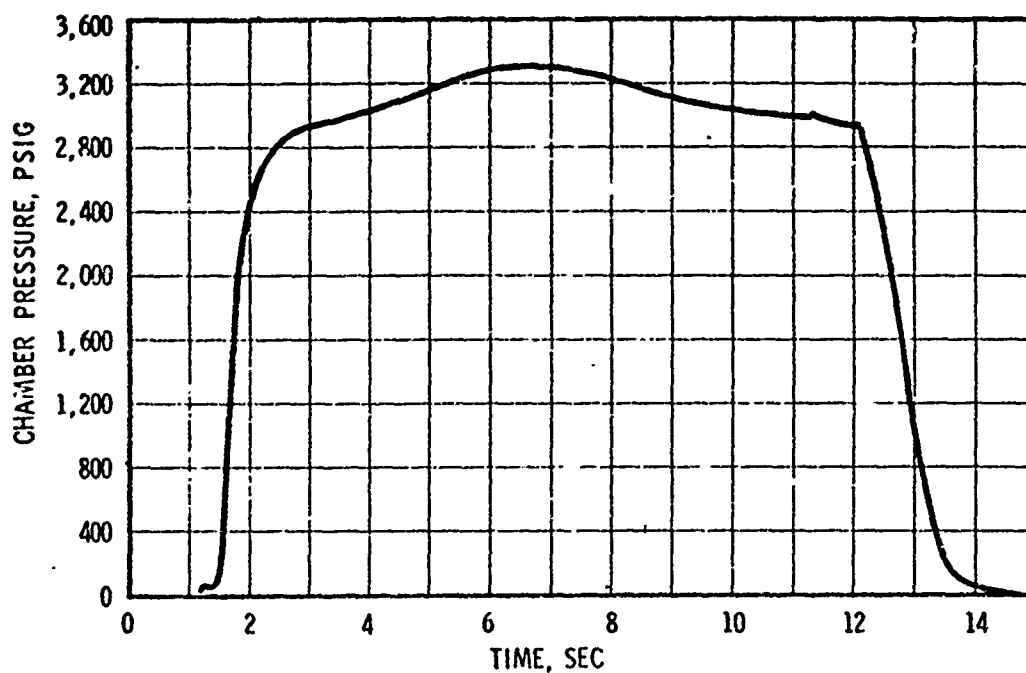


Figure 33. Pressure-Time Trace, Nozzle S/N 16

F.. The exit cone liner was eroded severely as would be expected based on the conditions of the Graph-i-tite G-90 located upstream.

The Graph-i-tite G-90 downstream of the throat apparently experienced higher-than-anticipated heat flux resulting in excessive erosion. The Graph-i-tite G-90 eroded to such a degree that it failed structurally due to the throat ejection loads transmitted to it resulting in the aft movement of the remaining Graph-i-tite G-90 and the throat insert. This caused a loss of the support for the pyrolytic graphite washer which fractured and was expelled from the nozzle.

## SECTION VIII

### PHASE IV - POSTTEST EVALUATION

#### 1. NOZZLE MATERIAL PERFORMANCE

##### a. Blast Tube and Ablative Components

The test nozzle appearance and ablation data show wider variations than reported in reference 2. This is probably due to a more severe propellant environment with CTPB binders than with PBAN, and to higher velocity flow fields in the entrance caps and blast tube.

Pretest and posttest dimensional profiles were made for all test nozzles to permit calculation of the total surface ablation of the nozzle contour. All measurements were taken from the nozzle centerline to the material surface. Use of a standard centering plate ensured accurate, repeatable measurements. This measurement technique eliminates the inherent measurement error which would be obtained by measuring from the nozzle backside due to allowable design tolerances and bondline thickness variation.

The data presented in this section have not been corrected for char swell.

##### (1) Aft Closure

Erosion data were obtained for four candidate materials: Durez 16771-1, Durez 16771-1/4, R155, and MX2625. All four materials exhibited similar erosion characteristics with the erosion rate increasing for smaller area ratios. The erosion rates experienced were two to five times as great as those experienced under contract No. F04611-69-C-0065 where a 16% aluminized PBAN propellant was used for tests having similar time-pressure histories.

The results are tabulated in table XI and shown as ablation versus area ratio in figure 34 for the 18% and 5% aluminum propellants. These data are not conclusive, but they do indicate several trends. Most of the available data are for Durez 16771.

- A. The variation in average ablation from test-to-test appears to be considerably larger for the 18% aluminized propellant. The available data show a variation of  $\pm 30\%$  to 50% on average ablation for the high aluminum tests while a variation of less than 10% is shown for the low aluminum propellants. The severity of the low aluminum propellant environment on material performance is primarily one of corrosivity to which glass and silica phenolics tend to be relatively immune. High aluminum propellant results in very high heat flux and a larger variation in material performance is expected. The Durez material is low cost, hence the quality control has to be significantly reduced, and more variation is anticipated.

TABLE XI  
EROSION DATA -- AFT CLOSURE

Test No.	Material	Initial Area Ratio	Erosion, in.			Average Erosion Rate mil/sec	Circumferential Variation Percent	Char Depth in.	Comments
			0°	45°	180°				
2	Durez 16771-1	26	.250	.201	---	11.8	±11.1	.130	
		15	.325	.306	---	27.6	± 3.8	.080	
	R-155	26	---	---	.274	.208	±13.3	.180	
		15	---	---	.341	.277	± 9.3	.120	
3	Durez 16771-1	25.6	.158	.26	---	11.8	±10.7	.045	
		14.9	.264	.15	---	11.1	± 3.9	.038	
	MX2625	25.6	---	---	.164	.247	±19.6	.420	
		14.9	---	---	.312	.275	± 6.8	.185	
4	Durez 16771-1	26.3	.201	.221	---	19.2	± 4.7	.060	
		15.2	.312	.307	---	27.2	± .8	.045	
	Durez 16771-1/4	26.3	---	---	.210	.208	± .1	.050	
		15.2	---	---	.293	.335	± 6.7	.035	
5	Durez 16771-1	26.0	.156	.215	---	17.6	±15.6	.088	
		15.0	.238	.345	---	27.6	±19.5	.050	
	R-155	26.0	---	---	.186	.149	±10.7	.235	
		15.0	---	---	.284	.233	± 9.7	.205	
8	Durez 16771-1	26.6	.179	.266	---	20.6	±19.3		
		15.4	.306	.410	---	33.2	±14.4		
	Durez 16771-1/4	26.6	---	---	.133	.027	±69.3		Keyhole Port
		15.4	---	---	.233	.194	± 7.5		Keyhole Port
9	Durez 16771-1	27.8	.196	.221	.228	.173	±13.4		
		16.4	.289	.283	.277	.294	27.8	± 2.8	
12	Durez 16771-1	26.85	.472	.046	.367	.196	N/A		
		15.66	.657	.053	.443	.357	N/A	N/A	
13	R-155	27.0	.185	.070	-.031	-.058	N/A		
		15.7	.205	.061	-.067	.106	N/A	N/A	
14	Durez 16771-1	27.0	.233	.223	.228	.228	± 2.2		
		15.7	.325	.345	.358	.383	33.3	± 8.4	
15	R155	27.0	.242	.279	.285	.272	±10.3		
		15.6	.278	.360	.318	.375	33.4	±16.7	
16	Durez 16771-1	---	---	---	---	---			

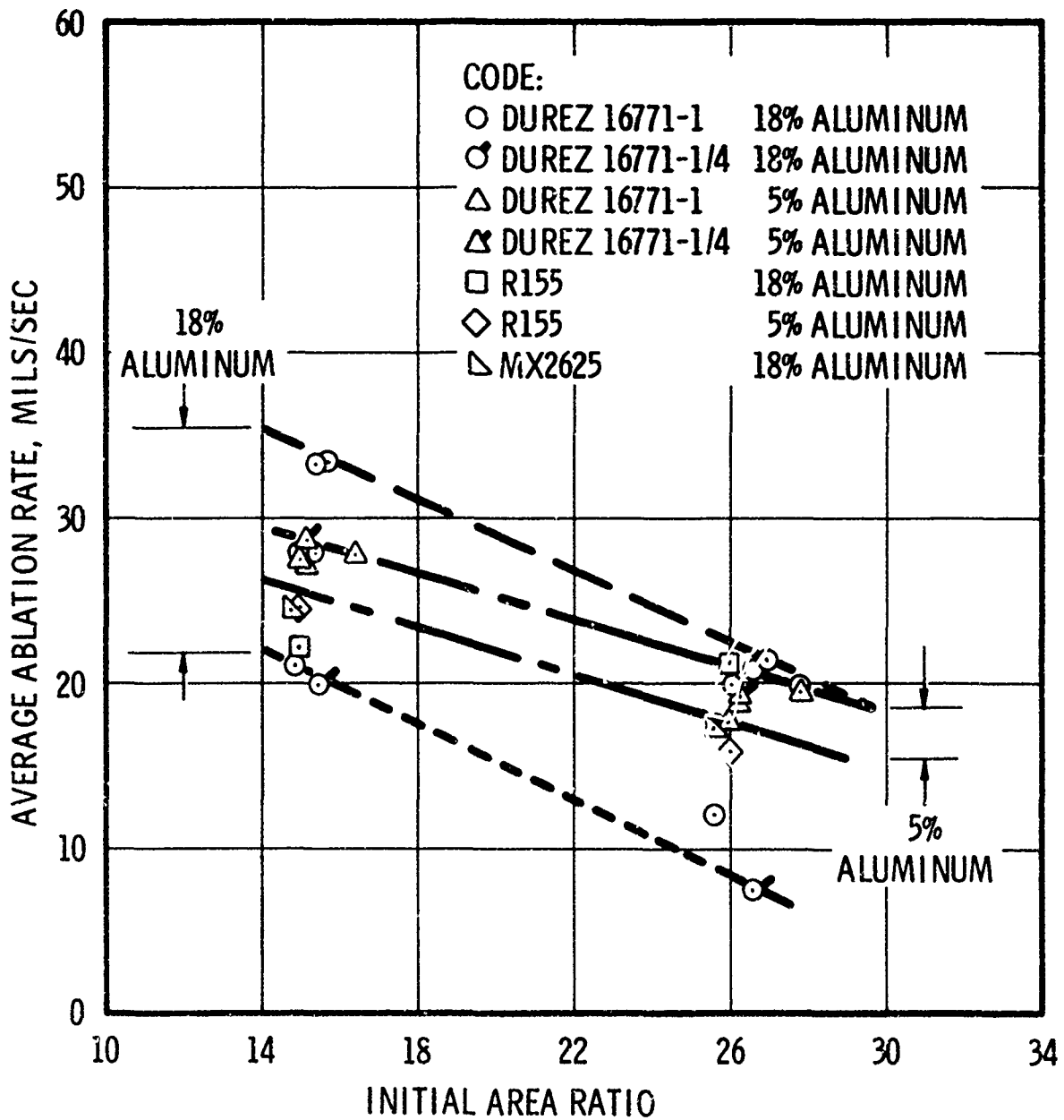


Figure 34. Aft Closure Materials, Average Ablation from Test-to-Test

- B. Due to the wide data scatter, it could not be determined whether the 0.25-in. (16771-1/4) or 1-in. (1577-1) fiber length offered any performance increase.
- C. The R155 data fell within the data scatter band and performance appears to be similar to the Durez material.
- D. The material performance data scatter is very pronounced for the low cost materials (i.e., Durez 16771-1, Durez 16771-1/4, and R155) while the limited data obtained for the higher cost MX2625 material exhibit erosion performance near the mean of the data scatter band (figure 34). Insufficient data are available for the higher quality MX2625 to state conclusively that the material performance is directly related to the material cost, but the data tend to suggest that the lower cost materials may lack reproducibility from batch to batch, i.e., a low level of quality control.

In addition to the test-to-test variation, a variation within any one test also exists. This total variation which has to be used for any design is the total variation, i.e., the sum of test-to-test and the circumferential variation within each test.

Excluding the keyhole port firings (nozzles S/Ns 12 and 13) the maximum variation in the circumferential direction fell within  $\pm 20\%$  for each individual component. A nonuniform circumferential profile was obtained behind the keyhole port slot, as expected.

#### (2) Forward Entrance Cap

Two materials were evaluated for use as a forward entrance cap: MXCE-280 and MX4926. This component is subjected to the severe temperature and corrosive environment and must withstand the high mechanical effects of turning the flow  $64.5^\circ$  under high velocity conditions. Table XII presents the test data. In the test environment, the flat laminate MX4926 material experienced approximately 25% less erosion than the molded MXCE-280. In addition, the MX4926 material eliminated the gouging previously experienced. Comparison of tests for nozzles S/N 02, S/N 03, S/N 04, S/N 08, and S/N 09 indicates that the effect of the aluminum content in the propellant was within the range of normal data scatter.

#### (3) Blast Tube

Silica-based and carbon-based materials, as well as Graph-i-tite G-90 and carbon-carbon composites, were examined for possible application as blast tube liner materials. Table XIII identifies the materials used and their performance in those tests which yielded valid material performance data.

TABLE XII

## EROSION DATA - FORWARD ENTRANCE CAP

Test No.	Material	Initial Area Ratio	Erosion, in.			Average Erosion Rate, mil/sec	Circumferential Variation Percent	Char Depth, in.	Comments
			0	45°	180				
2	MXCE-280	3.00 2.06	.330 .438	.348 .372	.328 .322	.329 .345	± 2.1 ± 14.7	1.02 1.55	
3	MXCE-280	2.43 1.31	.426 .456	.450 .490	.420 .500	.470 .501	± 5.0 ± 4.6		
4	MIXCE-280	2.89 2.06	.422 .482	.389 .403	.448 .440	.468 .442	± 8.8 ± 8.8	.242 .353	
5	MXCE-280	2.49 1.37	1.121 1.191	.390 .566	0.411 burn out	0.333 0.381	± 08.7 ± N/A	420 N/A	Severe gouging due to insufficient thermal expansion gap
8	MXCE-280	2.73 1.39	.383 .460	.425 .511	.351 .434	.249 .339	± 20.7 ± 21.0		Local gouging was encountered on entrance cap
9	MXCE-280	3.21 2.10	.332 .310	.368 .342	.305 .305	.319 .313	± 9.2 ± 5.6		
12	MX4926	2.58 1.33	.602 .533	.085 .144	.624 .590	.500 .505	± 84.3 ± 10.0		Keyhole port grain
13	MX4926	3.04 1.37	.351 .517	.396 .539	-.149 -.014	.216 .336	± 110 ± 108		Keyhole port grain
14	MX4926	4.21 3.17	.245 .262	.255 .247	.255 .254	.215 .261	± 7.0 ± 3.5		
15	MX4926	2.47 1.34	.427 .481	.417 .411	.399 .453	.393 .433	± 4.4 ± 8.3		Ejected throat insert near shutdown
16	MX4926								

**TABLE XIII**  
**EROSION DATA -- BLAST TUBE**

Test No	Material	Initial Area Ratio	Erosion, in.				Average Erosion Rate mils/sec	Distance From Fwd Face of B T	Circumferential Variation Percent	Char Depth in.	Comments	
			0°	45°	180°	225°						
2	MXCE-280	2.0	.403	.342	----	----	32.7	.250	± 8.1	.150		
			.384	.347	----	----	32.0	3.000	± 5.4	.145		
			.376	.314	----	----	30.2	5.000	± 8.7	.140		
			.271	.302	----	----	25.2	7.890	± 10.4	.130		
	MXSC-195	-----	-----	-----	-----	.328	.321	28.5	0.250	± 1.2	.075	
				-----	-----	.359	.366	31.6	3.000	± 0.8	.055	
MX4926	-----	-----	-----	-----	.543	.549	47.0	5.000	± 0.5	.150		
			-----	-----	.477	.493	42.3	7.890	± 1.6	.150		
3	MXCE-280	1.3	.471	.521	----	----	40.3	.250	± 5.1	.130		
			.440	.455	----	----	37.4	3.000	± 1.6	.105		
	G-90	-----	-----	.193	.199	----	----	16.4	5.000	± 1.5	----	
				.182	.157	----	----	15.4	7.890	± 1.4	----	
	MXCF-280	-----	-----	-----	-----	.438	.540	43.2	.250	± 5.1	.130	
				-----	-----	.450	.470	38.7	3.000	± 1.1	.100	
G-90	-----	-----	-----	-----	.200	.193	15.4	5.00	± 1.5	----		
			-----	-----	.204	.191	16.3	7.890	± 3.5	----		
4	MXSE-280	2.0	.354	.268	.326	.333	29.1	.250	± 14.7	.080		
			.248	.227	.250	.242	22.0	3.00	± 5.1	.060		
	MX2-25	-----	-----	.236	.217	.258	.244	21.6	5.000	± 8.4	.060	
				.234	.220	.222	.240	20.6	7.890	± 4.3	.045	
5	MXSE-280	1.3	.651	1.037	----	----	53.0	.250	± 23.5	.030	Gouging in entrance cap caused uneven erosion in blast tube	
			.422	0.700	----	----	53.1	5.000	± 26.3	.025		
	MX4926	-----	-----	.588	0.736	----	----	42.6	5.000	± 13.8		.085
				.512	0.593	----	----	52.3	7.890	± 7.2		.065
	MXCE-280	-----	-----	-----	-----	.468	.876	63.6	.250	± 31.0		.020
				-----	-----	.471	.565	49.1	3.000	± 8.7		.020
-----				-----	.526	.850	65.1	5.000	± 1.5	.030		
-----				-----	.416	1.224	77.7	7.890	± 42.8	.035		
8	MXCE-280	1.3	.443	.491	.400	.750	48.2	.250	± 29.1	.210	Local gouging on entrance cap	
			.496	.505	.505	.490	46.2	3.000	± 1.4	.155		
			.475	.475	.485	.470	44.1	5.000	± 1.7	.165		
			.412	.418	.422	.413	38.5	7.890	± 1.2	.160		
9	MXCE-280	2.0	.314	.333	.290	.296	29.9	.250	± 6.8	.105		
			.356	.376	.347	.324	34.1	3.00	± 7.4	.110		
			.346	.375	.347	.325	33.8	5.00	± 7.1	.100		
			.305	.328	.318	.285	30.0	7.890	± 5.3	.100		
12	MXCE-280	1.3	.527	.284	.212	.525	56.1	.250	± 41.1	.050	Keyhole port	
			.495	.321	.262	.394	53.3	3.000	± 44.7	.070		
			.494	.402	.258	.478	59.1	5.000	± 23.1	.060		
			.444	.381	.252	.426	54.5	7.890	± 29.0	.070		
13	MXCE-280	1.3	.449	.483	-.038	.340	27.9	.250	±101		Keyhole port	
			.491	.525	-.035	.441	31.5	3.000	±106			
			.500	.514	-.021	.443	31.2	5.000	±102			
			.504	.428	.002	.391	28.8	7.890	±101			
15	MXCE-280	1.3	.454	.436	.469	.463	46.0	.250	± 3.6		Ejected throat near shutdown	
			.533	.509	.578	.547	57.1	3.000	± 6.4			
			.553	.468	.549	.521	56.9	5.000	± 9.6			
			.519	.547	.584	.559	58.1	7.890	± 5.8			
16	MXCE-280	1.3	.499	.519	.484	.492	47.5	.250	± 3.0			
			.575	.595	.560	.570	54.8	3.000	± 3.1			
			.553	.568	.557	.542	52.8	5.000	± 2.3			
			.609	.643	.520	.511	54.4	7.890	± 10.2			

69/70

The Graph-i-tite G-90 material provides the best erosion resistance at the low contraction ratio stations. Problems associated with its high thermal conductivity, fabrication, cracking during test, thermal expansion gapping, assembly, and cost make it an undesirable blast tube material, especially since other materials are shown to be acceptable.

Most of the data was obtained for the baseline material, MXCE-280. Figure 35 shows the average ablation rate as a function of length down the blast tube. The average performance is fairly consistent. Maximum erosion occurs somewhat aft of the entrance except for the 1.3 initial area ratio for the 5% aluminum propellant test firings for nozzle S/N 05, and the higher pressure 18% aluminized propellant test firings for nozzles S/N 15 and 16. The blast tube for nozzle S/N 05 experienced very uneven erosion due to excessive gouging on the entrance cap, as discussed in the previous section. Based upon visual inspection, the measured erosion at the 5-in. station for S/N 05 was discarded and license was used in estimating the performance based on trends. The reason is not explained for the high ablation at the aft end of the higher pressure test firings (nozzles S/N 15 and 16).

A cross plot of this performance showing the maximum circumferential variation at the 3-in. station is shown in figure 36. The maximum circumferential variation is well within  $\pm 10\%$  for these firings at the same pressure. Also, the material performance for the 5% and 18% aluminized propellant tests falls within the data scatter for each firing. An increase in pressure ( $\sim 600$  psia) shows a definite increase of about 15% in the ablation experienced at the low contraction ratio. The ablation of nozzle S/N 16 was almost uniform circumferentially. Nozzle S/N 15 indicated a spread of  $\pm 7\%$ . Even though the throat was ejected essentially at shutdown on the nozzle S/N 15 test firing, the data still appear to be valid. Also shown on figure 36 are the data from reference 2 which are used only to aid in determining trends since these data are for a 20 sec test firing, a much milder environment of 16% aluminized PBAN, and a contraction ratio of 3.14.

While these rates are based on one firing and each condition and do account for circumferential variations, they are for a specific time (10 sec). The average ablation rate for shorter duration firings would be expected to be higher since the high erosion is rapidly reducing the local flow velocity. A counteracting factor is the finite time it takes for the surface temperature to approach equilibrium. Figure 6-19 of section VI, volume II shows the surface temperature reaches near maximum in approximately 1.0 sec. Therefore, the time required for surface temperature stabilization does not appear to be a major factor.

Even though the amount of data is limited, good agreement exists indicating that the test-to-test variation is probably small. Other

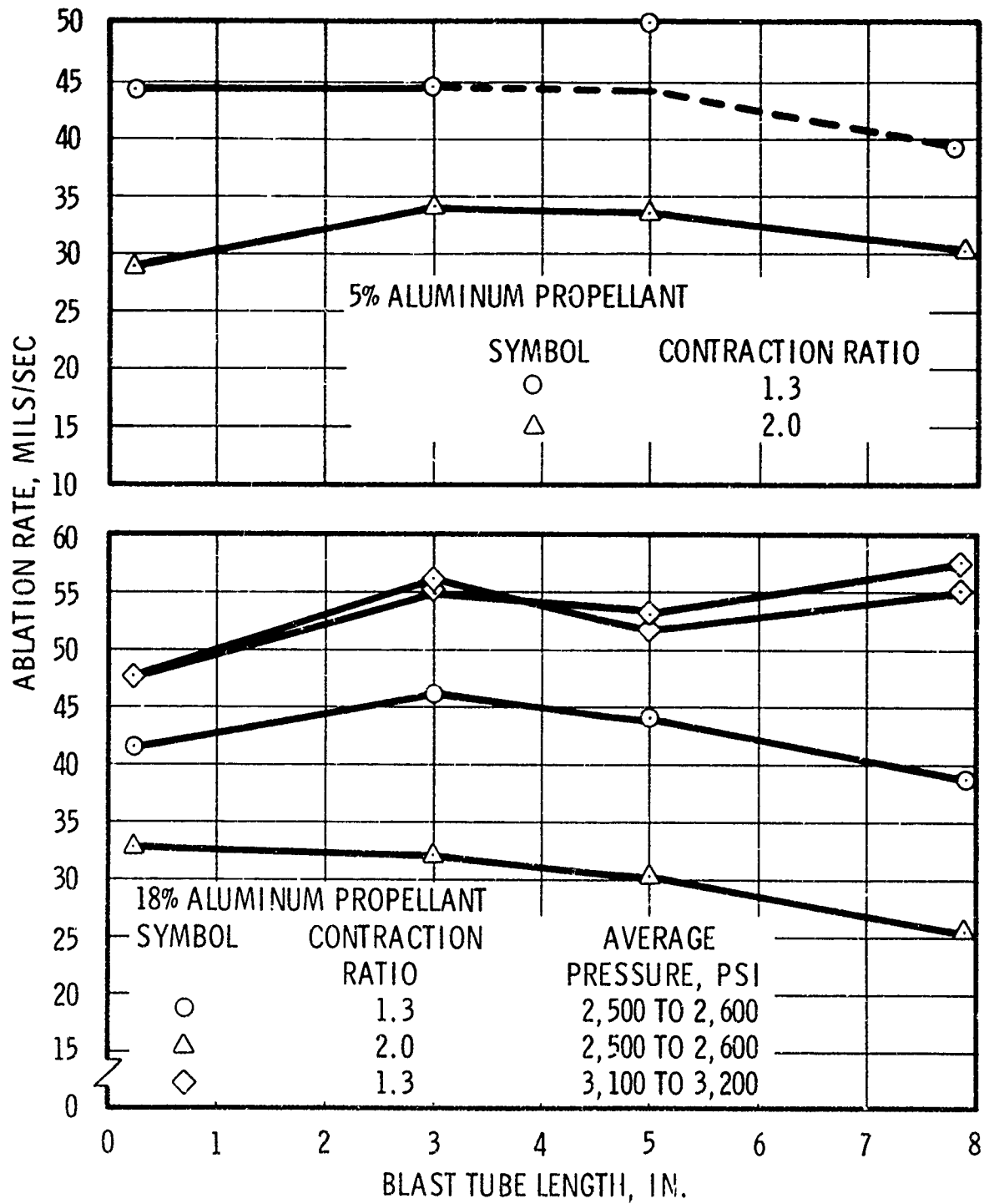


Figure 35. MXCE-280 Ablation vs Blast Tube Length

materials did not show any gain over the MXCE-280 except in the test for nozzle S/N 04 where the silica-phenolics MXSE-280 and MX2625 appear to offer a considerable gain of ~20 to 22 versus 30 to 35 mils/sec over the carbon phenolic at a contraction ratio of 2.0 for the low aluminum propellant. At a contraction ratio of 1.3 for nozzle S/N 05, the MXSE-280 did not offer any apparent gain; however, this blast tube eroded very unevenly. The other carbon-phenolic, MX4926, eroded in a very unpredictable manner. The charred surface appeared to fail locally during the firing so that a peeling effect was obvious only in discrete areas. This was noted on both firings of the 18% aluminum content propellants. The effect was not pronounced for the 5% aluminum content propellants. Since MX4926 is a flat laminate fabric molding, this effect would not be anticipated. No explanation is given. The MXCE-280 resulted in a considerably more uniform surface for this application, while the flat laminate considerably outperformed the molding compound in the forward entrance cap.

The hybrid carbon silica-phenolic, MXSC-195, did not offer any advantages. In addition, this material reportedly is no longer available and was dropped from the matrix early in the program.

Two carbon-carbon composites, Pycobond and Pyrostrand, were tested unsuccessfully in three firings. All resulted in throat ejection. Inadequately characterized properties and lack of design

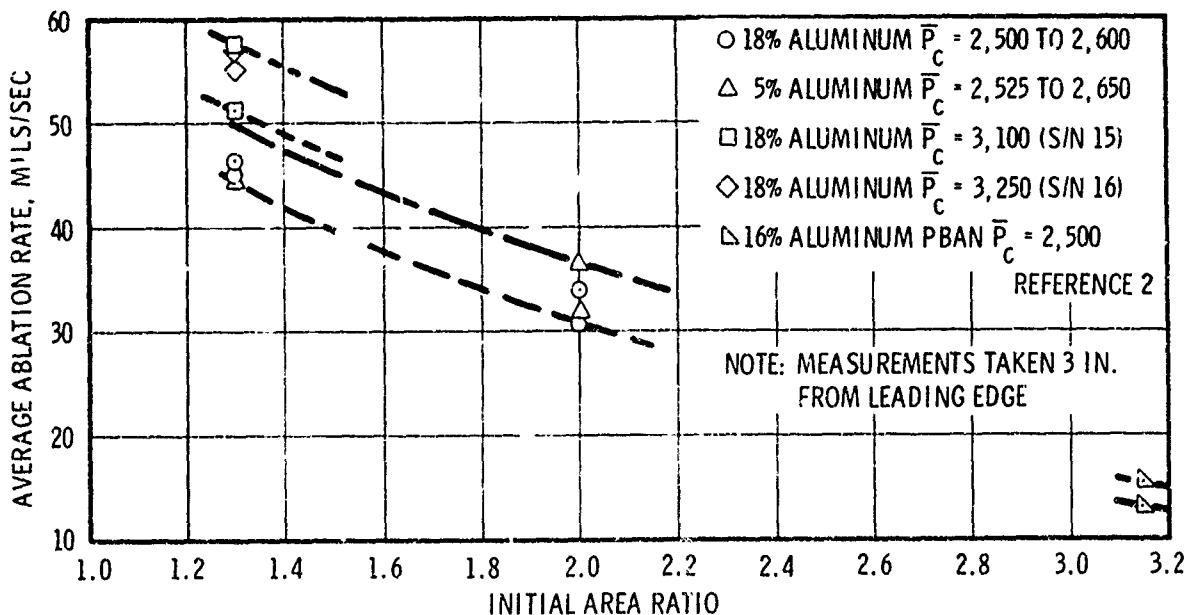


Figure 36. MXCE-280 Performance vs Blast Tube

data are blamed for these failures. The Pycobond expanded approximately five times as much as the original material properties indicated, thereby shoving out the throat insert at 7.5 sec in the nozzle S/N 06 test. The Pycobond remained in the nozzle while the motor continued to burn at reduced pressure for an additional 3.5 sec. Based on a normal 10 sec firing, an ablation rate of approximately 20 mils/sec was experienced which is relatively high for the contraction ratio of 2.0. These data are only approximate and should not be used for designs using this material. Tests for nozzles S/N 10 and 11 used 4-in.-long cylinders of Pycobond and Pyrostrand, respectively. These liners both appeared to fail structurally (i.e., fracturing) in the same manner, causing momentary throat blockage and resulting in throat ejections at approximately 9.0 sec. Adequate thermal expansion gaps were provided based on the higher expansion values. Small pieces of the Pycobond were found which ranged from approximately 0.25- to 0.38-in. thick indicating erosion rates of 15 to 28 mils/sec for the low contraction ratio blast tube. No pieces of the Pyrostrand liner were found. Based on these results, the carbon-carbon composites do not appear to be exceptionally strong candidates for the blast tube both from thermal-structural problems or performance.

The ablation performance of the aft closure insulation, entrance cap, blast tubes, and throat assemblies when used in conjunction with the keyhole port grain showed a definite effect of the slot. Figures 37 through 39 show photographs of the entrance and exit end of the blast tube, and the entrance end of the throat package for the 18% aluminum propellant (nozzle S/N 13). Diametrically opposite the slot there is a flat area which experiences essentially no erosion. At the forward end and in line with the slot (TDC), there was no noticeable increase in erosion over that normally experienced. The unevenness gradually transitioned down the blast tube until a "heart" effect resulted at the blast tube aft end. In line with the slot, there was additional erosion over that at the forward end. The flat area 180° from the slot transitioned into a rather sharp ridge. This effect was carried into the throat and is noticeable on the forward entrance cap and entrance throat washers. Minimal effect was experienced at the throat plane, with a slight flattening at 180°. The exit cone performance for the keyhole port grain firings showed more circumferential variation. The results for the 5% aluminized propellant (nozzle S/N 12) were essentially the same but not as pronounced.

#### (4) Aft Entrance Cap

Three polycrystalline graphites (Graph-i-tite G-90, P03, and Speer 8882) were tested for application as aft entrance cap materials. The test data are presented in table XIV and figure 40. The Graph-i-tite G-90 exhibited the best erosion resistance of the three materials tested, as would be expected based on a comparison of the relative bulk density. Less erosion was obtained for the Graph-i-tite G-90 as the aluminum content was increased. The keyhole port grain did not noticeably affect the average performance



Figure 37. Entrance View of Test-Fired Blast Tube S/N 13  
(Keyhole Port Grain Effect)

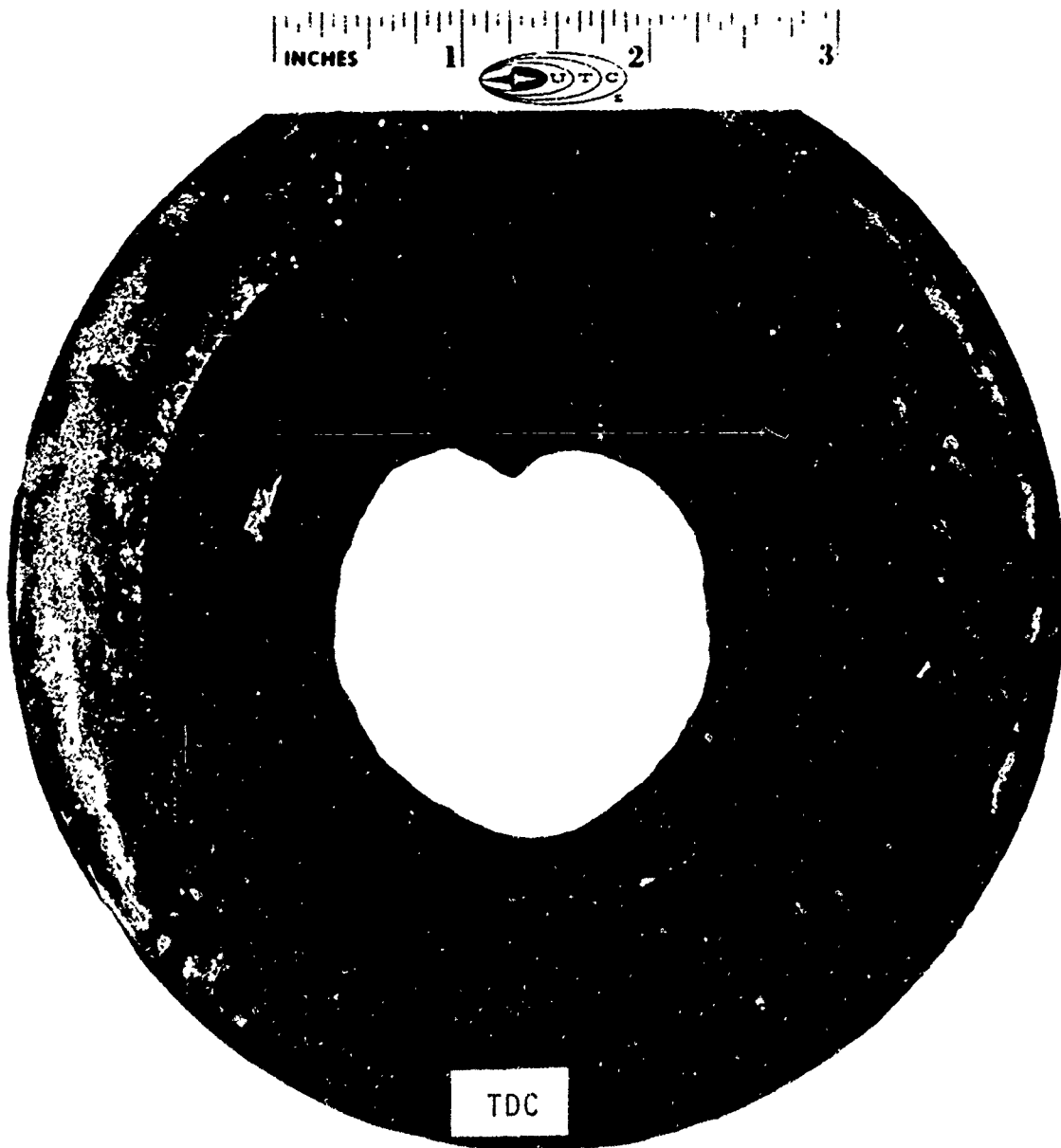


Figure 38. Aft End View of Test-Fired Blast Tube S/N 13  
(Keyhole Port Grain Effect)



Figure 39. Entrance View of Throat Package S/N 13  
(Keyhole Port Grain Effect)

TABLE XIV

## EROSION DATA -- AFT ENTRANCE CAP

Test No.	Material	Initial Area Ratio	Erosion, in.			Average Erosion Rate ml/sec	Circumferential Variation		Comments
			0°	45°	180°		225°	Percent	
2	G-90	1.89	.161	.147	---	---	13.5	± 5.2	
			.171	.157	---	---	14.4	± 4.7	
	P03	1.89	---	---	.213	.242	19.9	± 6.6	
			---	---	.209	.216	18.6	± 1.9	
3	G-90	1.22	.193	.248	---	---	18.4	± 11.8	
			.183	.241	---	---	17.6	± 14.2	
4	P03	1.22	---	---	.197	.240	18.2	± 17.6	
			---	---	.197	.226	17.6	± 13.4	
4	G-90	1.87	.199	.195	---	---	17.9	± 1.0	
			.208	.191	---	---	18.2	± 4.0	
5	8882	1.87	---	---	.269	.270	24.6	± 0.0	
			---	---	.256	.256	23.3	± 0.0	
5	G-90	1.23	.301	.413	---	---	33.8	± 15.3	
			.267	.343	---	---	28.9	± 13.1	
8	8882	1.23	---	---	.356	.631	46.8	± 28.0	
			---	---	.335	.419	35.7	± 10.7	
8	G-90	1.25	.225	.235	.244	.258	22.3	± 5.1	
			.184	.189	.195	.185	17.4	± 2.6	
9	G-90	1.89	.200	.221	.210	.182	19.7	± 10.0	
			.192	.207	.194	.175	18.6	± 7.9	
12	G-90	1.27	.269	.210	.092	.253	29.8	± 48.6	Keyhole port
			.251	.198	.091	.223	27.6	± 51.8	
13	G-90	1.28	.371	.279	.081	.186	19.9	± 63.6	Keyhole port
			.301	.173	.106	.149	15.3	± 50.5	
14	G-90	2.84	.125	.135	.137	.113	12.3	± 9.6	
			.146	.148	.178	.128	14.1	± 16.3	
16	G-90	1.88	.114	.122	.135	.101	11.1	± 14.4	
			---	---	---	---	19.6	± 5.0	

Entrance cap moved aft during firing.  
Thickness of part measured rather than profiled to get ablation. Variation appeared small on order of 0±5%.

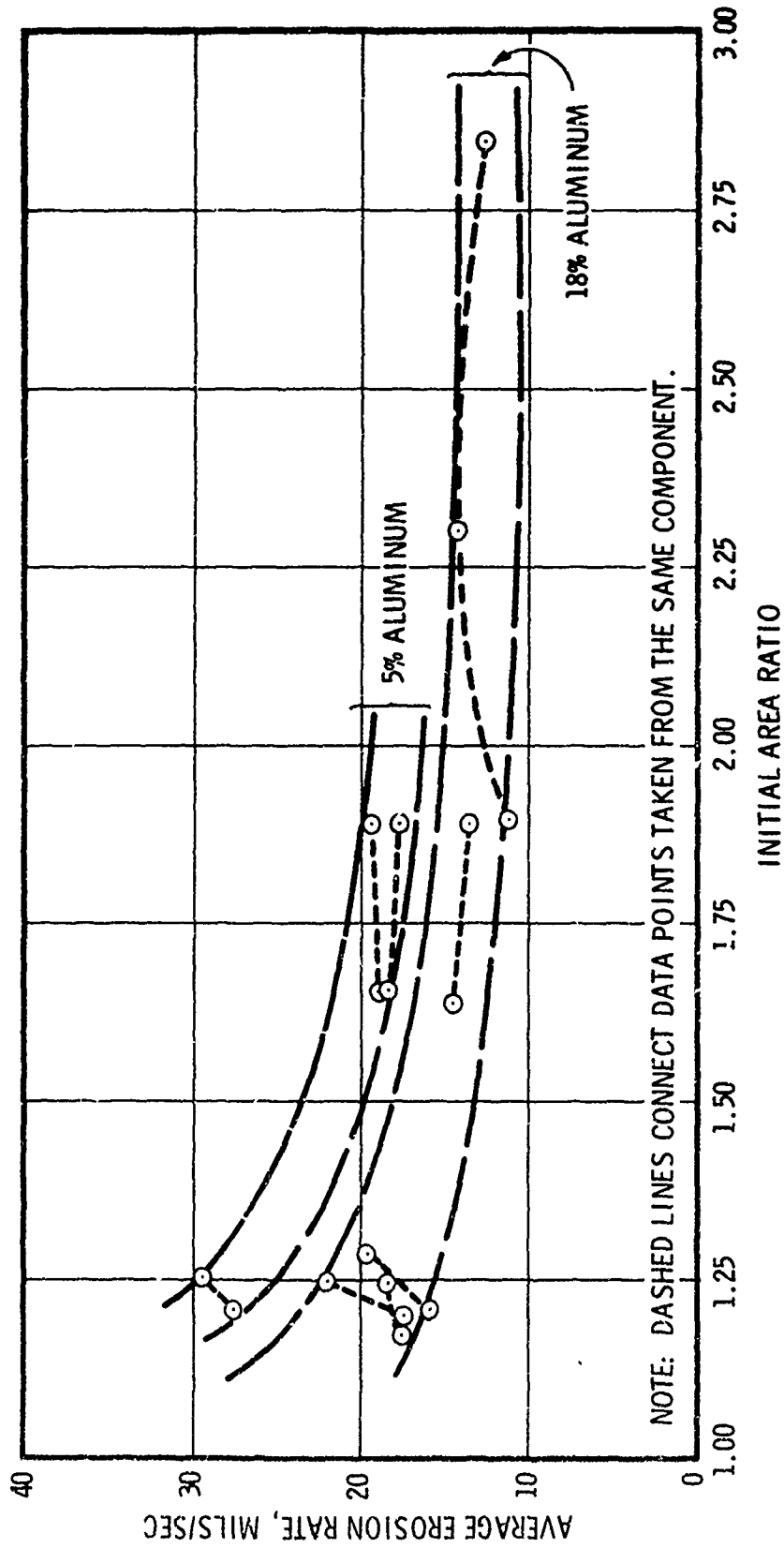


Figure 40. Aft Entrance Cap Average Performance of Graph-i-lite G-90 Material

of the aft entrance cap because all the available data fall within  $\pm 20\%$ ; however, localized effects were detected due to the keyhole port effect.

The circumferential variation for each aft entrance cap usually was within  $\pm 15\%$  except for those firings with the keyhole port grains.

#### (5) Exit Cone

Three materials were examined as exit cone liner candidates: FM5055, MX4926, and MX2600. The performance of these materials is summarized in table XV.

For expansion ratios in excess of approximately 5, the effect of the material used, chamber pressure, and propellant aluminum content are not determining factors in the erosion rate of the material. This is not the case, however, for area ratios under 4. Examination of the data shown in figure 41 indicates that low aluminum content propellants create higher average erosion rates for the same material under similar conditions (tests for nozzles S/N 04 and 05 versus tests for nozzles S/N 02 and 03, and 08).

For the 5% aluminized CTPB propellant, the silica-based MX2600 exhibited better erosion resistance than did the carbon-based MX4926. This result agrees with thermochemical analysis predictions. Relative performances of the silica-based materials versus carbon-based materials were not obtained for the 18% aluminized CTPB propellant.

Using the CTPB propellants, the erosion rates obtained were approximately two to three times greater than those obtained during contract No. F04611-69-C-0065 for a 16% aluminized PBAN propellant.

The circumferential variation in ablation for each test was generally within  $\pm 10\%$  with few exceptions. The exceptions occurred where the average erosion was small and the variations appeared large percentage-wise, but were not large in actual amount of material removed.

### b. Posttest Evaluation of Nozzle Throat Insert Performance

#### (1) Pyrolytic Graphite

Nozzle throat inserts fabricated from pyrolytic graphite and wire-wound tungsten were tested during this contract effort. The pyrolytic graphite throats (utilizing pyrolytic graphite from Super-temp and Pyrogenics) were tested with both a 5% and 18% aluminum CTPB propellant (UTP-13,615 and UTP-11,475 respectively) while the wire-wound tungsten insert was evaluated with the 18% aluminum CTPB propellant only.

Test results presented in table XVI and plotted in figure 42 demonstrate that, for the same average chamber pressure, the pyrolytic

TABLE XV

## EROSION DATA - EXIT CONE

Test No.	Material	Initial Area Ratio			Erosion, in.			Average Erosion Rate mils/sec	Circumferential Variation Percent	Char Depth in.	Comments
		0°	45°	180°	225°	180°	225°				
2	FM5055	2.26	.206	.191	.210	.199	17.6	± 4.5	.120	Visual inspection shows multiple streaks at A/A* = 4.19 0° and 45° data invalid as taken in the discontinuities.	
		4.19	.031	.052	.052	.057	4.2	± 4.0	.160		
		6.78	-.008	-.004	.000	-.007	- 0.5	± N/A	.125		
3	FM5055	2.24	.168	.203	.221	.172	15.9	± 12.5	.080	Visual inspection shows multiple streaks at A/A* = 4.19 0° and 45° data invalid as taken in the discontinuities.	
		4.19	.223	.216	.070	.082	12.3	± 56.2	.120		
		6.78	-.003	-.005	-.007	-.005	-0.4	± N/A	.150		
4	FM5055	2.26	.299	.351	-----	-----	29.5	± 7.7	.050	Visual inspection shows multiple streaks at A/A* = 4.19 0° and 45° data invalid as taken in the discontinuities.	
		4.24	.132	.121	-----	-----	11.5	± 4.7	.050		
		6.90	.019	.025	-----	-----	2.0	± 13.6	.070		
5	MX2600	2.26	-----	-----	.227	.262	22.2	± 7.5	.050	Visual inspection shows multiple streaks at A/A* = 4.19 0° and 45° data invalid as taken in the discontinuities.	
		4.24	-----	-----	.103	.111	9.8	± 3.7	.100		
		6.90	-----	-----	.028	.024	2.4	± 7.7	.120		
6	MX4926	2.26	.253	.427	-----	-----	32.2	± 28.3	.005	Visual inspection shows multiple streaks at A/A* = 4.19 0° and 45° data invalid as taken in the discontinuities.	
		4.24	.122	.124	-----	-----	11.6	± .8	.065		
		6.90	.025	.053	-----	-----	3.7	± 34.2	.080		
7	MX2600	2.25	-----	-----	.254	.261	24.4	± 1.6	.050	Visual inspection shows multiple streaks at A/A* = 4.19 0° and 45° data invalid as taken in the discontinuities.	
		4.24	-----	-----	.114	.102	10.2	± 5.6	.060		
		6.90	-----	-----	.032	.032	3.0	± 0.0	.080		
8	FM5055	2.21	.207	.229	.210	.206	19.7	± 5.4	.080	Visual inspection shows multiple streaks at A/A* = 4.19 0° and 45° data invalid as taken in the discontinuities.	
		4.20	.111	.120	.118	.107	10.6	± 5.3	.150		
		6.86	.008	.002	.012	.002	5.5	± N/A	.240		
9	MX2600	2.31	.219	.211	.213	.205	20.5	± 3.3	.050	Visual inspection shows multiple streaks at A/A* = 4.19 0° and 45° data invalid as taken in the discontinuities.	
		4.31	.081	.081	.086	.076	7.9	± 6.2	.050		
		6.97	.025	.018	.029	.021	2.2	± N/A	.085		
12	MX4926	2.30	.267	.368	.201	.367	43.5	± 29.8	.100	Keyhole port grain	
		4.27	.087	.195	.061	.086	15.5	± 50.0	.120		
		6.92	-.001	.007	.000	.014	0.7	± N/A	.105		
13	FM5055	2.28	.152	.138	.169	.163	13.5	± 7.4	.100	Keyhole port grain	
		4.25	.122	.016	.096	.037	5.4	± 100.6	.120		
		6.88	-.004	-.023	.009	.013	-1.0	± N/A	.105		
14	FM5055	1.81	.268	.261	.270	.252	24.8	± 3.4	.100	These data are not representative of the material due to the high erosion on the G-90 block upstream.	
		2.77	.461	.488	.516	.453	45.2	± 5.3	.120		
		5.02	.199	.261	.355	.204	24.0	± 28.1	.105		

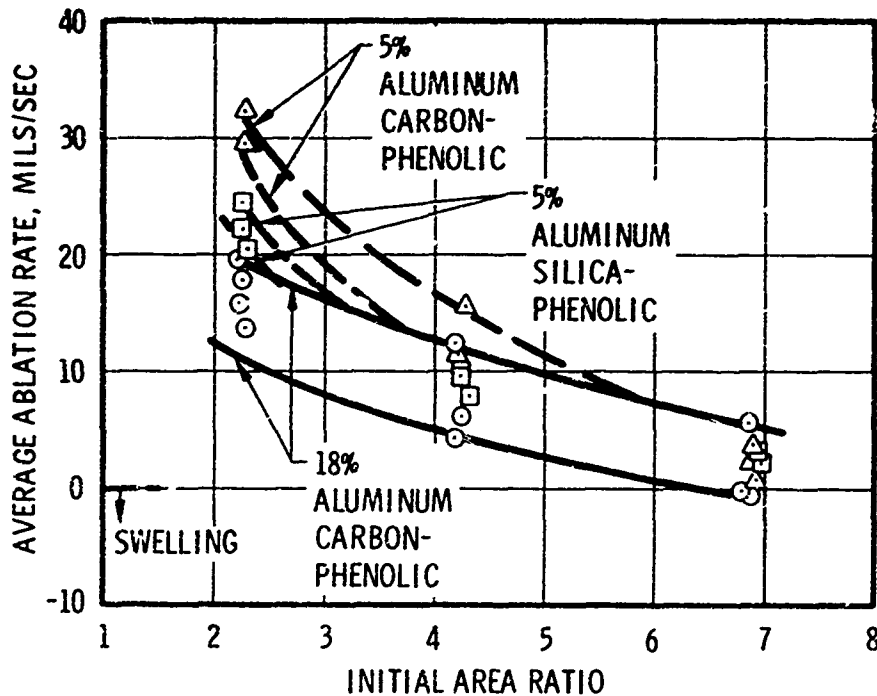


Figure 41. Average Ablation Rates from Test-to-Test in Exit Cone

graphite throat inserts experience considerably higher average erosion rates with CTPB propellants than with the PBAN propellants used during contract No. F04611-69-C-0065. Referring to figures 16, 17, 19, and 20, it is evident that at approximately 5 sec, a high erosion rate is encountered since the pressure rapidly decays while the thrust level is maintained. Until this time, a relatively low erosion rate is encountered, probably similar to that predicted by thermochemical analysis. The erosion rates presented are average over the entire duration and caution should be exercised in using these rates for other durations.

The wide variation in the average erosion rate for the pyrolytic graphite in the pressure range of 2,400 to 3,000 psi indicates that the limit for use of the graphite has been reached with this environment, i.e., CTPB or HTPB binder at 3,000+ psi. This effect is unexplained at this time. Further discussion of this phenomena from the thermochemical attack aspect is presented in section VI, volume II of this report. More definitive data are required at chamber pressures below 2,400 psi and above 2,700 psi to determine an accurate erosion rate band as a function of chamber pressure for the pyrolytic graphite. The insert eroded in a relatively symmetrical manner with no gouging or streaking evident. The data obtained under contract No. F04611-71-C-0051 conclusively demonstrates that:

- A. Pyrolytic graphite when used in conjunction with CTPB propellants erodes from 5 to 10 times as much as thermochemical calculations predict.

**SECTION XI**  
**RECOMMENDATIONS**

Based on the results of the program, the following recommendations are offered:

- A. Additional experimental and analytical work should be performed to define reasons for the high ablation rates of pyrolytic graphite washer throat inserts.
- B. An analytical model should be derived which accurately predicts the ablation performance of ablative materials downstream of a noneroding throat insert. This model should not only be based on accurate boundary layer analysis but also should include experimentally derived heat transfer multipliers for rearward facing steps as a function of step height, pressure level, and local Mach number.
- C. MXCE-280 material should be evaluated for application to lower than 1.3 contraction area ratio blast tubes. The additional data will provide material performance for design tradeoffs on the SRBDM.
- D. Configuration variables such as blast tube length, internal contour, subsonic splitline gaps, etc., should be evaluated to define their influence on material performance. The subsonic splitline gap may be the largest challenge based on the problems encountered during this contract with larger than 0.030-in. gaps at the blast tube entrance.
- E. A material is required for use downstream of the wire-wound tungsten throat insert which possesses higher ablation resistance and has structural properties equal to or greater than Graph-i-tite G-90. High density (>1.85 g/cc) carbon-carbon composites are recommended candidates. Possible alternates are pyrolytic graphite coatings or codeposited silicon carbide/pyrolytic graphite (SiCPG) on polycrystalline graphite substrates.

## REFERENCES

1. Stephen, Wendell A., Development of High Performance Materials for High Chamber Pressure Rocket Motor Applications, AFRPL-TR-69-222 Part I, Contract No. F04611-69-C-0065, United Technology Center, September 1969.
2. Stephen, Wendell A., Development of High Performance Materials for High Chamber Pressure Rocket Motor Applications, AFRPL-TR-71-78 Part I, Contract No. F04611-69-C-0065, United Technology Center, August 1970.
3. Wu, Jain-Ming, Michael W. Su, and Trevor H. Moulden, On the Near Flow Field Generated by the Supersonic Flow Over Rearward Facing Steps, ARL 71-0242, Aerospace Research Laboratories, November 1971.
4. Sandford, J., and J. J. Ginoux, Laminar, Transitional and Turbulent Heat Transfer Behind a Backward Facing Step in Supersonic Flow, Technical Note 38, von Karman Institute for Fluid Dynamics, Rhode-Saint-Genese, Belgium, October 1968.
5. Lamb, J. P., and C. G. Hood, "Theoretical Distributions of Heat Transfer Downstream of a Backstep in Supersonic Turbulent Flow," Transactions of the ASME, Journal of Heat Transfer, -87, February 1972.
6. Gerhart, Philip, "Heat Transfer Downstream of Attachment of a Turbulent Supersonic Shear Layer," AIAA Journal, Volume II, No. 1, January 1973.
7. Stephen, Wendell A., High Chamber Pressure Evaluation of Wire-Wound Tungsten Nozzles, AFRPL-TR-69-79, Contract No. F04511-68-C-0083.  
(CONFIDENTIAL)

**APPENDIX I  
MATERIAL PROPERTIES DATA**

**R155 INSULATION DATA SHEET  
(Asbestos filled rubber, randomly oriented fibers)**

Properties	Random Fiber*			
	77°F	170°F	-55°F	
Ultimate Elongation, %	20	14	13	
Ultimate Tensile Strength, psi	640	500	3,400	
Modulus (secant), psi	3,500	3,400	25,000	
Modulus (tangent), psi	7,000	6,000	75,000	
Density, lb/in. <sup>3</sup>				
Thermal Conductivity, Btu/hr-ft <sup>2</sup>	0.20 at 77° to 212°F			
Thermal Expansion (from molded block), in./in./°F				
Vertical orientation	15.4 x 10 <sup>-5</sup> at 78 to 33			
Vertical orientation	18.3 x 10 <sup>-5</sup> at 33 to -68			
Horizontal orientation	4.8 x 10 <sup>-5</sup> at 78 to 68			
Specific Heat, cal/°C	0.267 at 75°F			
	0.39 at 0°F			
	0.48 at 200°F			
	0.56 at 400°F			
	<b>Tensile Strength, psi</b>			
Bond Strength	-70°F	77°F	170°F	290°F
R155/Steel (primed with Chemlock 231)	1,220	566	466	418
R155 aged 2 weeks at 170°F	---	640	---	---
R155/EPT rubber liner (cure bonded)	746	209	134	106
R155 aged 2 weeks at 170°F	---	246	---	---

\* Tested at 20 in./min crosshead on Istron Tensile Tester

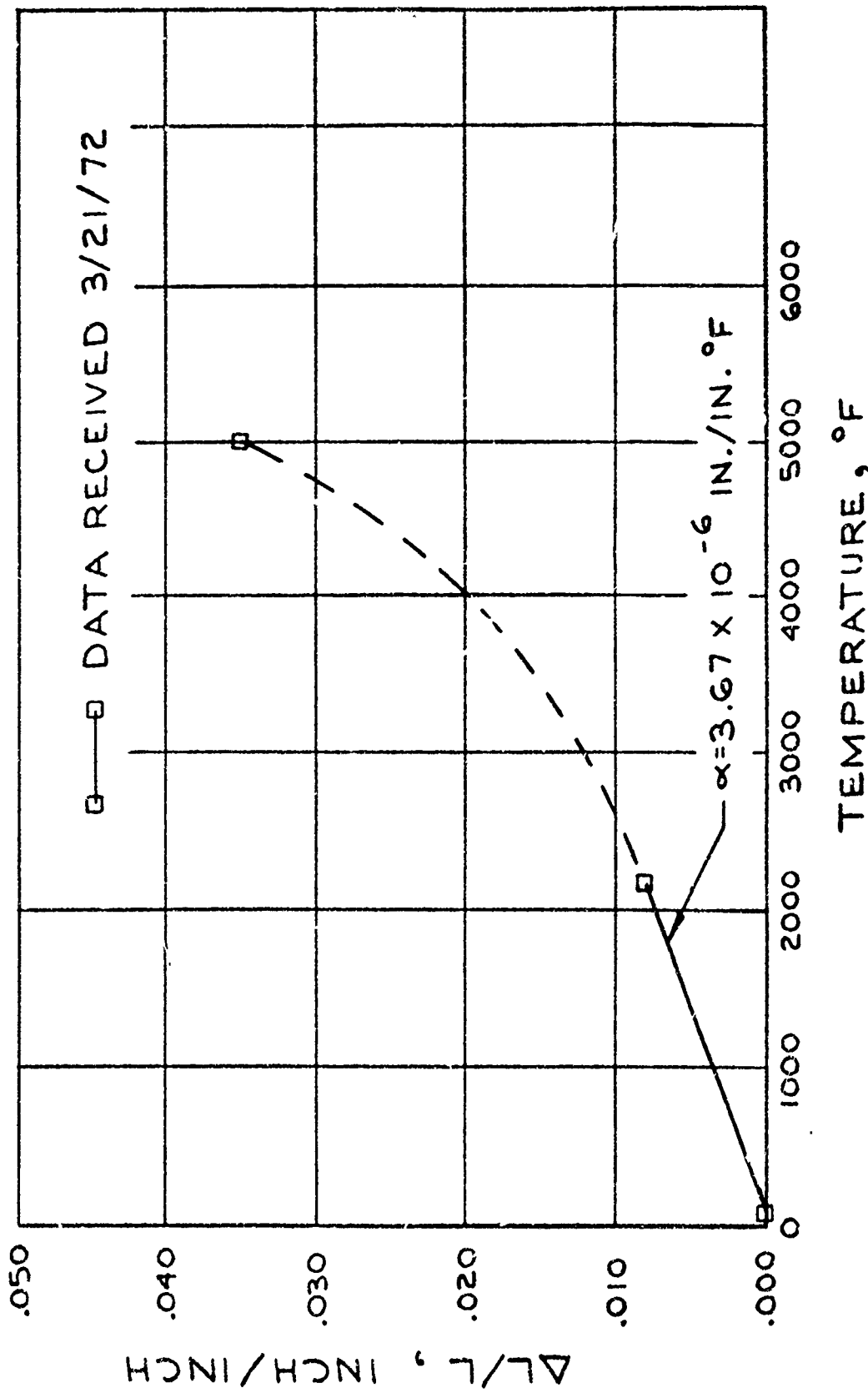


Figure 1. Thermal Expansion of Pycobond

## APPENDIX II

### THERMAL AND ABLATION ANALYSIS OF NOZZLES S/N 14 AND S/N 16

#### 1.0 INTRODUCTION

This thermal analysis report contains the results and conclusions of the work conducted by UTC during the later phases of Project 2410 on nozzles S/N-14 and S/N-16. This is not a complete analysis including all materials evaluated or configurations tested, but includes the analytical work conducted on the above referenced nozzles to determine the effect of the steps downstream of the Techmet<sup>R</sup> throat and the G-90 graphite ring.

#### 1.1 Scope of The Analysis

The following thermal analysis was conducted in order to determine the nozzle thermal adequacy as affected by the presence of the steps that were observed at the interfaces of the Techmet<sup>R</sup> throat and G-90, and the G-90 and Carbon Cloth Phenolic exit cone materials. It was observed in firing S/N-14, that there was significant ablation in the region of the nozzle downstream of the Techmet<sup>R</sup> throat package. The nozzle was very near a failure in the exit cone near the steel retainer ring which was exposed during the firing. Since the ablation of the G-90 was relatively large compared to firings conducted with ablating throats, and since the steel retainer ring was exposed, an extensive study was undertaken to attempt to understand what mechanisms could cause such a phenomenon. The primary objective was to model the ablation, and then apply the model to the subsequent static tests in order

to eliminate the high ablation. As a result, a few selected stations were chosen to be analyzed, assuming that the remainder of the nozzle was thermally adequate. This assumption is based upon prior test firing results with similar or the same configuration.

## 1.2 Nozzle Environment

The boundary conditions for the analysis were based upon the pressure trace of S/N-14 firing illustrated in figure 1. The propellant used throughout the analysis is UTP 11475 whose properties are given in table I.

FIGURE 1

CHAMBER PRESSURE VS. TIME FOR 2410 S/N 14 TEST

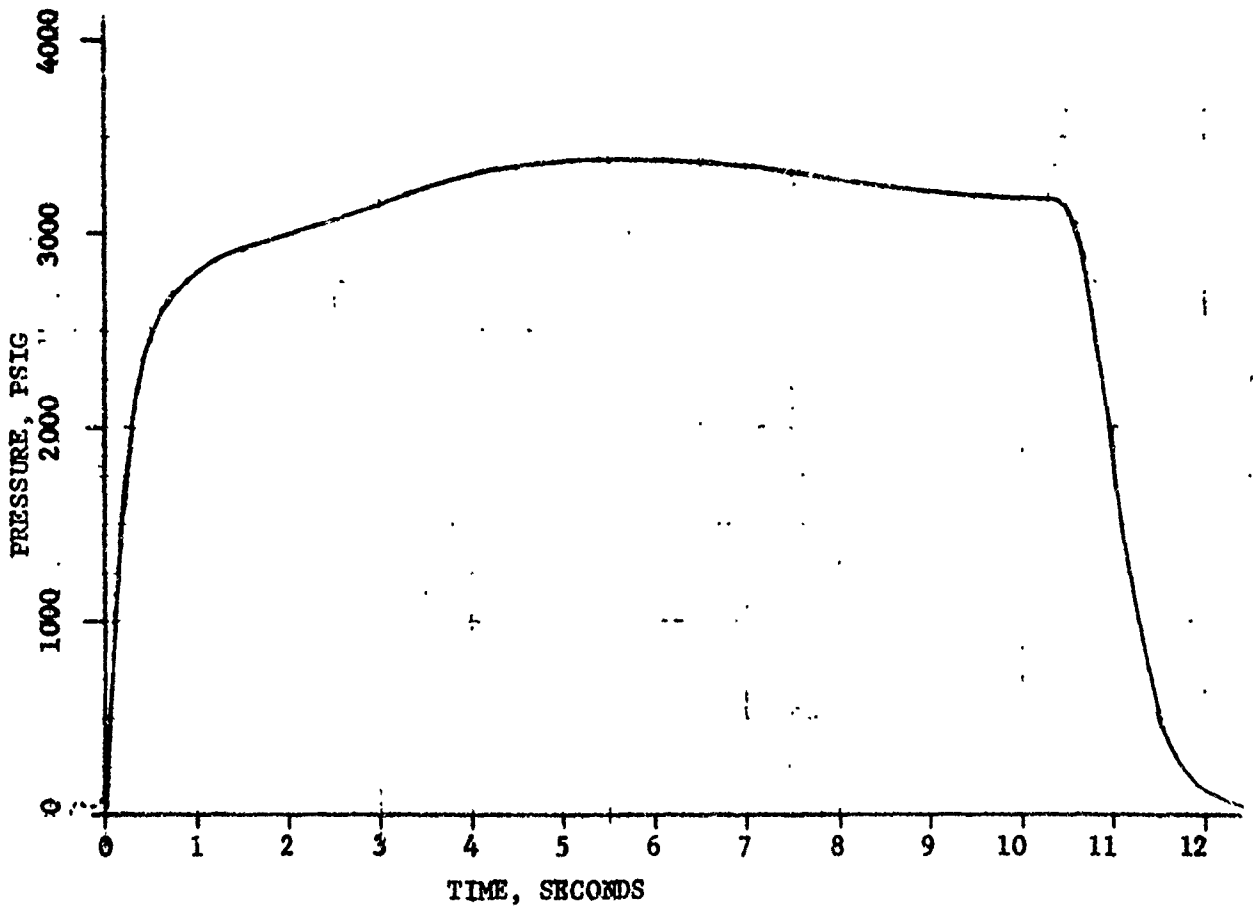


TABLE I  
GENERAL PROPELLANT DATA, UTP 11475

T-STAGNATION = 6692.4°R at 3250 PSIA  
 = 6704.5°R at 3500 PSIA

GAMMA = 1.141

PRANDTL NO. = 0.418

VISCOSITY =  $6.19 \times 10^{-5}$  Lbm/(ft. sec)

$C_p$ , FROZEN = 0.438

MOLECULAR WT. = 29.6 (combined gas, condensed)  
 = 20.37 (gal only)

$C_M/C_H$  = 0.693

ELEMENTAL COMPOSITION

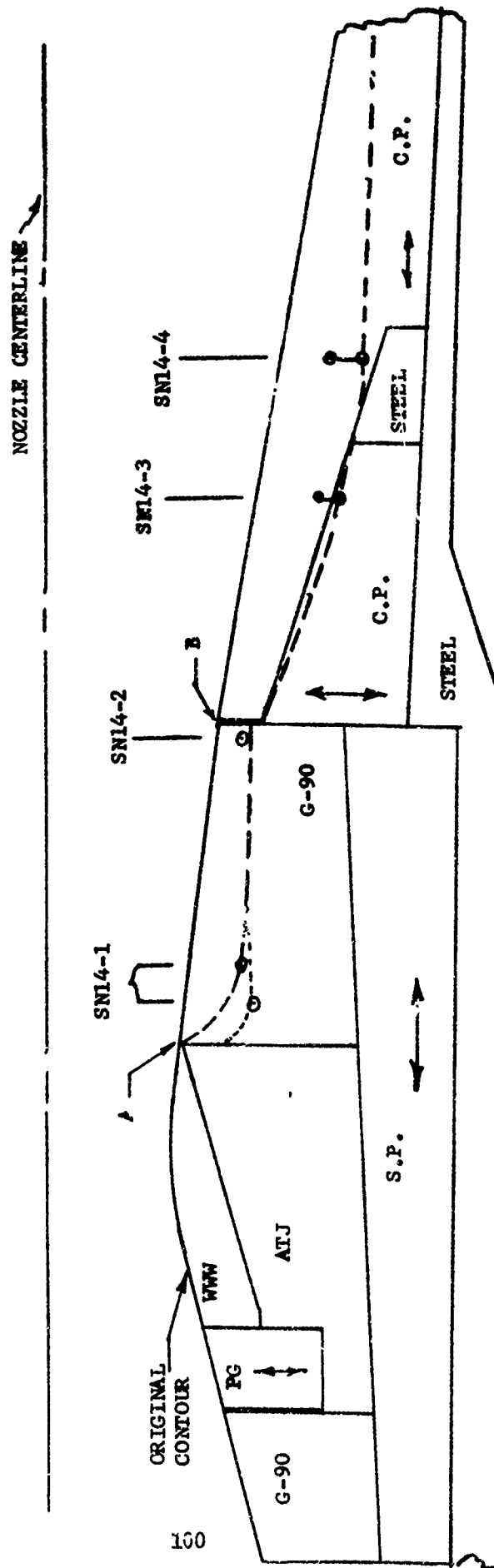
Hydrogen	3.677157
Carbon	0.826537
Nitrogen	0.600954
Oxygen	2.426413
Aluminum	0.667161
Chlorine	0.595745

## 2.0 SUMMARY OF THE RESULTS

The analysis was conducted in two basic parts, namely: (a) correlation of S/N-14 nozzle ablation, and (b) prediction of S/N-16 ablation performance downstream of the Techmet throat. The two throat schematics are shown in figures 2, and 3 including predicted and measured ablation depths for S/N-14 and S/N-16. Table II lists the analysis stations and the several parameters resulting from the analysis. The heat transfer coefficients and multipliers are included in addition to the predicted and measured ablation depths.

The results of the analysis have demonstrated that the heat transfer coefficients downstream of a step at low area ratios in the nozzle can increase anywhere from 1.4 (S/N-14) to 2.5 (S/N-16) times that at the upstream face of the step. The reasons for the range of the multipliers is not clear at this time. Subsequent studies are currently underway to clarify this difference, if possible. However, it may be necessary to take a significantly more sophisticated approach to prediction of the boundary layer and resultant separated region heat transfer than the one that has been taken in the present study. One approach would be to use a mass addition reacting boundary layer program (such as BLIMP) for more precise boundary layer calculations, and a laboratory testing program to measure the heating rates in the region of steps. The testing program should include extensive analysis and correlation and a parametric study to determine what factors can affect the step-region heat transfer.

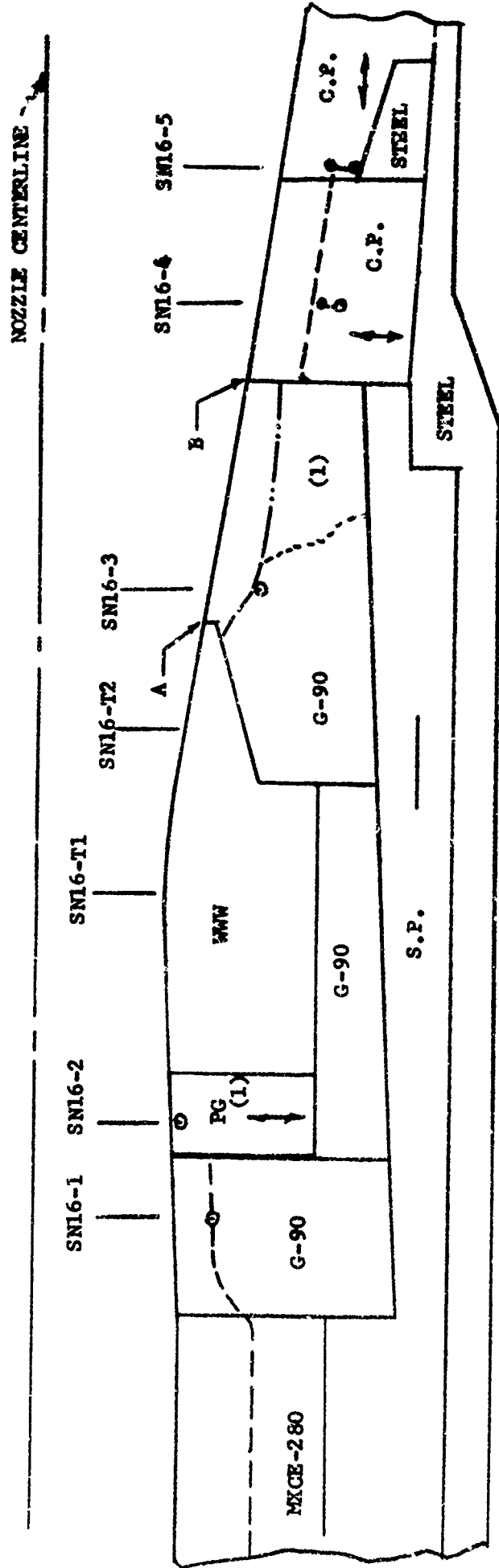
FIGURE 2-- S/M 14 NOZZLE



○ THERMOCHEMICAL CALCULATIONS  
 - - - - - POST-TEST MEASUREMENTS  
 ······ FRACTURED REGION

C.P. = CARBON PHENOLIC  
 S.P. = SILICA PHENOLIC

FIGURE 3 - S/N-16 NOZZLE



C.P. = CARBON PHENOLIC  
 S.P. = SILICA PHENOLIC

- ⊙ PRE-TEST THERMOCHEMICAL CALCULATIONS
- POST-TEST MEASUREMENTS
- ESTIMATED ABLATION, POST-TEST
- APPROXIMATE LOCATION OF FRACTURE

NOTE (1): THIS PORTION WAS MISSING  
 AFTER THE TEST

TABLE II

PROJECT 2410 ABLATION ANALYSIS SUMMARY

ANALYSIS STATION	MATERIAL ABLATED		HTC/C <sub>1</sub> at 3250 P <sub>PSIA</sub> (lbm/(ft <sup>2</sup> sec))	HTC MULTIPLIERS		INITIAL STATION RADIUS (IN.)
	PRED. (IN.)	MEAS. (IN.)		BARTZ	BOUNDARY LAYER	
SN14-1	0.481	0.45 <sup>#</sup>	5.580	1.2	2.1	1.06
SN14-1	0.352	0.35	3.627	0.8	1.37	1.06
SN14-2	0.179	0.22	2.402	-	1.0	1.25
SN14-3	0.440	0.54	2.420	-	1.0	1.45
SN14-3	0.580	0.54	3.025	-	1.25	1.45
SN14-4	0.343	0.55	1.949	-	1.0	1.60
SN14-4	0.531	0.55	2.924	-	1.5	1.60
SN16-1	0.256	0.25	3.081	-	0.75	0.98
SN16-2	0.066	**	3.260	-	0.75	0.94
SN16-3	0.326	0.30	3.877	1.2	2.50	1.225
SN16-3 <sup>*</sup>	0.185	-	2.731	1.0	1.75	1.225
SN16-4 SN16-5	***	0.35				

# This measurement reflects the region where the graphite was chipped away, not ablated.

\* This run had chemistry for no shock interaction and conventional flow gas dynamics.

\*\* This PG piece was missing after the test.

\*\*\* Predictions for these stations are the same as for SN14-3 and 4.

### 3.0 ANALYSIS

This section describes the details of the analysis conducted on the S/N-14 and S/N-16 nozzles. The first two subsections describe the computer programs and analytical methods used for this study and the thermal properties of the materials used. The third subsection describes the method of determining the boundary conditions used with the Charring Material Ablation (CMA) computer program. The next three subsections describe the details of the analysis for the S/N-14 and S/N-16.

### 3.1 DESCRIPTION OF THERMAL ANALYSIS COMPUTER PROGRAMS

#### 3.1.1 GASKET - Graphite Surface Kinetic Thermochemical Reactions

(Reference 1)\*

Program GASKET is used to describe the thermochemical reaction of a graphite (bulk or pyrolytic) with a gas environment assuming kinetically controlled reactions. The program can consider solid and liquid phases in equilibrium with the gas, and can compute the states of the exhaust gas within the chamber at different pressures, and expand isentropically to any Mach number. It can also consider normal or oblique shocks within the flow. Once the local static conditions are established by the program using appropriate input from the user, the program creates a table of temperature, enthalpy, chemical reaction terms, and non-dimensional ablation rates, for use with either program CMA or ASTHMA.

Typically, the program is first used to define the local thermodynamic properties of the exhaust gas at a specific nozzle location. This is done by using the elemental composition of the gas, the chamber temperature at 1,000 psia, the actual chamber pressure, and the Mach number of the location in question. The program then computes these states ending at the static conditions for the Mach number given. The next step is to determine the mass transfer coefficient to be used with the specific location of graphite ablation. This is computed from the boundary layer analysis and the value of  $C_M/C_H$  computed by GASKET. The next step is to use GASKET again, this time to compute the desired chemical tables to be used with the heat conduction program. The tables include the frozen edge (boundary layer edge conditions) table and the table of non-dimensional ablation rates mentioned earlier for the specific type of graphite in question. Generally, the tables are generated for a single pressure (average static pressure) and mass transfer coefficient,

\* References are listed on page 152.

but are applicable for small variations in pressure and mass transfer coefficient with little error. For large fluctuations in pressure, tables can be created for a series of pressures.

### 3.1.2 EST - Equilibrium Surface Thermochemistry (Reference 2)

This program is a general equilibrium thermochemistry program designed to provide non-dimensional ablation rate tables (similar to those from GASKET) for the CMA heat conduction program. The EST program, unlike GASKET, considers only diffusion controlled reactions (using equal or unequal diffusion factors) of the gas and surface material. The materials generally used with this program are the phenolic ablators such as graphite and carbon phenolics. These materials are charring ablators, such that they contain a resin that decomposes creating a gas which percolates through the material exhausting at the ablating surface. EST considers the surface reactions with the edge gas and the gases from the charring resin. During the ablation and charring processes, an infinite combination of surface material and gas reactions can take place. Therefore, a map of non-dimensional gas rates and non-dimensional surface removal rates are generated by EST for each designated pressure. CMA then takes these maps and uses interpolation to find the correct thermochemical state point for each step in time while the material is ablating and charring.

For this contract, the program was used for carbon phenolics (MXCE-280 and MX-4926). Generally, GASKET is used to get the local static state of the gas, and EST is subsequently used to generate the non-dimensional ablation rate and gas rate tables. Usually one pressure, the average pressure of the firing, is considered. Unlike GASKET, EST does not require a mass transfer coefficient.

**3.1.3 UARLED - Energy Deficit Integral Boundary Layer Program  
(United Aircraft Research Corp.)**

This program solves the boundary layer equations using an integral energy deficit technique. It can handle laminar and turbulent flow including transition from laminar to turbulent flow. The program assumes frozen flow with constant specific heat along the boundary layer. The nozzle contour and local Mach numbers are input, and wall temperature can be input as a constant or variable. Thermodynamic properties from GASKET are used to provide gas state data. This program is used to provide the local boundary layer properties and heat transfer coefficients.

### 3.1.4 CMA - Charring Material Ablation Computer Program (Reference 3)

For detailed thermal analysis of chemically ablating and charring materials, a complex thermochemical and heat conduction model is used which accounts for surface chemical reactions of the exhaust gas and surface materials as well as in-depth thermal degradation. This model is CMA or the Charring Material Ablation computer program. This program is used in conjunction with either EST or GASKET which provide thermochemical boundary condition tables of temperature, enthalpies, chemical reaction terms, and non-dimensional ablation rates. CMA can consider a surface material as well as back-up materials that are allowed to char, general back-wall boundary conditions, time varying heat transfer coefficient, pressure, recovery enthalpy, and radiation heat flux. Material thermal properties are input as functions of temperature and char state for the charring ablators. The program accepts virgin and char properties separately and internally combines them based upon the fraction of char that has taken place. Non-charring back-up material properties can also be functions of temperature. The solution to the one-dimensional heat equation is an implicit finite difference scheme which includes the effect of the non-homogeneous materials which may decompose in-depth. Internal decomposition is controlled by Arrhenius type reactions, one describing the matrix, and two describing the resin. For graphites, these reactions are not allowed to take place. Boundary conditions may include the full thermochemical reaction calculation which generates transient ablation rates on the surface, surface and in-depth temperatures and in-depth material decomposition for charring ablators. Two other boundary condition options are available where the surface ablation rate and temperature are assigned by

the user, but where the material is allowed to char in-depth; and one where the model is allowed to soak-out where the energy exchange to the surroundings is by radiation only. This option also allows in-depth charring. Output options in the program allow the user to get plots of the material surface and interfaces versus time, temperature profiles, and plots of the ablation rate and depth versus time.

The use of CEA for the nozzle analysis completes the sequence of operations for conducting a thermal analysis at one location. The necessary flow information has been generated yielding the Mach numbers for the boundary layer program. The boundary layer results, in the form of heat transfer coefficients, are used with the thermochemical data from GASKET or EST to form the set of boundary conditions necessary to complete the input data when joined with the geometrical specification and material property data. The resulting ablation rates and temperatures are then used in subsequent structural analysis, in addition to being checked for correlation with the design and analysis criteria.

### 3.1.5 LA15ZAZ - One-Dimensional Heat Conduction Computer Program (Reference 4)

Program LA15ZAZ is a UTC-developed one-dimensional heat conduction computer program which contains many boundary condition and geometry options. The program numerically solves the one-dimensional, axisymmetric heat equation by means of a backward difference or implicit finite difference technique. The solution allows the heat conduction model to contain several materials in series where the material thermal properties are functions of temperature. (Charring, however, is not considered in this program) The finite difference nodal structure can be spatially varied to accurately model regions of high thermal gradient with a greater number of nodes than areas where gradients are low. Surface erosion or ablation can be simulated by a node dropping scheme from either or both internal and external surfaces of the cylindrical model. Boundary conditions may include impressed surface temperature as a function of time, time and temperature dependent heat transfer coefficient with time dependent fluid recovery temperature, and incident radiant heat flux with re-radiation where the incident heat flux can be functions of time or of the surface temperature. The surface ablation imposed on either surface also can be time dependent and be combined with any of the above boundary conditions.

If desired, material interface resistance can be modeled by a constant conductance or one which is computed from radiation and conduction across a gas gap. Convenience features, such as the built-in convective heat transfer correlation of Bartz (reference 5), are included to aid in rapid analysis of nozzle components. Output features include normal tabular listing of temperature profiles at preselected times, and plots of temperature histories (of selected nodes) and temperature profiles (at selected times).

### 3.1.6 Radiation Heat Flux Calculations

Radiation heat flux is a required boundary condition to the heat conduction programs in addition to the convective heat flux. For most nozzle applications, the heat flux is computed as if the nozzle wall and exhaust gas are two parallel surfaces of infinite extent. This allows the use of the closed form of the equation of emissivity between two parallel planes:

$$\epsilon_{\text{eff}} = \frac{1}{1/\epsilon_{\text{wall}} + 1/\epsilon_{\text{gas}} - 1}$$

where:

$\epsilon_{\text{eff}}$  is the effective combined emissivity and view factor

$\epsilon_{\text{wall}}$  is the wall emissivity (usually assumed to be 0.89)

$\epsilon_{\text{gas}}$  is the gas emissivity described below.

The heat flux can then be computed from the following equation:

$$Q_{\text{rad}} = \epsilon_{\text{eff}} \sigma (T_{\text{gas}}^4 - T_{\text{wall}}^4)$$

where:

$\sigma$  is the Stefan-Boltzmann constant

$T_{\text{gas}}$  is the gas static temperature

$T_{\text{wall}}$  is the instantaneous wall temperature

The gas emissivity is computed by a form of the Beer's equation using constants developed at UTC for particle laden gas stream (Reference 5).

The equation is:

$$\epsilon_{\text{gas}} = 1 - e^{-(\rho cd)}$$

where:

$\rho$  is the local static stream density ( $\text{lb}/\text{ft}^3$ )

$d$  is the local diameter or view length (inches)

$c$  is a coefficient determined from Reference 6

The absorption coefficient,  $\rho c$ , of a particle-laden gas stream is proportional to the effective beam length and the number density of the particles. The number density of the particles is, in turn, a function of the gas density. The constant,  $c$ , varies directly with the amount of  $Al_2O_3$  in the exhaust products.

The tests in Reference 6 were made with UTP 3001 propellant where the constant,  $c$ , is 0.808. The constant for UTP 11475 is 0.883 and is determined from the ratio of  $Al_2O_3$  in the given propellant to that of UTP 3001 at the throat multiplied by 0.808.

### 3.2 Material Thermal Properties

The thermal properties used in this analysis are presented in Tables III through XI. For the charring materials, which are those ablative materials used in the Charring - Material Thermal Response and Ablation Program (CMA), the thermal conductivity, specific heat, and density are presented for both the virgin and char states. When charring materials are used with the non-charring heat conduction computer programs, or as backup materials in the CMA program, a single composite curve is used which represents the virgin properties at low temperatures and the char properties at high temperatures, with the point of transition at approximately 750°F.

Where a charring material wrap angle is indicated, 0° wrap refers to a material wrapped parallel to the nozzle centerline and 90° wrap refers to materials wrapped perpendicular to the centerline. For a material that is wrapped at an angle,  $\theta$ , between 0° and 90°, the thermal conductivity may be computed from:

$$K = K_{0^{\circ}} \left[ 1 + \left( \frac{K_{90^{\circ}}}{K_{0^{\circ}}} - 1 \right) \text{SIN } \theta \right] \quad (\text{Reference 7})$$

For anisotropic materials, the thermal conductivity is presented for the directions of maximum and minimum conductivity, indicated by "with grain", "with laminate", and "against grain", "against laminate", or "low K" and "high K" direction.

TABLE III

G-90 GRAPHITE, AGAINST GRAIN

DENSITY = 0.068000 LB/IN<sup>3</sup>  
 DISK PROPERTY NO. = 28

TEMPERATURE DEG F	SPECIFIC HEAT BTU/(LB. F)	THERMAL CONDUCTIVITY BTU/(IN. SEC. F)
0.00	0.15250	2.02500E-03
750.00	0.36083	1.29200E-03
1250.00	0.41000	9.25900E-04
1500.00	0.43000	7.98600E-04
2000.00	0.46000	6.59700E-04
2500.00	0.48000	5.67100E-04
3000.00	0.49000	4.88400E-04
3500.00	0.50000	4.32900E-04
4000.00	0.51000	3.93500E-04
4500.00	0.52000	3.72700E-04
5000.00	0.52500	3.61100E-04
5500.00	0.53000	3.58800E-04

TABLE IV

G-90 GRAPHITE, WITH GRAIN

DENSITY = 0.068000 LB/IN<sup>3</sup>  
 DISK PROPERTY NO. = 29

TEMPERATURE DEG F	SPECIFIC HEAT BTU/(LB. F)	THERMAL CONDUCTIVITY BTU/(IN. SEC. F)
0.00	0.15250	2.31500E-03
750.00	0.36083	1.48800E-03
1000.00	0.39000	1.30000E-03
1500.00	0.43000	1.00200E-03
2000.00	0.46000	8.21700E-04
2500.00	0.48000	7.06000E-04
3000.00	0.49000	6.25000E-04
3500.00	0.50000	5.69400E-04
4000.00	0.51000	5.32400E-04
4500.00	0.52000	5.16200E-04
5000.00	0.52500	5.04600E-04
5500.00	0.53000	5.00000E-04

TABLE V

## PYROLYTIC GRAPHITE, HIGH CONDUCTIVITY DIRECTION

DENSITY = 0.079500 LB/IN<sup>3</sup>  
 DISK PROPERTY NO. = 9

TEMPERATURE DEG F	SPECIFIC HEAT BTU/(LB, F)	THERMAL CONDUCTIVITY BTU/(IN, SEC, F)
0.00	0.25000	5.20800E-03
250.00	0.28000	5.09200E-03
500.00	0.31000	4.79100E-03
650.00	0.32800	4.62900E-03
1000.00	0.37000	4.05000E-03
1250.00	0.39500	3.47200E-03
1500.00	0.42000	2.89300E-03
1900.00	0.46000	2.31400E-03
2450.00	0.50600	1.73600E-03
2850.00	0.53100	1.44600E-03
3350.00	0.55400	1.15700E-03
4000.00	0.58000	9.00000E-04
4500.00	0.59000	7.50000E-04
5000.00	0.60000	6.50000E-04
5500.00	0.61000	5.50000E-04
6000.00	0.62000	5.00000E-04

TABLE VI

## ATJ GRAPHITE

DENSITY = 0.062470 LB/IN<sup>3</sup>  
 DISK PROPERTY NO. = 7

TEMPERATURE DEG F	SPECIFIC HEAT BTU/(LB, F)	THERMAL CONDUCTIVITY BTU/(IN, SEC, F)
0.00	0.13500	1.50000E-03
700.00	0.35675	1.00000E-03
1000.00	0.39250	8.40000E-04
1500.00	0.43300	6.70000E-04
2000.00	0.45800	5.40000E-04
3000.00	0.49000	3.70000E-04
4000.00	0.51322	3.10000E-04
5000.00	0.53365	2.90000E-04

TABLE VII

TECHMET, WIRE-WOUND TUNGSTEN COMPOSIT

DENSITY = 0.574000 LB/IN\*3  
 DISK PROPERTY NO. = 13

TEMPERATURE DEG F	SPECIFIC HEAT BTU/(LB. F)	THERMAL CONDUCTIVITY BTU/(IN. SEC. F)
50.00	0.03310	8.69000e-05
662.00	0.03464	8.02200e-05
932.00	0.03467	8.28500e-05
1292.00	0.03490	1.04300e-04
1652.00	0.03530	1.63100e-04
2012.00	0.03610	3.01000e-04
2372.00	0.03690	4.33200e-04
2732.00	0.03770	5.05400e-04
2912.00	0.03820	5.22800e-04
3272.00	0.03920	5.14700e-04
3632.00	0.04020	4.99000e-04
7032.00	0.05156	2.08000e-04

TABLE VIII

4130 STEEL

DENSITY = 0.283000 LB/IN\*3  
 DISK PROPERTY NO. = 23

TEMPERATURE DEG F	SPECIFIC HEAT BTU/(LB. F)	THERMAL CONDUCTIVITY BTU/(IN. SEC. F)
0.00	0.11000	5.80000e-04
200.00	0.11500	5.75000e-04
400.00	0.12000	5.70000e-04
600.00	0.13500	5.42000e-04
800.00	0.14900	5.20000e-04
1000.00	0.16500	4.75000e-04
1200.00	0.18000	4.42000e-04
1300.00	0.18750	4.42000e-04

TABLE IX

THERMAL PROPERTIES FOR CMA

MX-4926, CARBON PHENOLIC, FIBERS PARALLEL TO C.L. (O-WRAP)

---REACTION KINETIC CONSTANTS---

REACTION	KH00 (LB/CU FT)	RHOR (LB/CU FT)	B (1/SEC)	PSI	E (DEG R)	T REAC (DEG R)
A	60.75	32.40	4.480E+09	3.00	3.680E+04	600.
B	20.25	0.00	1.400E+04	3.00	1.540E+04	1000.
C	94.56	94.56	0.000E+00	0.00	0.000E+00	90000.

MASS FRACTION = 0.34500

RESIN RESIDUAL = 0.40000

VIRGIN ::: DENSITY = 89.397 LB/CU FT      HEAT FORM. = -379.50 BTU/LB

TEMPERATURE (DEG R)	SPECIFIC HEAT (BTU/LB-DEG R)	THERMAL CONDUCTIVITY (BTU/FT-SEC-DEGR)    (BTU/IN-SEC-DEGR)	
530.00	0.210000	1.3900E-04	1.1583E-05
800.00	0.360000	1.5800E-04	1.3167E-05
1160.00	0.360000	1.8300E-04	1.5250E-05
1500.00	0.472000	1.8300E-04	1.5250E-05
2000.00	0.484000	1.8300E-04	1.5250E-05
3000.00	0.493000	1.8300E-04	1.5250E-05
4000.00	0.498000	1.8300E-04	1.5250E-05
5000.00	0.500000	1.8300E-04	1.5250E-05
6000.00	0.500000	1.8300E-04	1.5250E-05

CHAR ::: DENSITY = 70.892 LB/CU FT      HEAT FORM. = 0.00 BTU/LB

TEMPERATURE (DEG R)	SPECIFIC HEAT (BTU/LB-DEG R)	THERMAL CONDUCTIVITY (BTU/FT-SEC-DEGR)    (BTU/IN-SEC-DEGR)	
530.00	0.210000	1.8300E-04	1.5250E-05
1000.00	0.430000	1.9000E-04	1.5833E-05
1500.00	0.472000	1.9500E-04	1.6250E-05
2000.00	0.484000	2.3500E-04	1.9583E-05
3000.00	0.493000	5.4000E-04	4.5000E-05
4000.00	0.498000	1.1650E-03	9.7083E-05
5000.00	0.500000	1.8800E-03	1.5667E-04
6000.00	0.500000	2.6500E-03	2.2083E-04

TABLE X

THERMAL PROPERTIES FOR CMA

MX-4926, CARBON PHENOLIC, TAPE PERPENDICULAR TO CL, (90-WRAP)

---REACTION KINETIC CONSTANTS---

REACTION	RH00 (LB/CU FT)	RHOR	B (1/SEC)	PSI	E (DEG R)	T REAC (DEG R)
A	60.75	32.40	4.480E+09	3.00	3.680E+04	600.
B	20.25	0.00	1.400E+04	3.00	1.540E+04	1000.
C	94.56	94.56	0.000E+00	0.00	0.000E+00	90000.

MASS FRACTION = 0.34500

RESIN RESIDUAL = 0.40000

VIRGIN : : : DENSITY = 89.397 LB/CU FT      HEAT FORM. = -379.50 BTU/LB

TEMPERATURE (DEG R)	SPECIFIC HEAT (BTU/LB-DEG R)	THERMAL CONDUCTIVITY (BTU/FT-SEC-DEGR)      (BTU/IN-SEC-DEGR)	
530.00	0.210000	2.3600E-04	1.9667E-05
800.00	0.360000	2.6900E-04	2.2417E-05
1160.00	0.360000	3.1100E-04	2.5917E-05
1500.00	0.472000	3.1100E-04	2.5917E-05
2000.00	0.484000	3.1100E-04	2.5917E-05
3000.00	0.493000	3.1100E-04	2.5917E-05
4000.00	0.498000	3.1100E-04	2.5917E-05
5000.00	0.500000	3.1100E-04	2.5917E-05
6000.00	0.500000	3.1100E-04	2.5917E-05

CHAR : : : DENSITY = 70.892 LB/CU FT      HEAT FORM. = 0.00 BTU/LB

TEMPERATURE (DEG R)	SPECIFIC HEAT (BTU/LB-DEG R)	THERMAL CONDUCTIVITY (BTU/FT-SEC-DEGR)      (BTU/IN-SEC-DEGR)	
530.00	0.210000	3.1100E-04	2.5917E-05
1000.00	0.430000	3.1500E-04	2.6250E-05
1500.00	0.472000	3.2000E-04	2.6667E-05
2000.00	0.484000	4.1500E-04	3.4583E-05
3000.00	0.493000	8.9500E-04	7.4583E-05
4000.00	0.498000	1.4700E-03	1.2250E-04
5000.00	0.500000	2.1250E-03	1.7708E-04
6000.00	0.500000	2.8350E-03	2.3625E-04

TABLE XI

THERMAL PROPERTIES FOR CMA

MX-2600, SILICA PHENOLIC, TAPE PARALLEL TO CENTERLINE (O-WRAP)

---REACTION KINETIC CONSTANTS---

REACTION	KHOD (LB/CU FT)	RHOR	B (1/SEC)	PSI	E (DEG R)	T REAC (DEG R)
A	20.25	0.00	1.400E+04	3.00	1.540E+04	600.
B	60.75	40.50	4.480E+09	3.00	3.680E+04	1000.
C	128.98	128.98	0.000E+00	0.00	0.000E+00	90000.

MASS FRACTION = 0.31500

RESIN RESIDUAL = 0.50000

VIRGIN :: DENSITY = 108.700 LB/CU FT      HEAT FORM. = -4805.85 BTU/LB

TEMPERATURE (DEG R)	SPECIFIC HEAT (BTU/LB-DEG R)	THERMAL CONDUCTIVITY (BTU/FT-SEC-DEGR) (BTU/IN-SEC-DEGR)	
530.00	0.260000	9.4000E-05	7.8333E-06
800.00	0.275000	9.4300E-05	7.8583E-06
1160.00	0.310000	9.4400E-05	7.8667E-06
1500.00	0.472000	9.4400E-05	7.8667E-06
2000.00	0.484000	9.4400E-05	7.8667E-06
3000.00	0.493000	9.4400E-05	7.8667E-06
4000.00	0.498000	9.4400E-05	7.8667E-06
5000.00	0.500000	9.4400E-05	7.8667E-06

CHAR :: DENSITY = 91.580 LB/CU FT      HEAT FORM. = -5293.00 BTU/LB

TEMPERATURE (DEG R)	SPECIFIC HEAT (BTU/LB-DEG R)	THERMAL CONDUCTIVITY (BTU/FT-SEC-DEGR) (BTU/IN-SEC-DEGR)	
530.00	0.210000	2.9400E-04	2.4500E-05
1000.00	0.430000	3.0600E-04	2.5500E-05
1500.00	0.472000	3.2000E-04	2.6667E-05
2000.00	0.484000	3.3100E-04	2.7583E-05
3000.00	0.493000	2.5700E-04	2.1417E-05
3500.00	0.495000	3.6800E-04	3.0667E-05
4000.00	0.498000	3.9600E-04	3.3000E-05
5000.00	0.500000	5.4500E-04	4.5417E-05

F = FUNCTION, WHERE:  $K = F1(X) \times KVIRGIN(TEMP) + F2(X) \times KCHAR(TEMP)$

X=VIR. MASS FR.	F1(X), VIRGIN	F2(X), CHAR
0.0000	0.0000	1.0000
0.2500	0.0000	1.0000
0.5500	0.5000	0.0000
0.8000	0.5000	0.0000
1.0000	1.0000	0.0000

### 3.3 Heat Transfer Boundary Conditions Including Shock and Boundary Layer Interaction

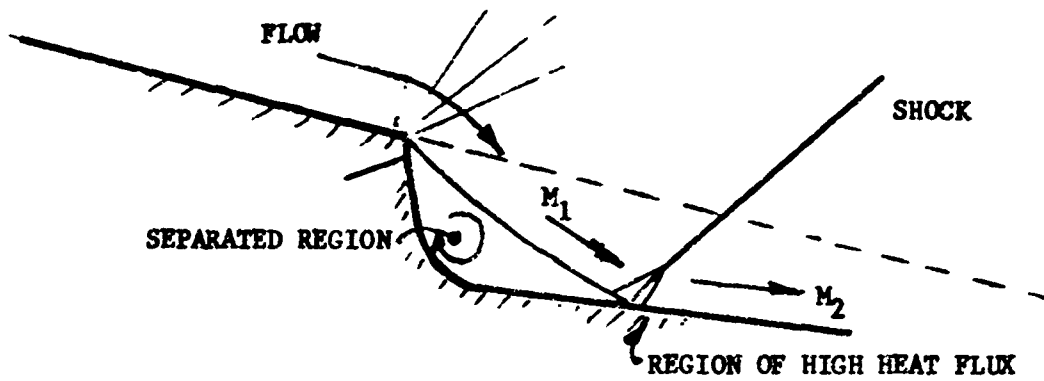
#### 3.3.1 Rationale and Assumptions

Analysis of the ablation downstream of a step in a supersonic stream poses a difficult and complex challenge, since there are not available state-of-the-art analytical techniques that can handle the computation of the flow over the resultant separated region. Figure 4 shows the nature of the flow within this region and the shock model used for the analysis. Limited heat transfer data are available as to the effect of the flow re-attachment and shock interaction on the downstream surface for flat-plate steps, but there is virtually no heat transfer data for steps within accelerating flows. For the flat-plate data available, the presence of the step does not increase the general free stream Mach number. For the nozzles investigated here, just the opposite is true; the nozzle is diverging and the step increases the Mach number beyond that of the normal divergence effect.

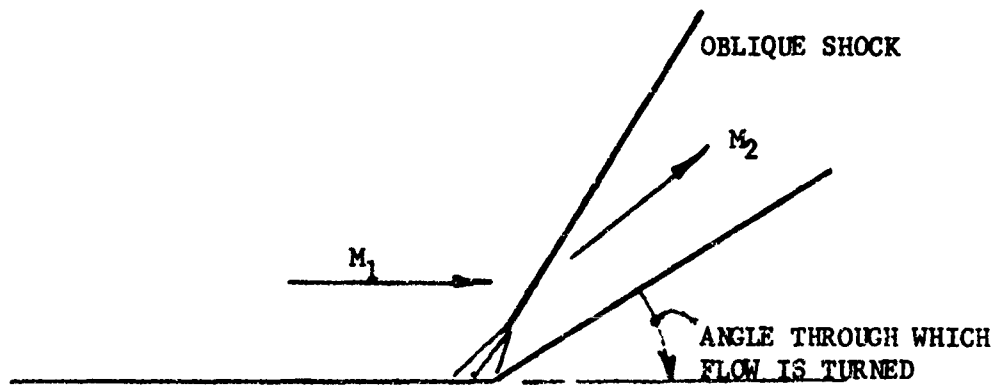
With limited outside data available, it was decided that the best data was that of the nozzle S/N-14 where the G-90 ring downstream of the Techmet throat was available for ablation correlation. As with other observers that correlate heat transfer data in regions of steps, the logical approach for correlation was to base the estimated heat transfer rates in the re-attachment region, on the heat transfer coefficient at the upstream lip of the step. Therefore, starting with that value, one could iterate with heat transfer multipliers until a multiplier was found that matched the ablation measured downstream of the step. This of course, would be an average multiplier, since the nozzle wall does not start out as a step, but one

develops as time becomes greater during a motor test. Once a small step develops, it is assumed that a similar pattern of flow and shock develops, independent of the step size, as long as the step is outside of the subsonic portion of the boundary layer. With these ideas in mind, the assumptions for the analysis were formulated and are summarized below:

1. The heat flux downstream of the face of the step can be defined by a multiplier on the heat flux at the point just upstream of the step. This multiplier would apply to the maximum heat flux encountered.
2. An energy integral boundary layer analysis will be used to predict local heat fluxes upstream of steps.
3. One dimensional gas dynamics will apply for the calculation of local Mach numbers and shock angles based upon the angle of the wedge.
4. The upstream Mach number approaching the oblique shock will be computed using the local diameter at the wall where the shock attaches.
5. The point of re-attachment of the flow coming over the step is assumed to be approximately 1.8 times the step height, downstream of the step face (reference 8).
6. The gas dynamics through the shock are computed by means of thermochemical calculations (program GASKET); and the subsequent ablation is defined by bulk graphite kinetic reaction calculations using program GASKET.



SCHEMATIC OF AFT FACING STEP IN NOZZLE EXIT



WEDGE FLOW MODEL OF AFT FACING STEP IN NOZZLE EXIT

FIGURE 4 - OBLIQUE SHOCK FLOW MODELS FOR ABLATION ANALYSIS

### 3.3.2 Boundary Layer Calculations

During a preliminary phase of the analysis correlation, the Bartz turbulent heat transfer correlation was used to estimate the heat transfer coefficients. Subsequently, an energy integral boundary layer program was used (UARLED, section 3.1.3) to obtain improved results. The resultant heat transfer coefficients are plotted in figures 5 and 6 for a wall temperature of 5000°F and the propellant properties listed in table I. The point marked "A" in the two figures defines the heat transfer coefficient at the step lip that was used as the baseline for the correlation and prediction.

For nozzle S/N-14, the boundary layer was re-started at each re-attachment point. The conditions at the restart point, just downstream of the shock, include an increase of the energy deficit and momentum thickness by 10% of the value at the lip of the step. This increase is an engineering estimate of the conditions at the restart based upon examination of references 8 and 9. In addition, the stagnation pressure was taken as that for the downstream shock state, either  $P_{02}$  or  $P_{04}$ , as shown in figure 7. The Mach numbers in each region (II and III, figure 7) are determined by defining an effective throat diameter that will result in the downstream oblique shock Mach number,  $M_2$  or  $M_4$ , for the corresponding local diameter. The flow was then expanded appropriately using the local diameters, the effective throat diameter and one-dimensional gas dynamic relations. The result of this procedure was to define the boundary layer and heat transfer coefficients for the regions in the G-90 downstream of the first step, and that in the carbon phenolic downstream of the G-90. No heat transfer estimates were made for the separated regions between the steps and the re-attachment points. It is notable that the effect of the step is to increase the heat transfer coefficients downstream, over those of the smooth nozzle. For

each of the boundary layer runs, the boundary layer was started within the aft closure using a turbulent start criteria.

For this phase of the analysis, reference 8 was used to estimate the length of the separated region downstream of the step. This reference indicated that the value of 1.8 times the step height could be used. Since the analysis was completed, other references (9, 10, 11) have been obtained and reviewed which suggested a better approach. A subsequent analysis is currently underway to re-evaluate the data from motor firings for nozzles S/N 14 and 16 using these new references.

### 3.3.3 Shock Region Calculations

Once the boundary layer results were obtained, the thermo-chemistry could be computed in order to obtain non-dimensional ablation rate curves at the points in question. The procedure listed below outlines the method of obtaining the chemistry behind the shock at the re-attachment location.

1. Determine an average Mach number using an average diameter in the region downstream of the step face, as that Mach number entering the shock caused by flow re-attachment.
2. Using GASKET, expand the flow from chamber conditions to the upstream Mach number, and then through the shock to get static conditions behind the shock. The angle the flow is turned is determined by the geometry of the step and exit cone half-angle. This angle then can be used to determine the oblique shock angle that is required by GASKET.
3. Using the static conditions behind the shock, the bulk graphite kinetics can be computed by GASKET to yield the  $\dot{B}$  curve and recovery enthalpy with which to run CMA. CMA will then predict transient ablation rates and in-depth temperatures.

When the correlation was complete, the heat transfer multipliers were then applied to the S/N-16 configuration. For this calculation, an estimated ablation depth was made in order to obtain the separated region geometry.

FIGURE 5

S/N 14 BOUNDARY LAYER ANALYSIS

HEAT TRANSFER COEFFICIENT VS. DISTANCE

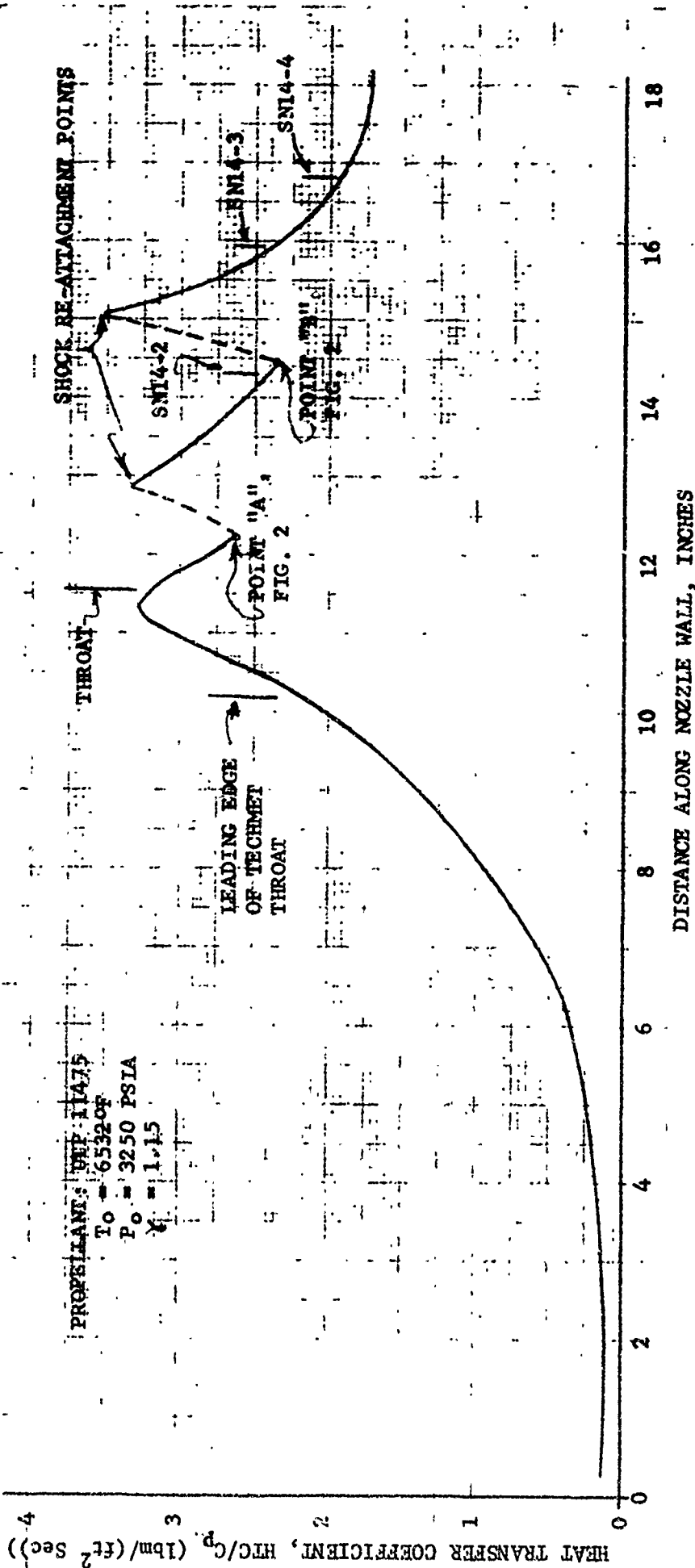


FIGURE 6

S/N - 16 BOUNDARY LAYER ANALYSIS  
HEAT TRANSFER COEFFICIENT VS. DISTANCE

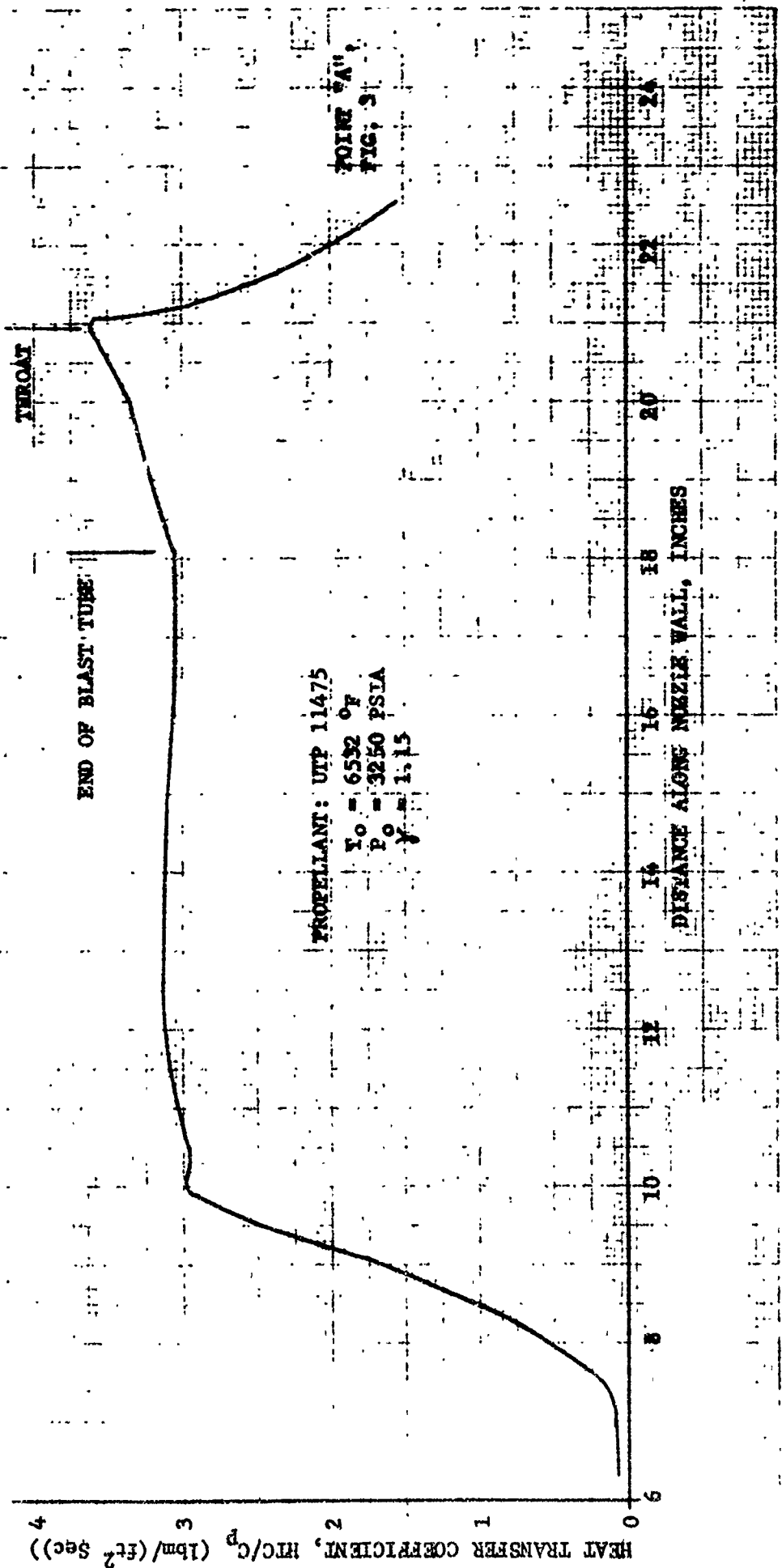
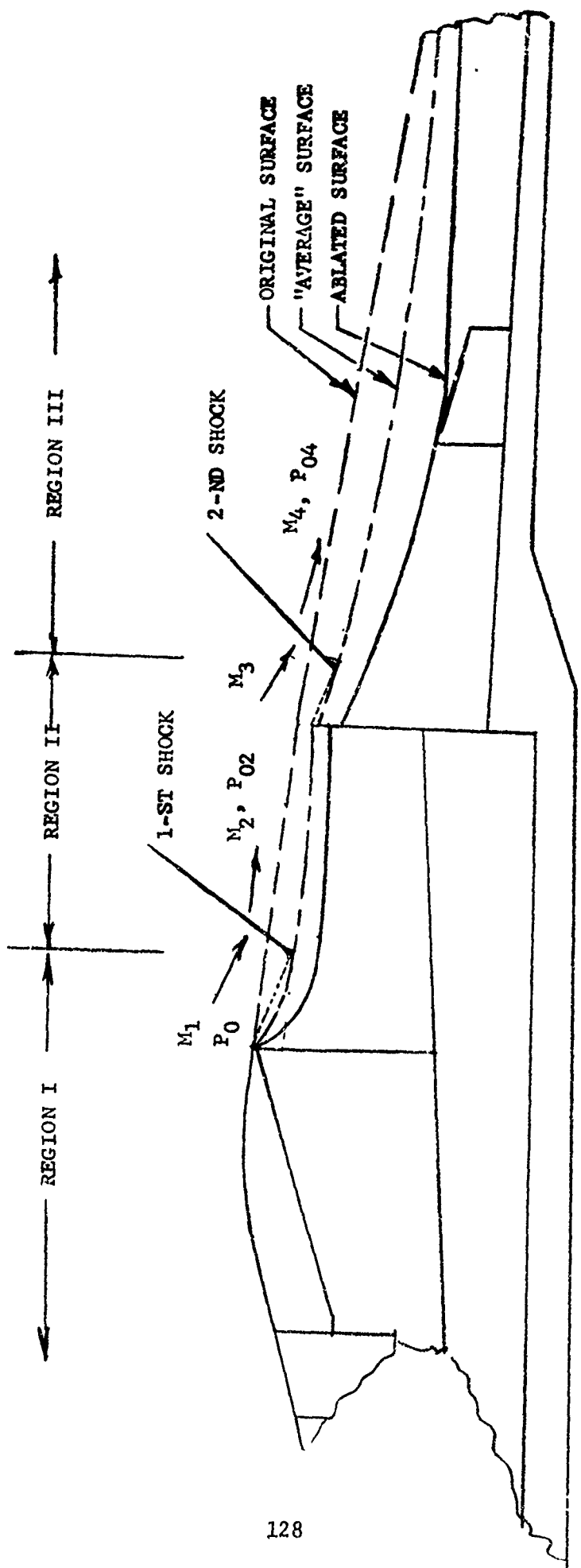


FIGURE 7 - FLOW AND SHOCK STRUCTURE FOR S/N-14 NOZZLE



### 3.4 Correlation of S/N-14 Nozzle Ablation

#### 3.4.1 Initial Calculations for S/N-14 and S/N-16

The ablation correlation of the G-90 ring downstream of the TECHMET throat was initiated using the Bartz heat transfer correlation for an estimate of the heat transfer rate at the nozzle step lip. For this first phase, it was generally unimportant how the heat transfer coefficient (HTC) was obtained, since one was to be found that would match the measured ablation data. This initial heat transfer coefficient was modified using the pressure trace of figure 1 to account for the pressure changes with time. It was found that a multiplier of 1.2 on the Bartz HTC would predict the downstream ablation. In order to provide preliminary design support, this same multiplier was used for an analysis of the step that was predicted in the S/N-16 throat using the Bartz heat transfer coefficient correlation. Subsequently, when the boundary layer runs were made, the resultant HTC values were significantly different than those of the Bartz calculations. It was noted that the new heat transfer coefficient ratios were no longer the same for the two nozzles (see Table II).

Initially, a maximum ablation depth of S/N-14 was reported to be 0.45 inches, downstream of the throat, thus providing a value that was to be matched. However, when the G-90 region was later re-examined, it was found that those highly "ablated" regions were actually located where the graphite had chipped away, failing structurally, rather than ablating away. Figure 2 reflects both of these contours. Prior to this discovery, however, the prediction of S/N-14 had been made. Since this prediction would be conservative, however, no new predictions were made.

Examination of the corrected ablation contour of S/N-14 showed that the maximum ablation depth was 0.35 inches. During the correlation sequence using the Bartz heat transfer coefficient, a run was made for a multiplier of 0.8. This run shows remarkable agreement with the measurement. When the boundary layer run was made, the values of the heat transfer multipliers were re-evaluated and found to be 2.1 for the run that matched the erroneous ablation depth, and 1.37 for that matching the actual maximum ablation depth. For the S/N-16 nozzle, this revised multiplier was 2.5. Since much of the G-90 ring aft of the TECHMET throat in S/N-16 was missing after the test, the measured ablation data is questionable. There was about  $\frac{1}{2}$  inch of usable data, and it was apparent that the location of the maximum ablation depth was probably downstream of the existing part. However, if one extrapolates the ablation as shown in figure 3, using the experience of S/N-14, one generates the dashed line indicated in figure 3. Using this extrapolation, the maximum ablation depth is apparently 0.3 inches. This compares reasonably well to the prediction of 0.326 inches which came from the original prediction based upon the Bartz heat transfer coefficient. It is obvious that if the 1.37 heat transfer coefficient multiplier were used for S/N-16, the ablation depth would have been significantly under predicted. This fact suggests that there is some significant factor necessary for accurate prediction that is being ignored in this analysis. Suggested approaches to finding the missing link will be discussed in section 4.0, the Conclusions.

A summary of the results of the two runs at station SN14-1 (figure 2) is given in table II. The non-dimensional ablation rate curves for the two runs are shown in figure 8, the temperature profiles in figures 9 and 10, and the transient ablation rates in figure 11. Although the ablation is severe, the silica phenolic insulation provides sufficient protection to the nozzle shell.

#### 3.4.2 Other Stations Analyzed on the S/N-14 Nozzle

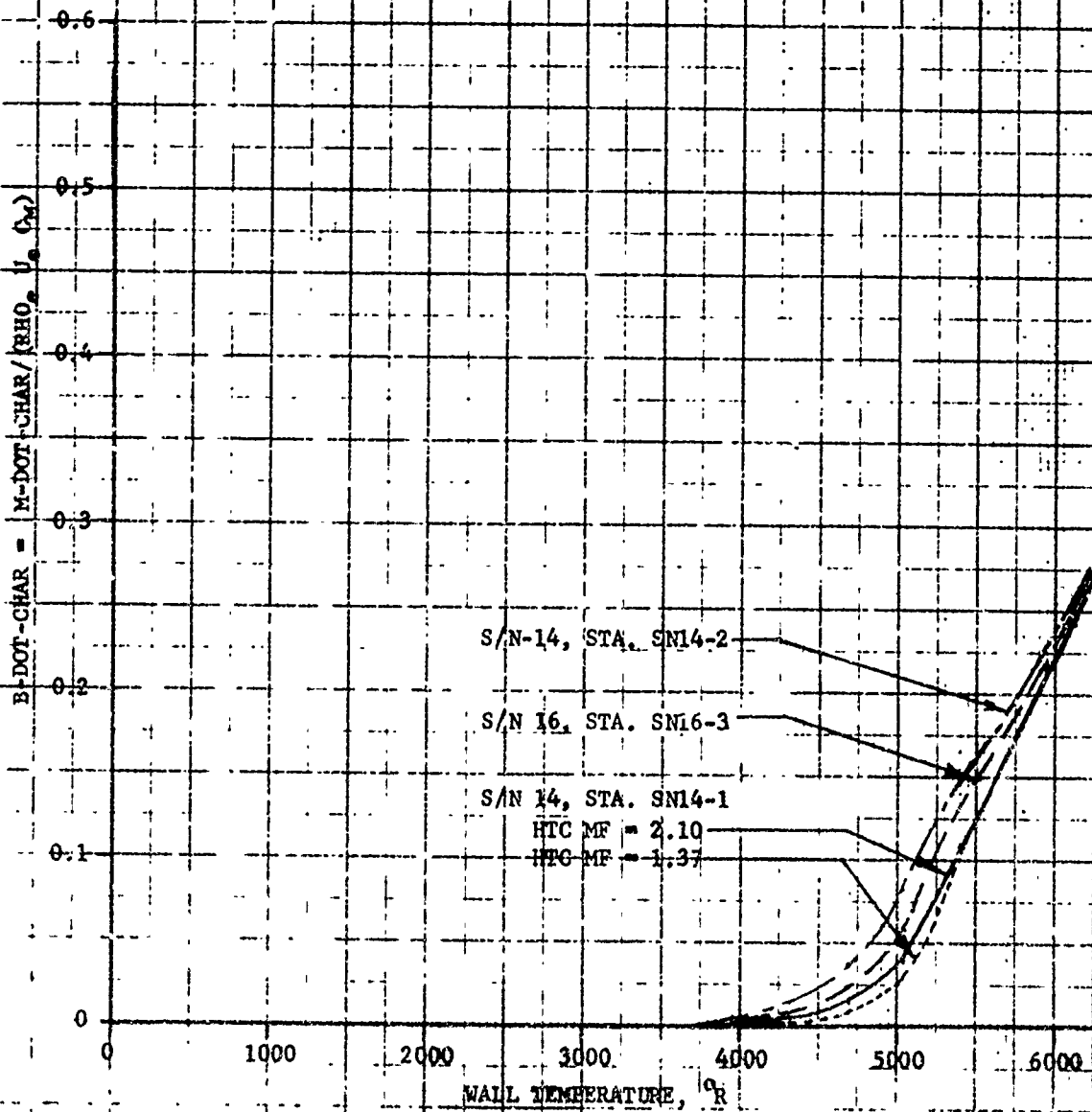
In addition to station SN14-1, 3 other stations were examined to correlate ablation downstream of the first step. Station SN14-2 was chosen to see if that region would be predicted using the re-start boundary layer approach. The results indicated that by using the boundary layer value of the heat transfer coefficient with no multiplier, the ablation was under predicted by about 18%. This suggests that some shock and re-attachment interaction is still present, or that the model used needs improvement. The non-dimensional ablation rate curve is shown in figure 8, the temperature profiles in figure 12 and the transient ablation rate in figure 13.

Two additional stations (SN14-3 and 4) in the carbon phenolic region of the exit cone were studied to see if there was any correlation of the ablation data with conventional diffusion controlled thermochemical prediction techniques that have been used on other nozzles. It was apparent from an examination of the post test exit cone that there may have been some mechanical removal of the surface layer of carbon phenolic due to the wrap orientation (parallel to the nozzle centerline). However, an attempt to predict the ablation at two locations was made. The boundary layer run was made using a contour half way in between the initial and final contours, starting it downstream of the apparent re-attachment point. At the locations of SN14-3 and 4, an attempt was made to match the ablated depth. Table II lists the results of the four runs that were made, where multipliers of

1.0, 1.25, and 1.5 were applied to the local value of the predicted heat transfer coefficient. Since the actual mechanism of ablation was not apparent, no further correlation attempt was made. It was felt that the final contour of the nozzle was much too divergent from the initial smooth contour, such that additional attempts to estimate heat transfer coefficients and ablation depths would not be fruitful. The results obtained, however, were felt to be reasonably conservative and were subsequently used as estimates of the performance of the S/N-16 nozzle exit cone. The results indicated in figure 3 and in table II seem to substantiate this assumption.

FIGURE 8

NON-DIMENSIONAL G-90 GRAPHITE ABLATION RATES (B)  
VERSUS WALL TEMPERATURE



20 DEC 1972

# S/N 14 HIGH PRESS. NOZZLE, G-90

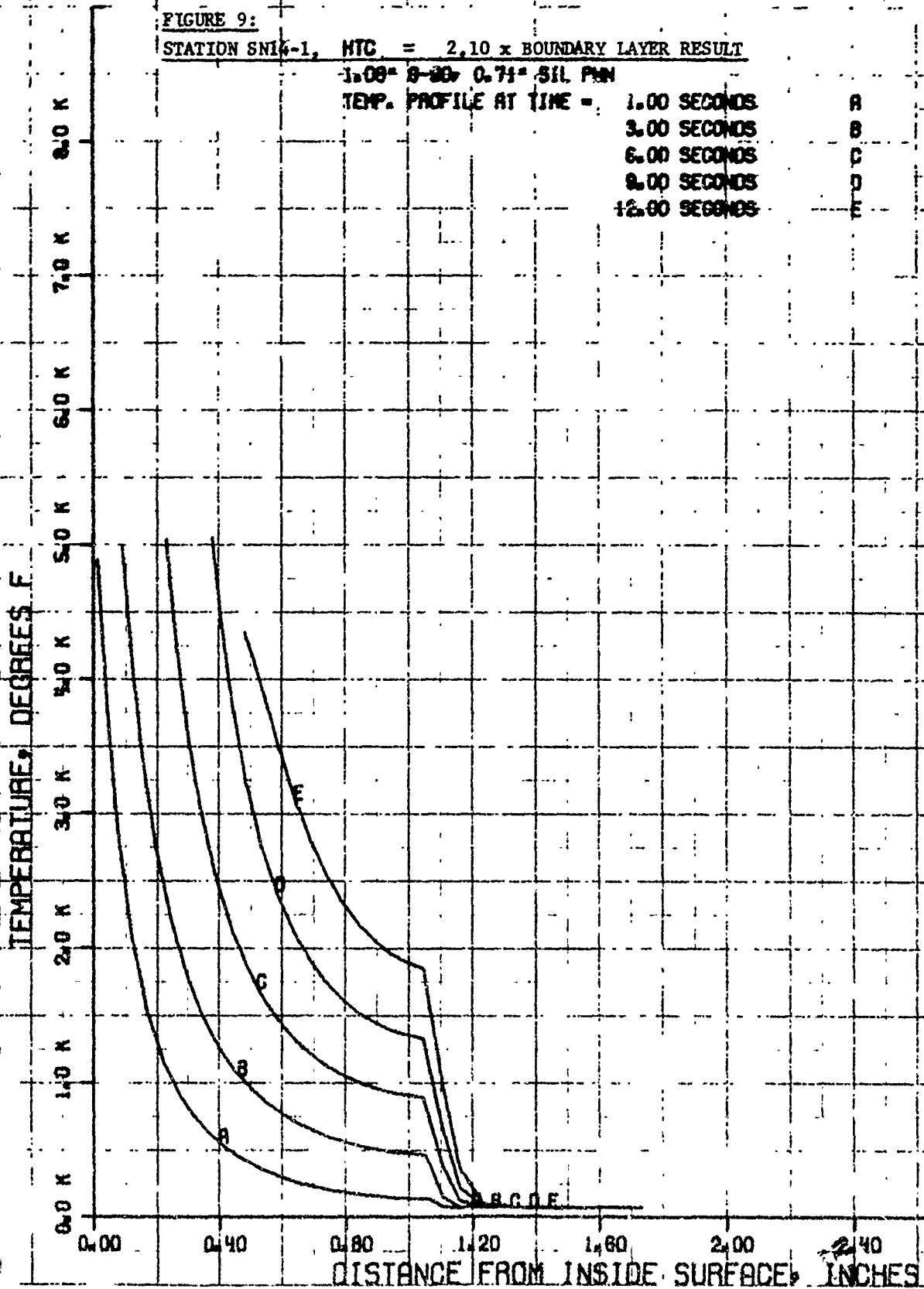
FIGURE 9:

STATION SNI-1,  $HTC = 2.10 \times$  BOUNDARY LAYER RESULT

$1.00 \times 8-20 \times 0.71 = 511 \text{ PPM}$

TEMP. PROFILE AT TIME =

1.00 SECONDS	A
3.00 SECONDS	B
6.00 SECONDS	C
9.00 SECONDS	D
12.00 SECONDS	E



20 DEC 1972

# S/N 14 HIGH PRESS. NOZZLE, 0-90

FIGURE 10:

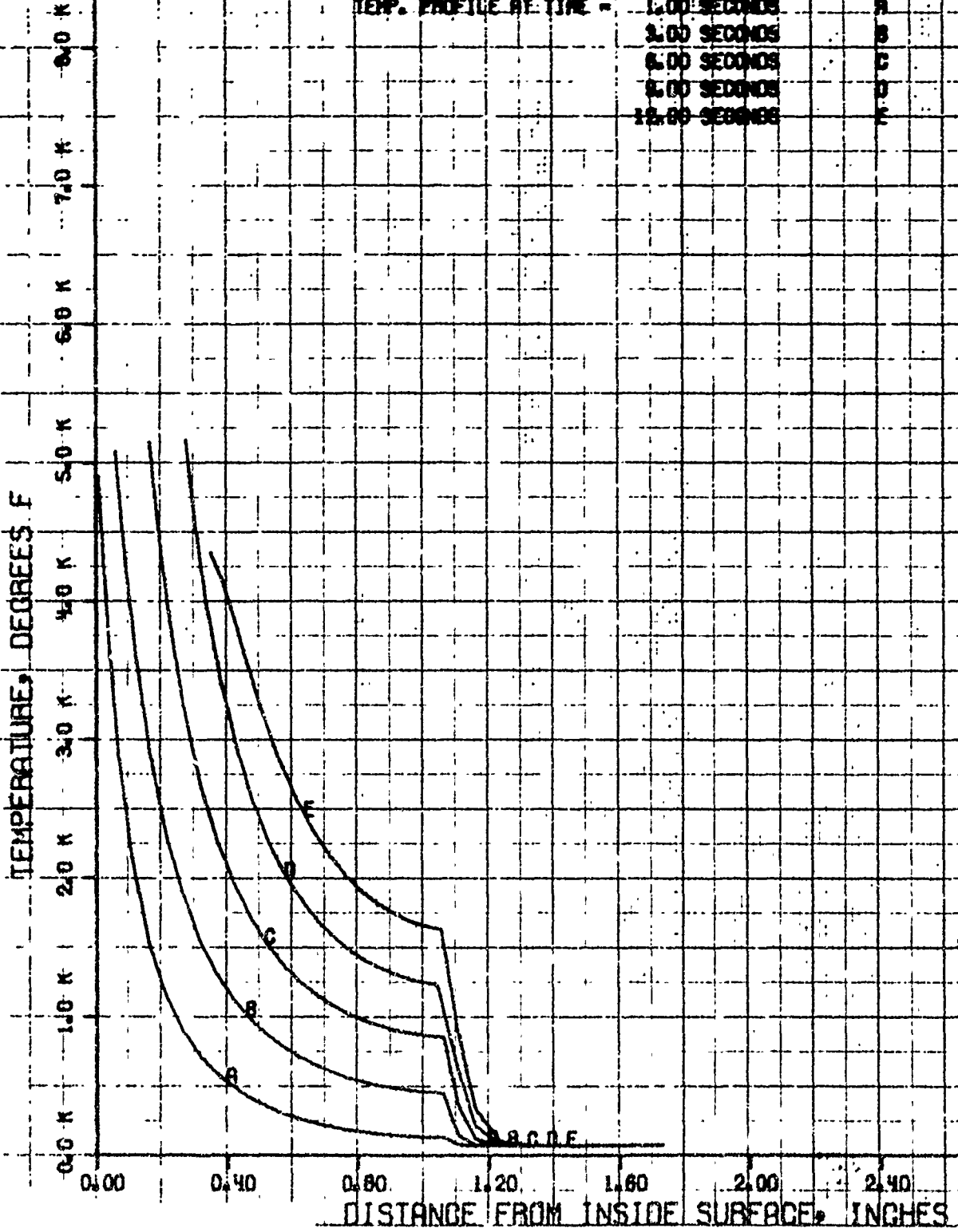
STATION SN14-1,

HTC = 1.37 x BOUNDARY LAYER RESULT

1.00 - 6.00 - 0.717 SIL FILM

TEMP. PROFILE BY TIME =

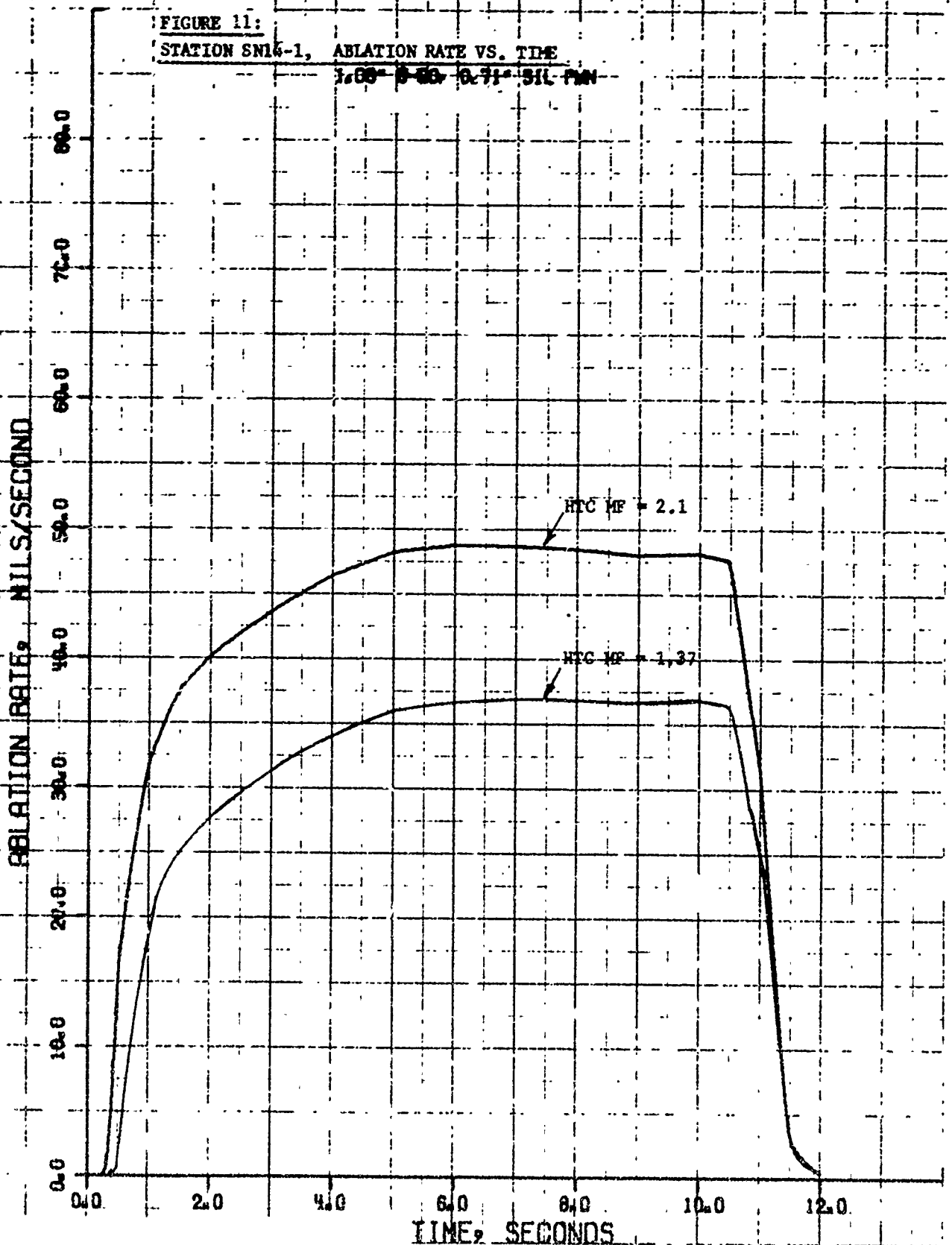
- 1.00 SECONDS A
- 3.00 SECONDS B
- 6.00 SECONDS C
- 9.00 SECONDS D
- 12.00 SECONDS E



20 DEC 1972

# S/N 14 HIGH PRESS. NOZZLE, G-90

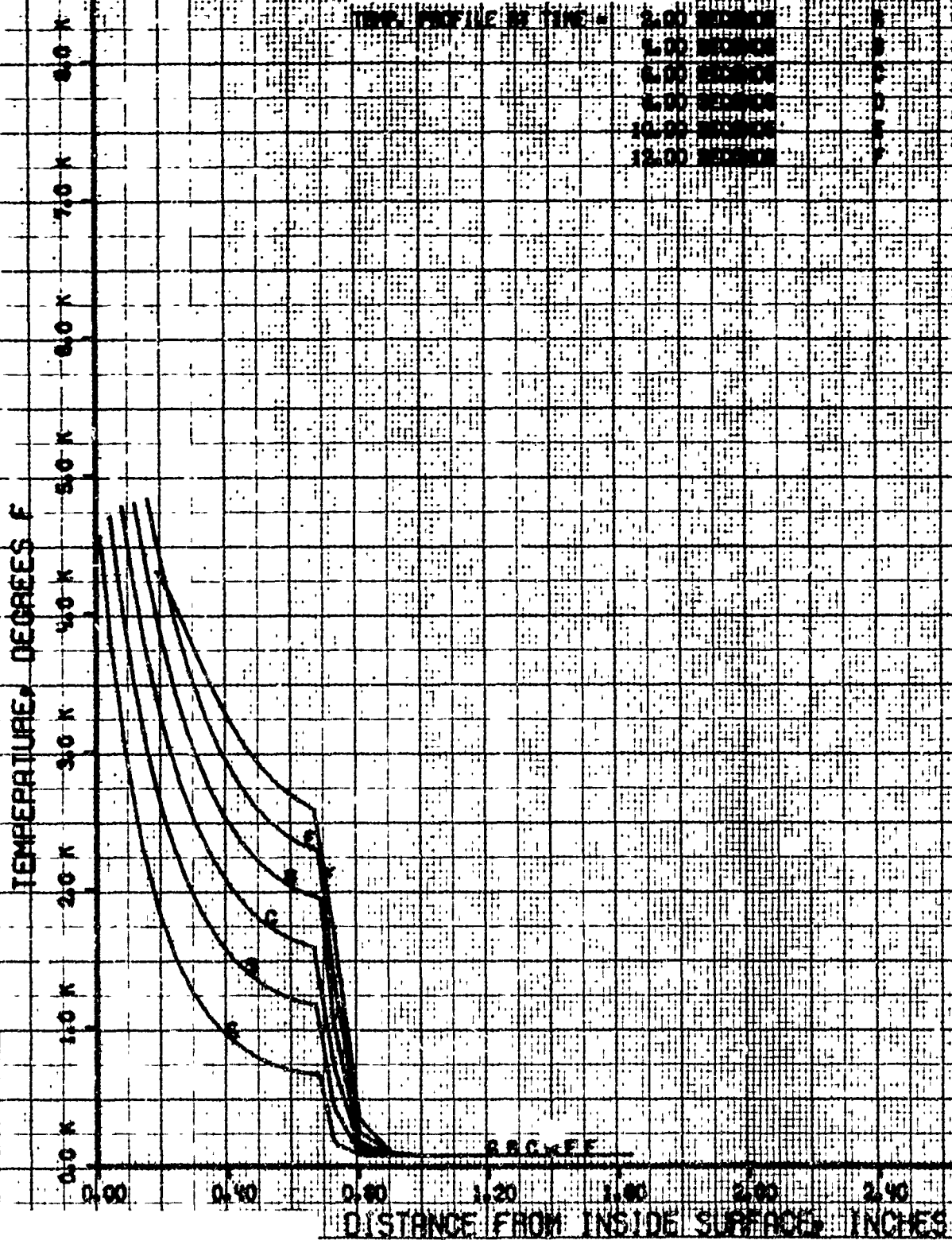
FIGURE 11:  
STATION SN14-1, ABLATION RATE VS. TIME  
1.00" Ø 50, 0.71" Ø I.L. PIN



25 JUN 1973

# H/P MOTOR S/N 11 ONE

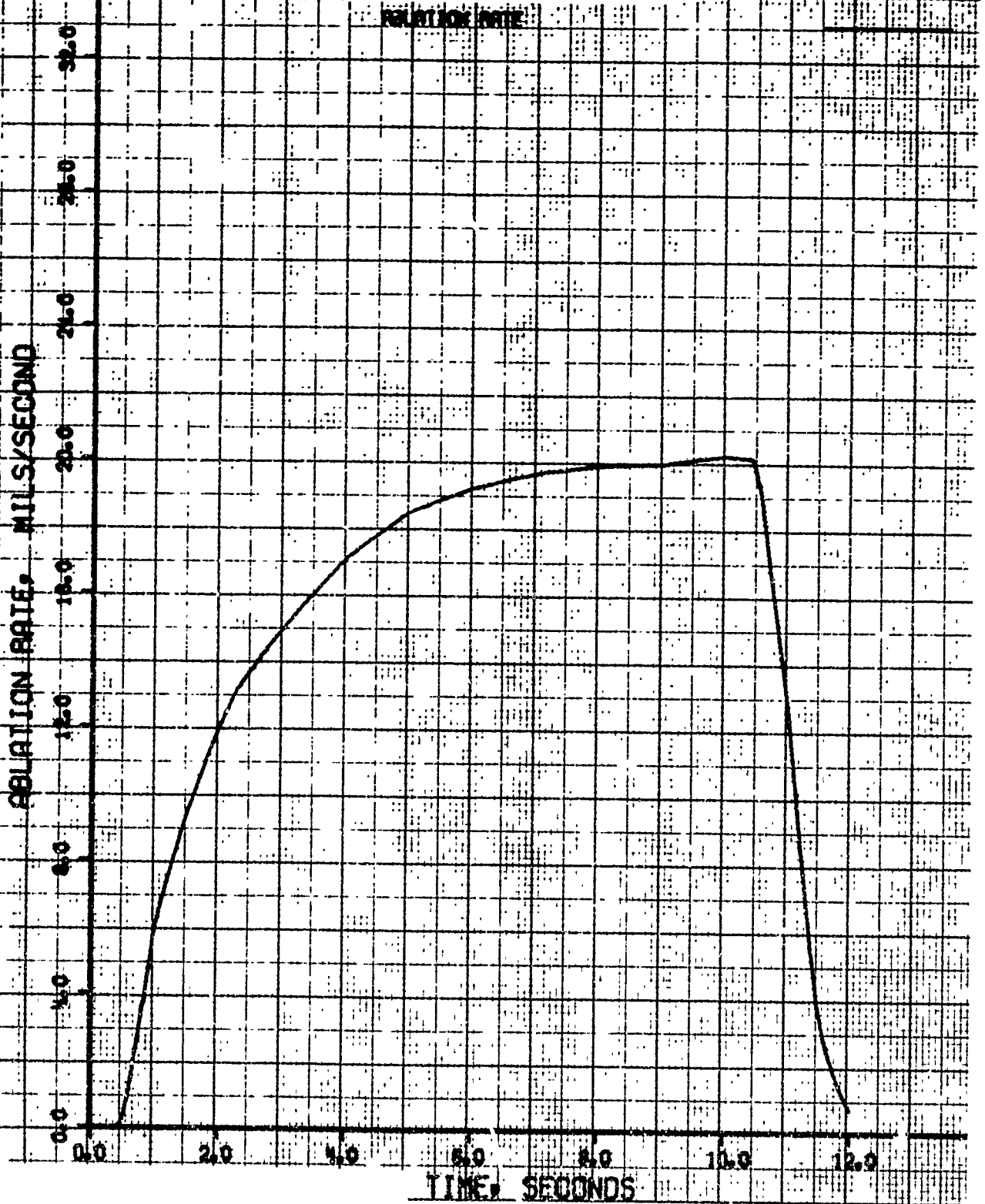
FIGURE 12: TEMPERATURE PROFILES FOR SECTION 11A  
R-25-157-10-1700-1-20100



21 JUN 1973

# H/P MOTOR S/N 14 CM9

FIGURE 13: ABLATION RATE VS. TIME FOR STATION S14-2  
H/P MOTOR S/N 14 CM9, Q-25 STEEL



### 3.5 Analysis of S/N-16 Nozzle Ablation and Thermal Performance

As described in section 3.4.1, the region downstream of the TECHMET throat (station SN16-3) was analyzed using the correlation technique developed for the S/N-14 nozzle. At the outset of the analysis, the Bartz heat transfer coefficient was used, subsequently to be updated with the boundary layer results shown in figure 6. The temperature profiles and the transient ablation rate results are shown in figures 14 and 15, where the predicted G-90 material removal is 0.326 inches using the HTC multiplier of 2.5. The apparent measured value was 0.3 inches, which indicates that a multiplier of approximately 2.4 would probably predict the measured ablation performance. If the multiplier of 1.37 from S/N-14 were used for station SN16-3, the predicted ablation would be only 40% of the measured value.

In addition to the station SN16-3, stations SN16-1 and 2 were evaluated using thermochemical ablation techniques. These materials, G-90 and "edge-oriented" pyrolytic graphite, were predicted using program CMA. The heat transfer coefficients were predicted by program UARLED, and thermochemistry from program GASKET for bulk and edge oriented pyrolytic graphite. The resultant non-dimensional ablation rates are shown in figure 16. Figures 17 and 18 show the predicted temperature profiles and the transient ablation rate for station SN16-1 and likewise for station SN16-2 in figures 19 and 20. For these runs, a heat transfer coefficient multiplier of 0.75 was used to modify the boundary layer results to account for upstream mass addition altered chemistry. This multiplier value is typical for similar nozzles in the region upstream of the throat. The post test examination revealed that the PG ring at station SN16-2 had been ejected during the test. As a result, there was no data with which to compare the predicted ablation of 0.066 inches. However,

the G-90 ring at station SN16-1 did remain and the measured ablation matched quite closely with the predicted results (table II). It is likely that the pyrolytic graphite ring ablated more than predicted due to the nature of its location relative to the G-90. Inspection of the ring in a similar position in nozzle S/N-14 showed more ablation at a slightly higher area ratio.

In order to support the structural analysis where the throat region was to be analyzed two-dimensionally, some additional heat transfer runs were made at the stations indicated as SN16-T1 and T2. These stations were analyzed with program LA15ZAZ since they would not ablate. The temperature profiles resulting from this analysis are shown in figures 21 and 22. With these results, and those at the other stations, two-dimensional isotherms were constructed on the structural analysis grids to represent an estimate of the temperature distribution. For the purpose of the structural analysis, this procedure was considered to result in conservative temperature distributions which would tend to maximize the structural response. These isotherm plots are presented in section VI subsection II of this report.

No additional carbon phenolic predictions were made at stations SN16-3 and 4, but the results of stations SN14-3 and 4 were plotted on figure 3 for comparisons. Table II indicates that the ablation depth measured for the S/N-16 firing just downstream of the G-90 exit cone region was approximately 0.35 inches. This compares reasonably well with the predictions of stations SN14-3 and 4, considering that there is a lack of complete definition of the flow structure and boundary layer downstream of the TECHMET lip.

# S/N 16 HIGH PRESSURE NOZZLE G-90

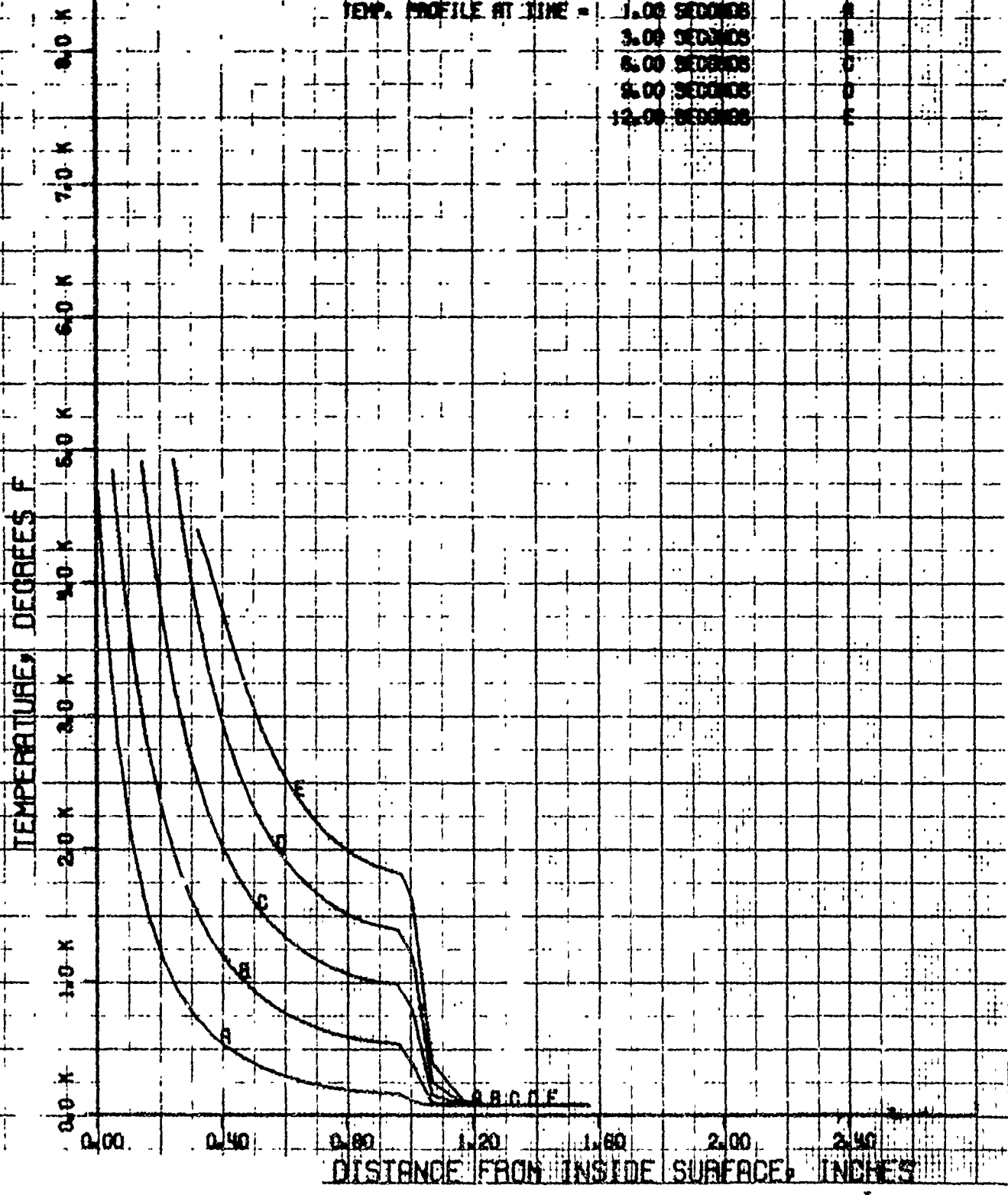
FIGURE 14: TEMPERATURE PROFILES FOR STATION SML6-3

1.00" O.D. x 0.25" I.D. (NO. 1) CHAMFER

HTC = 2.5 x BOUNDARY LAYER RESULT

TEMP. PROFILE AT TIME =

1.00 SECONDS	A
3.00 SECONDS	B
6.00 SECONDS	C
8.00 SECONDS	D
12.00 SECONDS	E

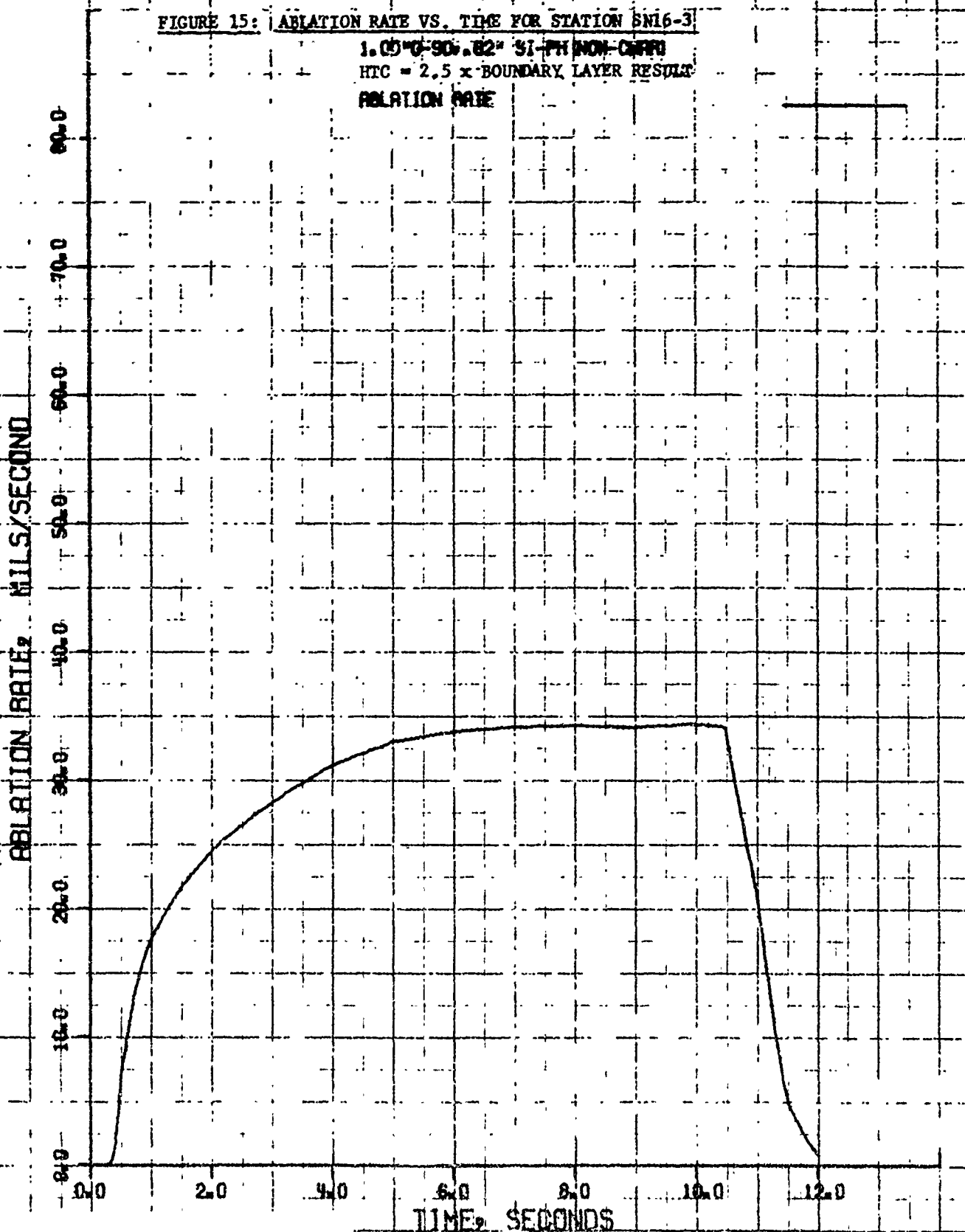


18 DEC 1972

# S/N 16 HIGH PRESSURE NOZZLE G-90

FIGURE 15: ABLATION RATE VS. TIME FOR STATION BN16-3

1.05" G-90 .82" SI-PH NON-CORRO  
HTC = 2.5 x BOUNDARY LAYER RESULT  
ABLATION RATE



22 MAY 1973

# 5/16-18 HIGH PRESSURE MOTOR

FIGURE 16:

NON-DIMENSIONAL RELATION RATES

STN. 5/16-1 (0-20) & 5/16-2 (0-EDGE)

P-STATIC = 186.369 ATM. KINETIC CONTROLLED

P-STATIC = 179.295 ATM. KINETIC CONTROLLED

$B-DOT-CHAR = MDOTCHAR / (RHOEXUE \times CM)$

0.80  
0.70  
0.60  
0.50  
0.40  
0.30  
0.20  
0.10  
0.00

1.0 K 2.0 K 3.0 K 4.0 K 5.0 K 6.0 K 7.0 K

TEMPERATURE, DEG. R

STATION 5/16-1,  
G-90 GRAPHITE

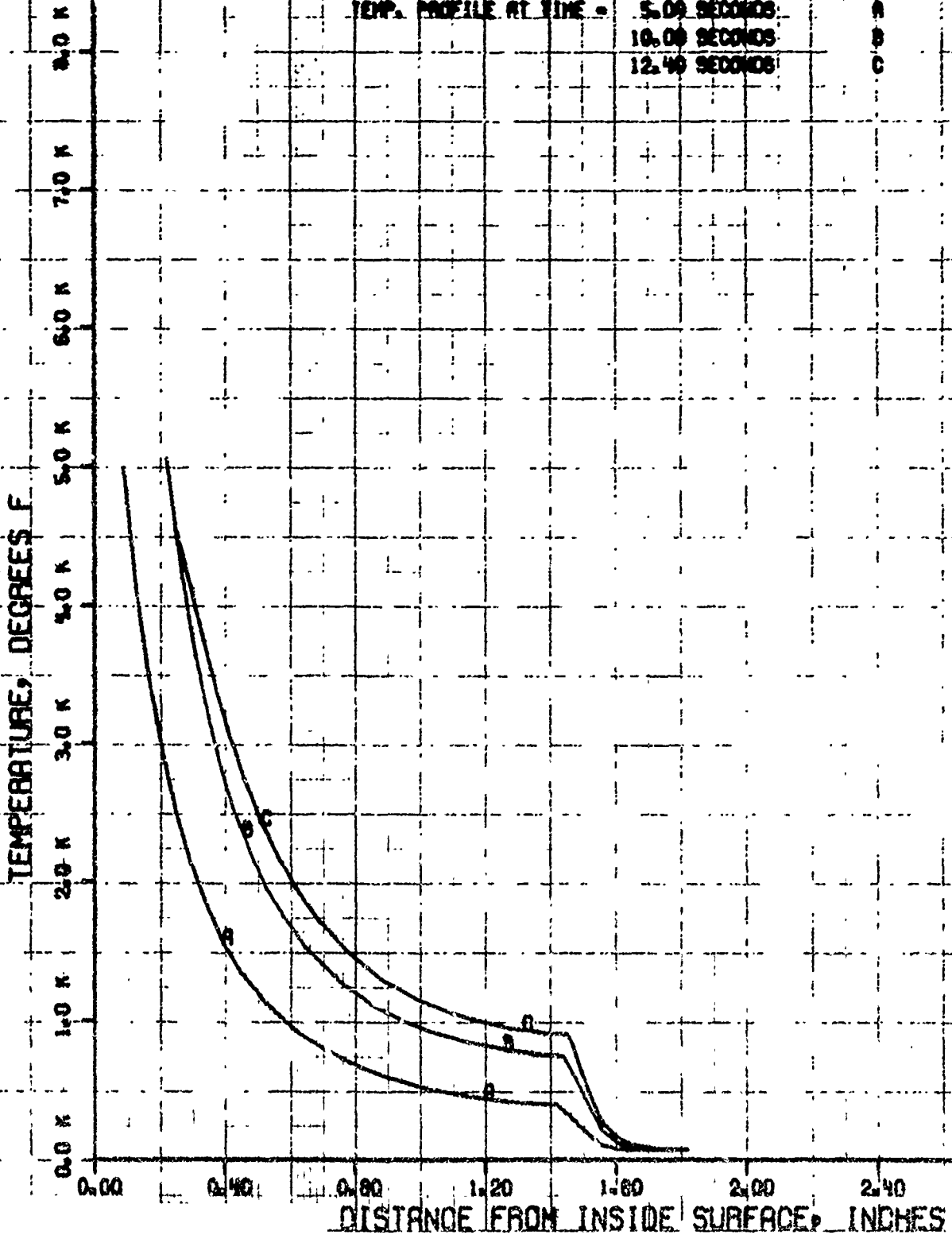
STATION 5/16-2,  
Pyralytic  
Graphite, Edge  
Oriented

22 MAY 1973

# S/N-16 NOZZLE ENTRANCE

FIGURE 17:

STATION S/N-16: 1.75" x 0.00"  
0.25" HOLE - 2.1" W x 0.75" H TEMPERATURE PROFILES  
TEMP. PROFILE AT TIME - 5.00 SECONDS A  
10.00 SECONDS B  
12.40 SECONDS C



22 MAY 1973

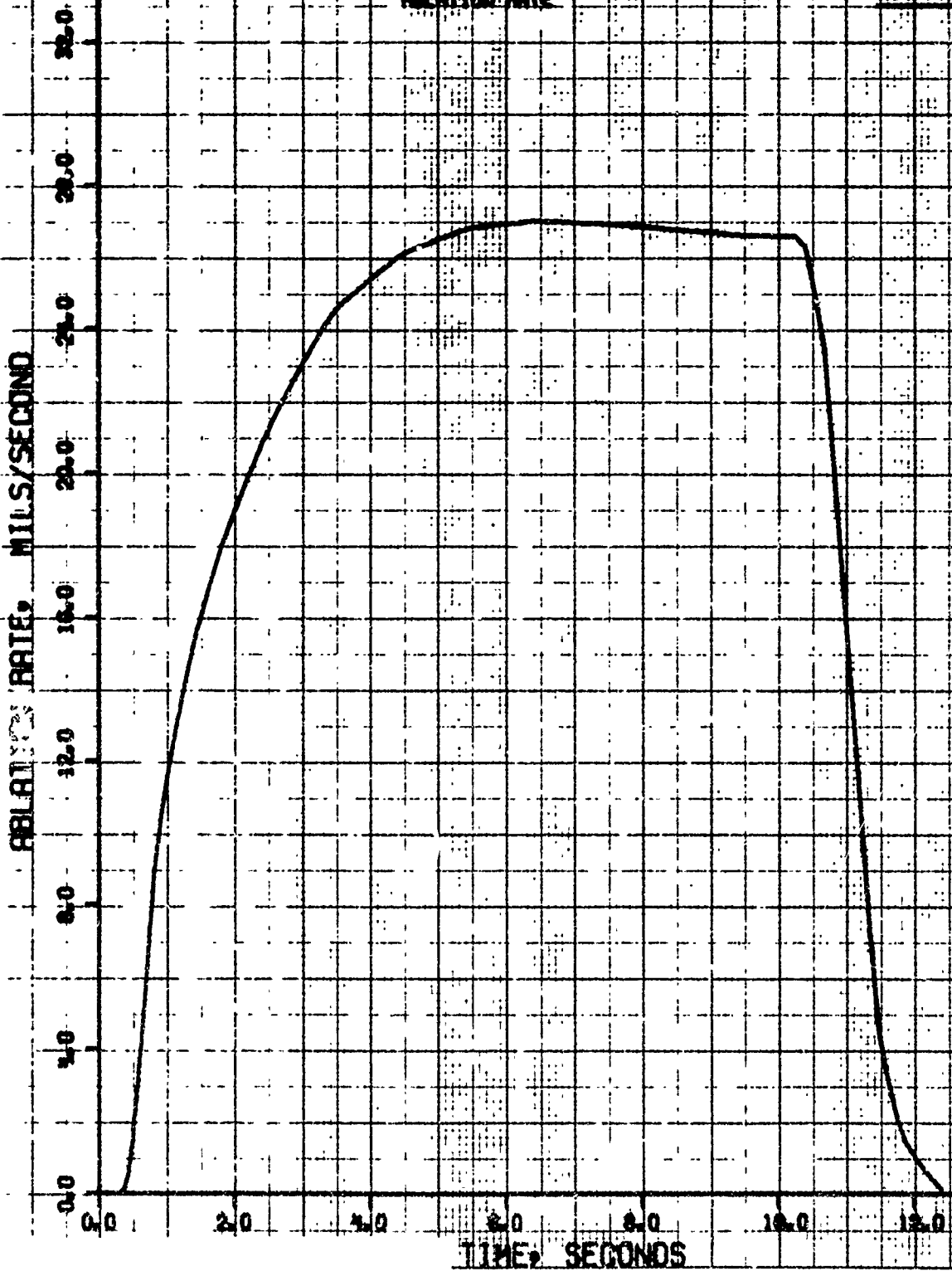
# S/N-16 NOZZLE ENTRANCE

FIGURE 18: ABLATION RATE VS. TIME FOR STATION S/N-16

STATION S/N-16: 1.78 - 0.30

0.37 - 0.000 - 0.1 - 0.75

ABLATION RATE



# HIGH PRESSURE

# NOZZLE

FIGURE 19: TEMPERATURE PROFILES FOR STATION SM16-2

0.98" PD (90%), .50" OD (40%), .42" SP (0W)

WF = 0.75

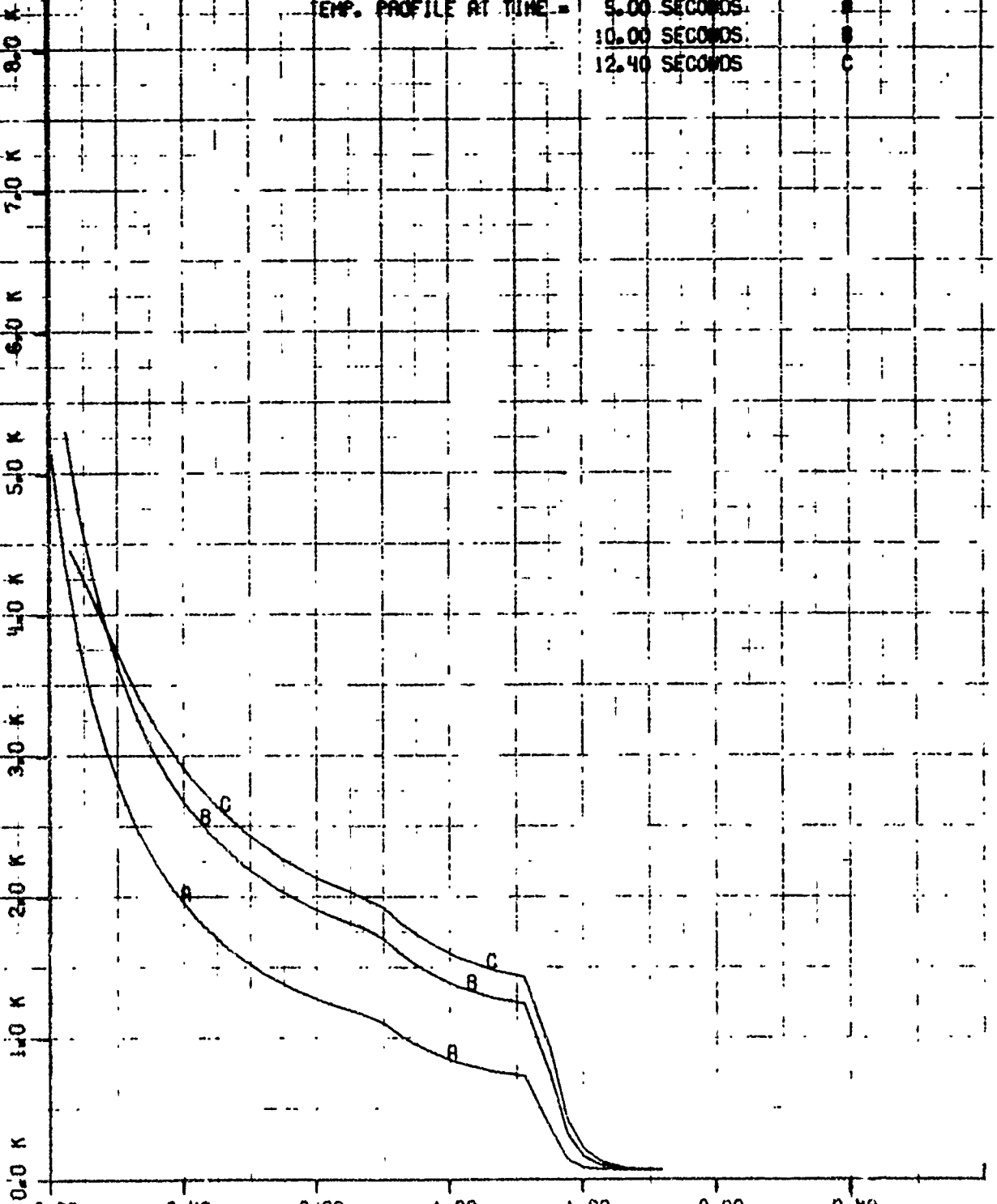
TEMP. PROFILE AT TIME =  
5.00 SECONDS  
10.00 SECONDS  
12.40 SECONDS

TEMPERATURE, DEGREES F

8.0 K  
7.0 K  
6.0 K  
5.0 K  
4.0 K  
3.0 K  
2.0 K  
1.0 K  
0.0 K

0.00 0.40 0.80 1.20 1.60 2.00 2.40

DISTANCE FROM INSIDE SURFACE, INCHES

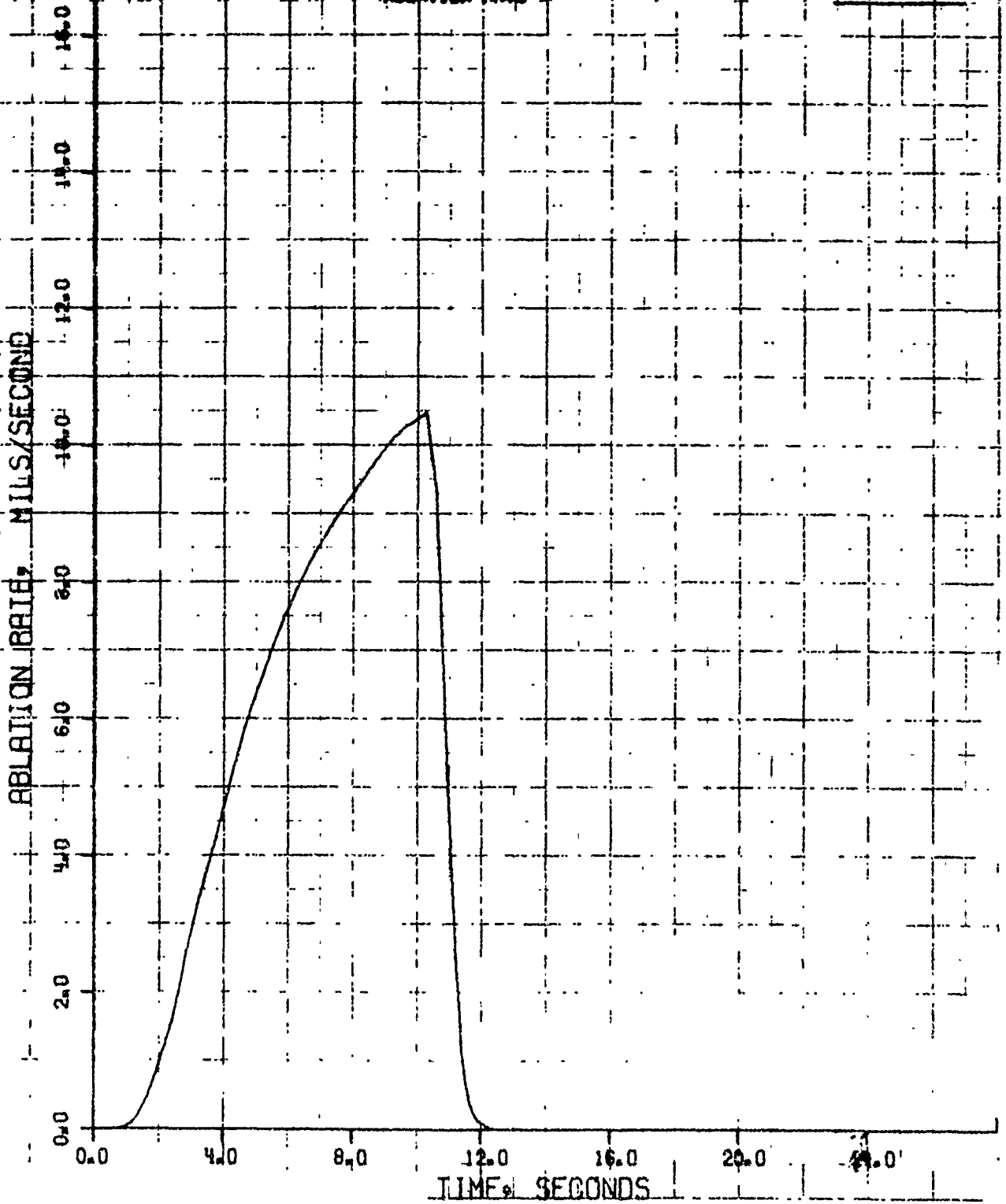


P

HIGH PRESSURE

NOZZLE

FIGURE 20: ABLATION RATE VS. TIME FOR STATION SW16-2  
(.58" P (30%), .50" (20%), .42" (30%)  
NF-0.75  
ABLATION RATE



18 DEC 1972

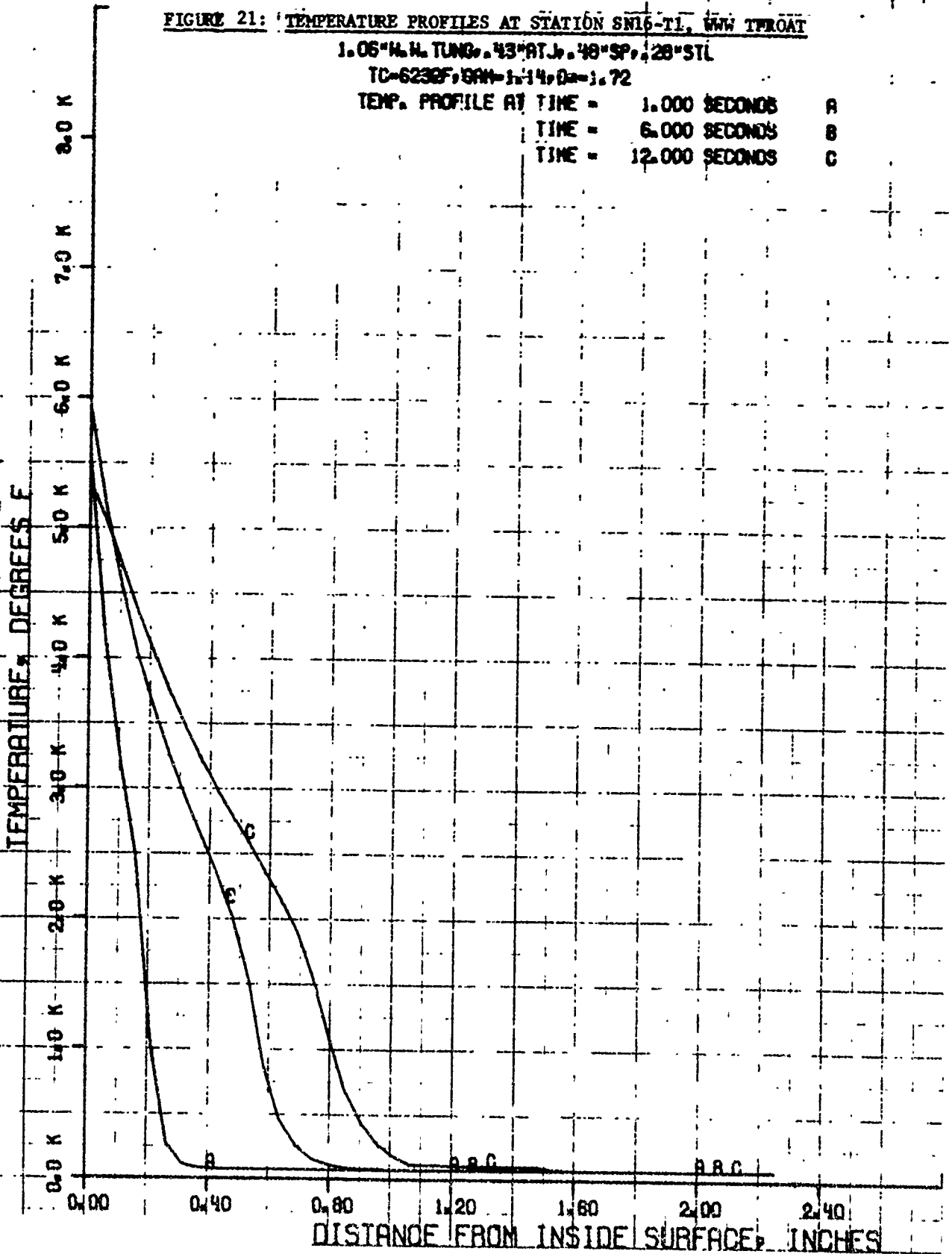
# 24110 W3 THROAT

FIGURE 21: TEMPERATURE PROFILES AT STATION SN16-T1, WW TPROAT

1.05" H. H. TUNG, 43" AT, 48" SP, 28" STL

TC-6238F, GAN-1, 14, 0 = 1.72

TEMP. PROFILE AT TIME =	1.000 SECONDS	A
TIME =	6.000 SECONDS	B
TIME =	12.000 SECONDS	C



21 MAY 1973

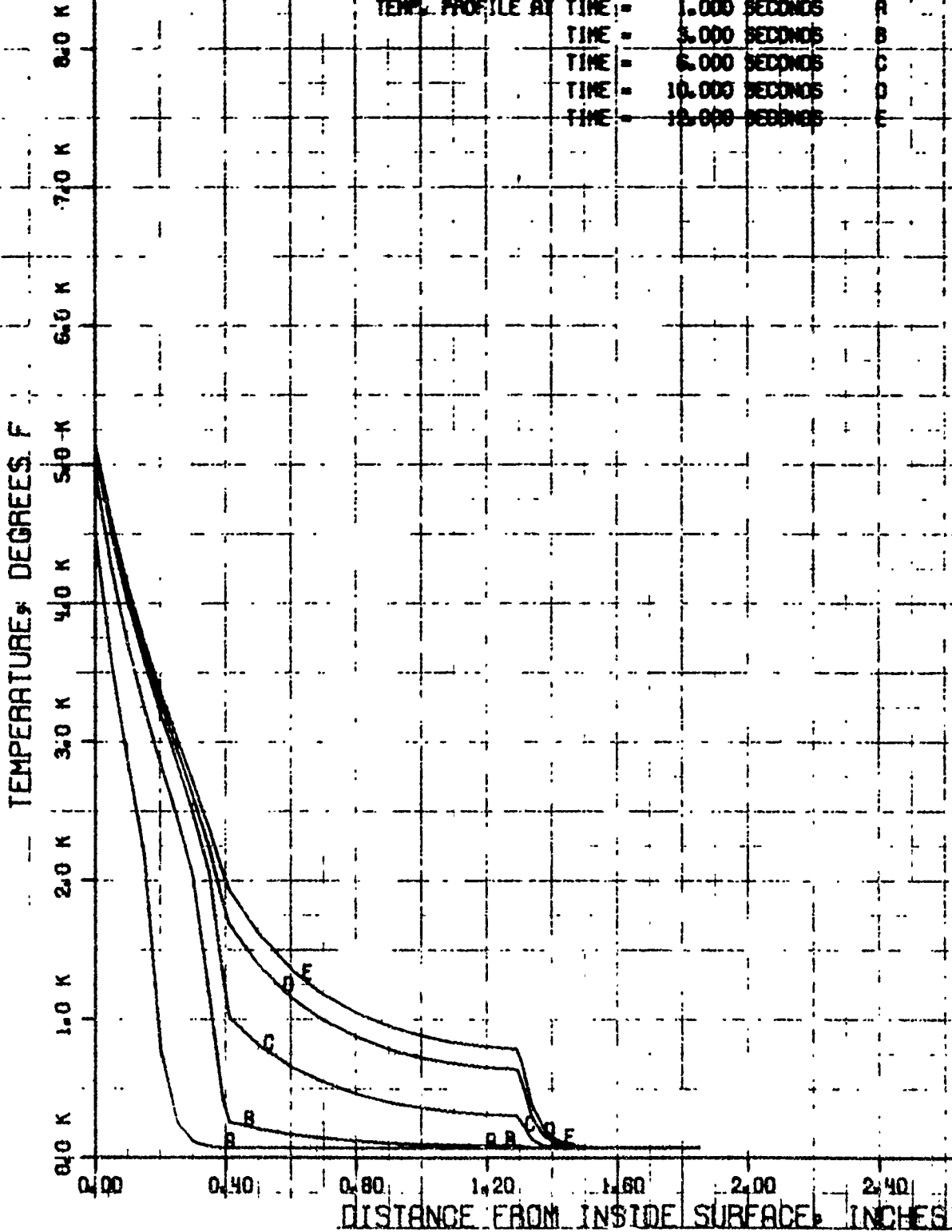
S/N-116 WNW

FIGURE 22: TEMPERATURE PROFILES AT STATION SNI6-72

STATION SNI6-72 0.4" DIA. TL 8-80

0.55" SP. 1.05" UNRAID B

TEMP. PROFILE AT TIME =	1.000 SECONDS	A
	3.000 SECONDS	B
	6.000 SECONDS	C
	10.000 SECONDS	D
	12.000 SECONDS	E



#### 4.0 CONCLUSIONS

An analysis of two high pressure nozzles, S/N-14 and 16 has been conducted to attempt the correlation of ablation data in the vicinity of supersonic, downstream facing steps at the interface between the TECHMET throat and the G-90 graphite cone. The results of the analysis have shown that the ablation can be predicted by using heat transfer coefficients computed at the upstream surface of the step and by then multiplying the result by a number somewhere between 1.3 and 2.5. To apply this analysis to future nozzles, the prediction should include a boundary layer analysis and thermochemical prediction techniques using graphite kinetics. It should be noted that these resultant multipliers can be considered as applicable only for durations, conditions, and geometries similar to those shown in this analysis. Extrapolation to other configurations is not necessarily valid until a theory is developed that can explain the divergence of the multipliers for the two test nozzles.

Current literature suggests that the heat transfer downstream of supersonic steps, may be a non-linear function of the Mach number besides being a specific function of the flow and step configuration. There may also be an effect of accelerating flow that has apparently not been treated in that current literature. Continuing studies with the two nozzles (S/N-14 and 16) have shown that the flow angle leaving the step lip can have a significant affect on the heat transfer coefficients downstream of a re-attachment shock. As a result of the questions raised during this analysis, the best analytical procedure available for prediction of heat transfer downstream of a step is to evaluate a nozzle fired under similar conditions to those to be analyzed, and to then extrapolate the results. It is expected, however, that the analytical approach outlined here could be conservatively applied to other nozzle configurations by assuming an increase in heat transfer downstream of the step by as much as 2.5 to 3.

Although increased ablation downstream of a step is observed on all rocket motor nozzles having ablative material interfaces, this difference is not a significant problem if the motors are generally low in pressure (in the neighborhood of 1000 psia) and the materials on both sides of the material interface are both ablating materials. For the current contract however, both of these two factors have been reversed and the step becomes quite significant. Since rocket motors will continue to be required that must operate at high pressures, it is recommended that research be initiated that can investigate the particular problem of nozzle heat transfer in the vicinity of forward and rearward facing steps in converging and diverging nozzle regions. The research should be designed to gather heat transfer data and to study the various parameters that can affect the flow and heat transfer in the separated regions. Correlated data would then be available for estimating the heat transfer for flow over steps in accelerating flow.

The current state-of-the-art analytical techniques cannot handle the separated flow, but somewhat more sophistication can be introduced to the boundary layer and thermochemical analysis. A more precise estimate of the heat transfer rates may be obtained by means of currently available mass addition, reacting boundary layer computer programs. However, until heat transfer data is available, the analyst must still rely on the empirical correlation of test data.

## REFERENCES

1. "User's Manual, Aerotherm Graphite Surface Kinetics Computer Program", AFRPL-TR-72-23, Volume I, January 1972 (Aerotherm Report No. UM-72-25).
2. "User's Manual, Aerotherm Equilibrium Surface Thermochemistry Computer Program, Version 3", AFRPL-TR-70-93, Volume I, April 1970 (Aerotherm Report No. UM-70-13).
3. "User's Manual, Aerotherm Charring Material Thermal Response and Ablation Program, Version 3", AFRPL-TR-70-92, Volume I, April 1970 (Aerotherm Report No. UM-70-14).
4. Kennedy, W. S., "A One-Dimensional, Axisymmetric, Transient Heat Conduction Solution by Finite Differences", UTC Technical Memorandum TM-14-62-U13, April 16, 1962.
5. Bartz, D. R., "A Simple Equation for Rapid Estimation of Rocket Nozzle Convective Heat Transfer Coefficients", Jet Propulsion, January 1957, p. 49.
6. Allport, John J., "Results of a Measurement of the Emissivity and Temperature of the Combustion Products in the Throat of a TM-3 End-Burner" UTC Technical Memorandum TM-33-61-U1, June 6, 1961.
7. Schaefer, J. W. & Dahm, T. J., "Studies of Nozzle Ablative Material Performance for Large Solid Boosters", NASA CR-72080, Aerotherm Corporation Report No. 66-2, Contract NAS 7-405.
8. Jain-Ming Wu, Michael W. Su, Trevor H. Moulden, "On the Near Flow Field Generated by the Supersonic Flow Over Rearward Facing Steps", Aerospace Research Laboratories, ARL 71-0242, November 1971.
9. J. Sandford, J. J. Ginoux, "Laminar, Transitional and Turbulent Heat Transfer Behind a Backward Facing Step in Supersonic Flow", von Karman Institute for Fluid Dynamics, Technical Note 38, October 1968, Rhode-Saint-Genese, Belgium.
10. J. P. Lamb, C. G. Hood, "Theoretical Distributions of Heat Transfer Downstream of a Backstep in Supersonic Turbulent Flow", Transaction of the ASME - Journal of Heat Transfer, February 1972, p. 87.
11. Philip M. Gerhart, "Heat Transfer Downstream of Attachment of a Turbulent Supersonic Shear Layer", AIAA Journal, Vol. II, No. 1, January 1973.

### APPENDIX III

#### STRUCTURAL ANALYSES OF NOZZLE THROAT EJECTION LOADS AND STEEL SHELLS (MEOP = 3,600 psia)

Included in this appendix are safety factor calculations for both the throat ejection loads and verification of the aft closure and nozzle shells for operation at 3,500 psi with an MEOP of 3,600 psia. The first portion includes the ejection load calculations which are as follows:

The dimensions and pressure conditions are:

$$P_1 = 2,910$$

$$\gamma_A = 0.96 \text{ in.}$$

$$l_A = 0.95 \text{ in.}$$

$$\gamma_B = 1.91 \text{ in.}$$

$$l_B = 0.99 \text{ in.}$$

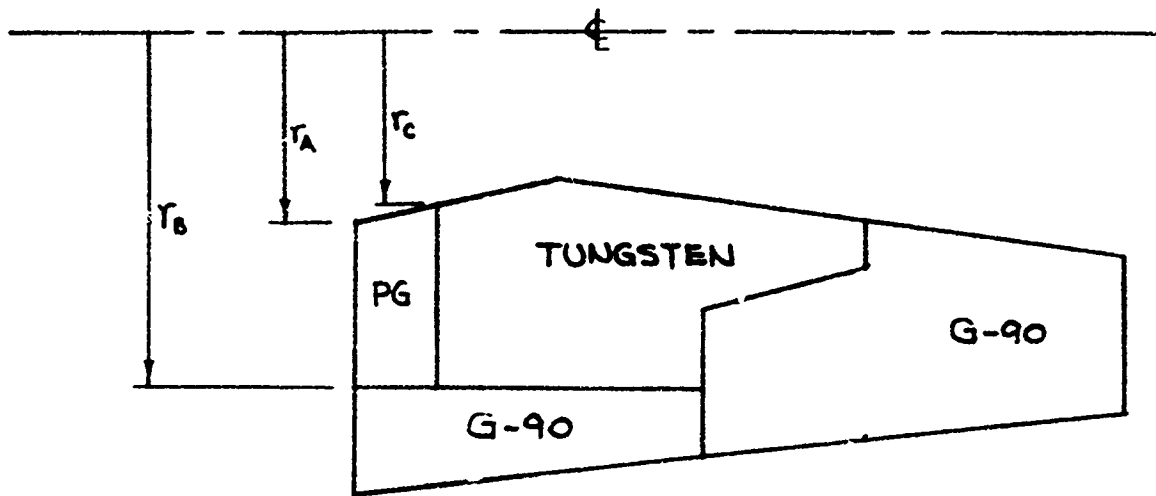
$$\gamma_C = 0.92 \text{ in.}$$

$$\theta_B =$$

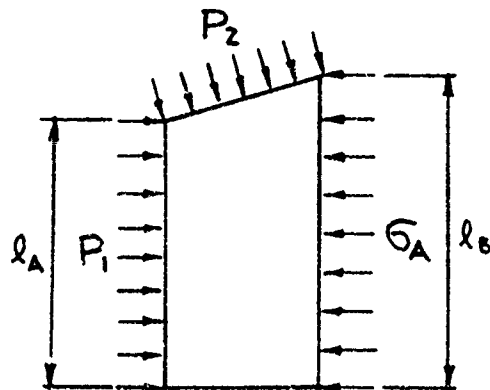
$$\gamma_E = 1.11 \text{ in.}$$

The models are

## CALCULATION OF EJECTION LOAD STRESSES



### PYROLYTIC GRAPHITE



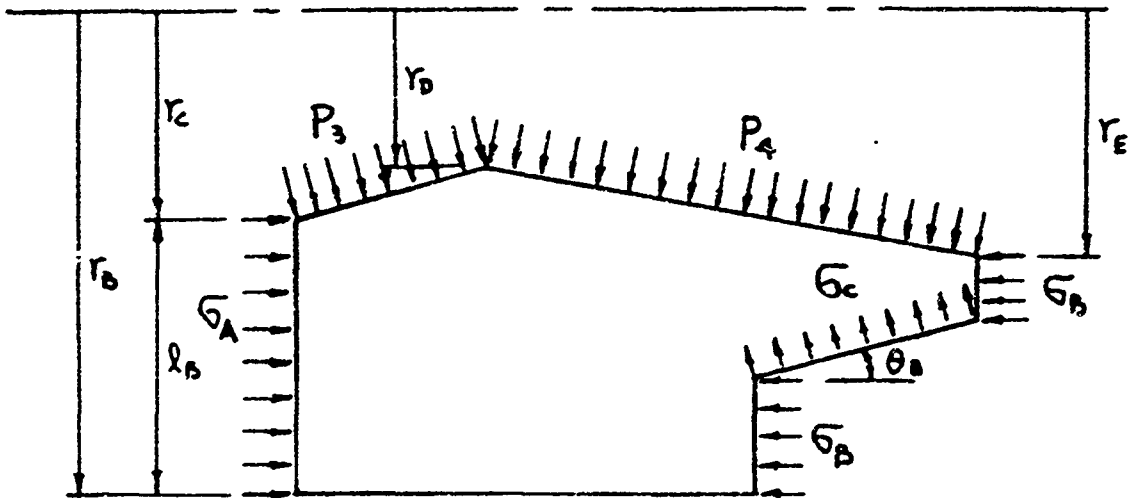
a) NEGLECT  $P_2$  EFFECTS

b)  $\Sigma F_{\rightarrow} = 0$

$$P_1 l_A (2\pi) \frac{(r_B + r_A)}{2} = \sigma_A l_B (2\pi) \frac{(r_B + r_C)}{2}$$

$$\Rightarrow \sigma_A = P_1 \frac{l_A}{l_B} \frac{(r_B + r_A)}{(r_B + r_C)}$$

# TUNGSTEN



$$\sigma_B = \sigma_C \sin \theta_B$$

$$\Sigma F_{\rightarrow} = 0$$

$$\sigma_A l_B (2\pi) \frac{(r_B + r_C)}{2} = \sigma_B (r_B - r_E) (2\pi) \frac{(r_B + r_E)}{2}$$

$$\sigma_B = \sigma_A \frac{l_B}{(r_B - r_E)} \left( \frac{r_B + r_C}{r_B + r_E} \right)$$

$$P_1 = 2910 \text{ psi}$$

$$r_A = 0.96 \text{ in.}$$

$$l_A = 0.95 \text{ in.}$$

$$r_B = 1.91 \text{ in.}$$

$$l_B = 0.99 \text{ in.}$$

$$r_C = 0.92 \text{ in.}$$

$$\theta_B =$$

$$r_E = 1.11 \text{ in.}$$

The resulting stresses are:

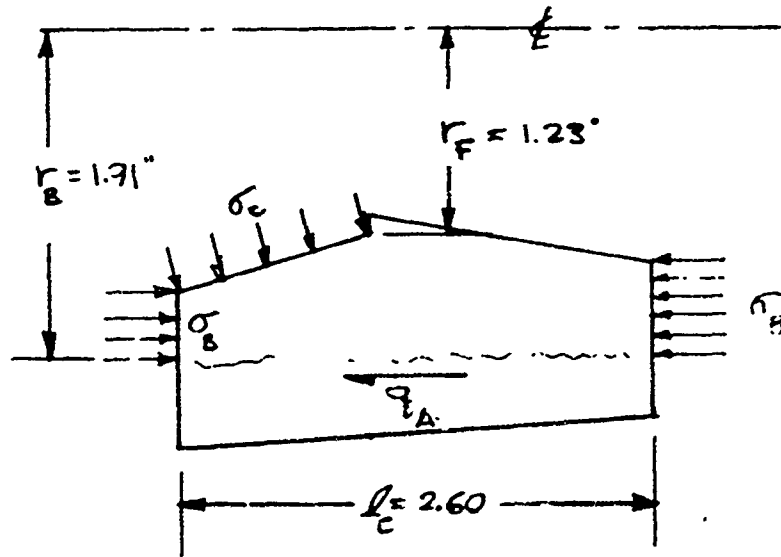
$$\sigma_A = 2,830 \text{ psi}$$

$$\sigma_B = 3,280 \text{ psi}$$

$$\sigma_C = 12,700 \text{ psi}$$

$$\text{Critical safety factor} = \frac{27700}{12700} = \underline{\underline{1.57}} @ 1000^\circ\text{F}$$

### G-90 THROAT RETENTION BLOCK



$$[ZF = 0]$$

$$\sigma_B (r_B - r_F) (2\pi) \left( \frac{r_F + r_B}{2} \right) = q_A l_c (2\pi) r_B$$

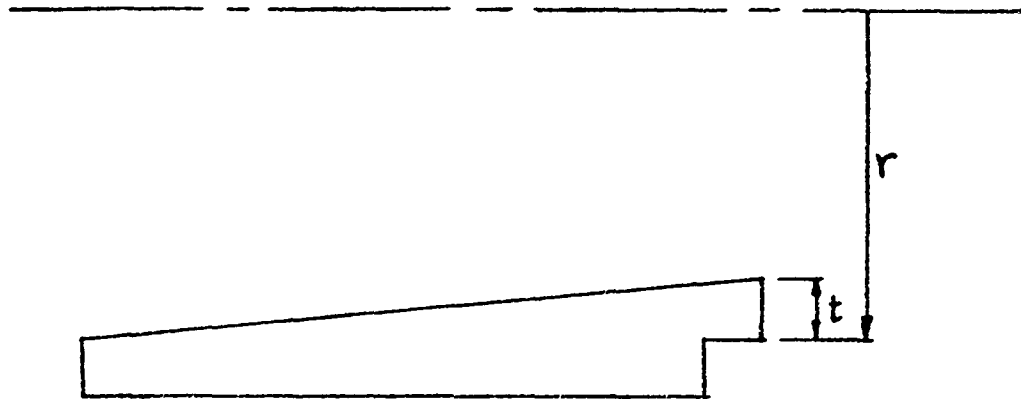
$$q_A = \sigma_B \left( \frac{r_B - r_F}{l_c} \right) \left( \frac{r_F + r_B}{2 r_B} \right)$$

$$q_A = (2280) \left( \frac{1.91 - 1.23}{2.60} \right) \left( \frac{1.91 + 1.23}{2 \cdot 1.91} \right)$$

$$q_A = 705 \text{ PSI}$$

$$\text{Safety Factor} = \frac{1850}{705} = \underline{\underline{2.62}}$$

# HOOP STRESS IN SILICA-PHENOLIC THROAT INSULATION



$$\sigma = \frac{Pr}{t}$$

$$P \sim 350 \text{ psi}$$

$$r = 2.53 \text{ IN.}$$

$$t = 0.3 \text{ IN.}$$

$$\sigma = 2950 \text{ psi}$$

$$\text{Safety Factor} = \frac{10,000}{2950} = \underline{\underline{3.39}}$$

## NOZZLE AND AFT CLOSURE STEEL SHELL ANALYSIS

The lightweight nozzle and aft closure steel shells were analyzed structurally. This internal loads analysis was made using UTC computer code (LI11ZBZ) which has the capability of performing a complete redundant shell-ring analysis. A schematic of the aft closure is shown in figure 1. A free-body diagram, as considered in the analysis, is shown in figure 2. All these calculations were made for the hydrotest condition at a pressure of 5,400 psi, which includes a safety factor of 1.5 over the MEOP of 3,600 psi. Table I presents the margins of safety that result from the analysis of the redesigned configuration.

TABLE I

MARGINS OF SAFETY FOR AFT CLOSURE AND NOZZLE SHELL

<u>Description</u>	<u>Margin of Safety</u>
Aft closure shell (at maximum radius)	0.50 (based upon 4340 steel with ultimate strength of 200 ksi)
Aft closure, thread shear	7.63
Nozzle shell, thread shear	4.22
Nozzle shell, membrane stress	0.36

Justification of these margins of safety are included in the following paragraphs.

(1) Aft Closure Shell

At minimum thickness

$$\sigma_{\theta} = \frac{PR}{t \cos \alpha} = \frac{(3600)(1.5)(4)}{(0.43)(0.50)}$$

$$\sigma_{\theta} = 100,200 \text{ psi}$$

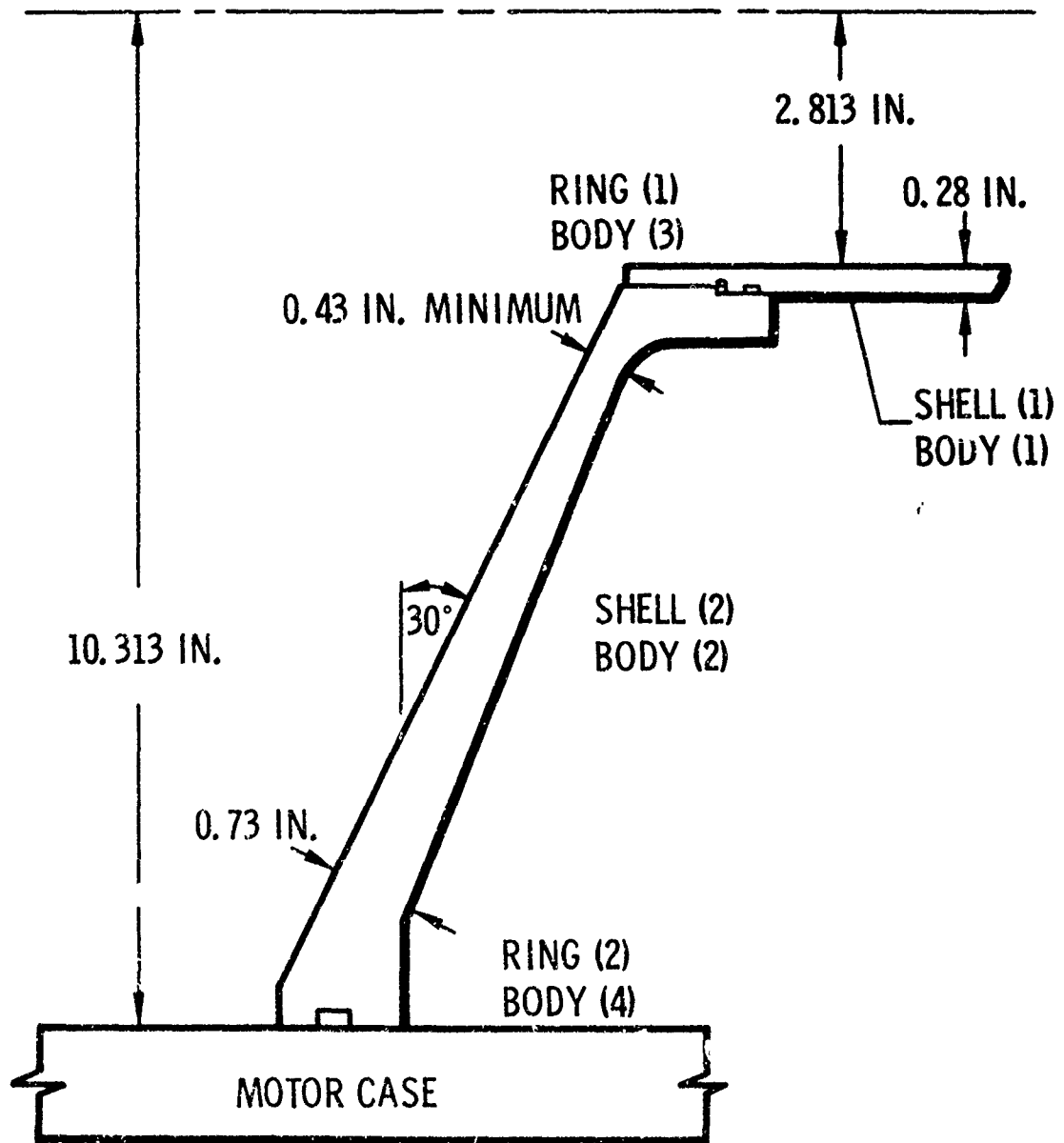


Figure 1. HIPPO Motor Aft Closure

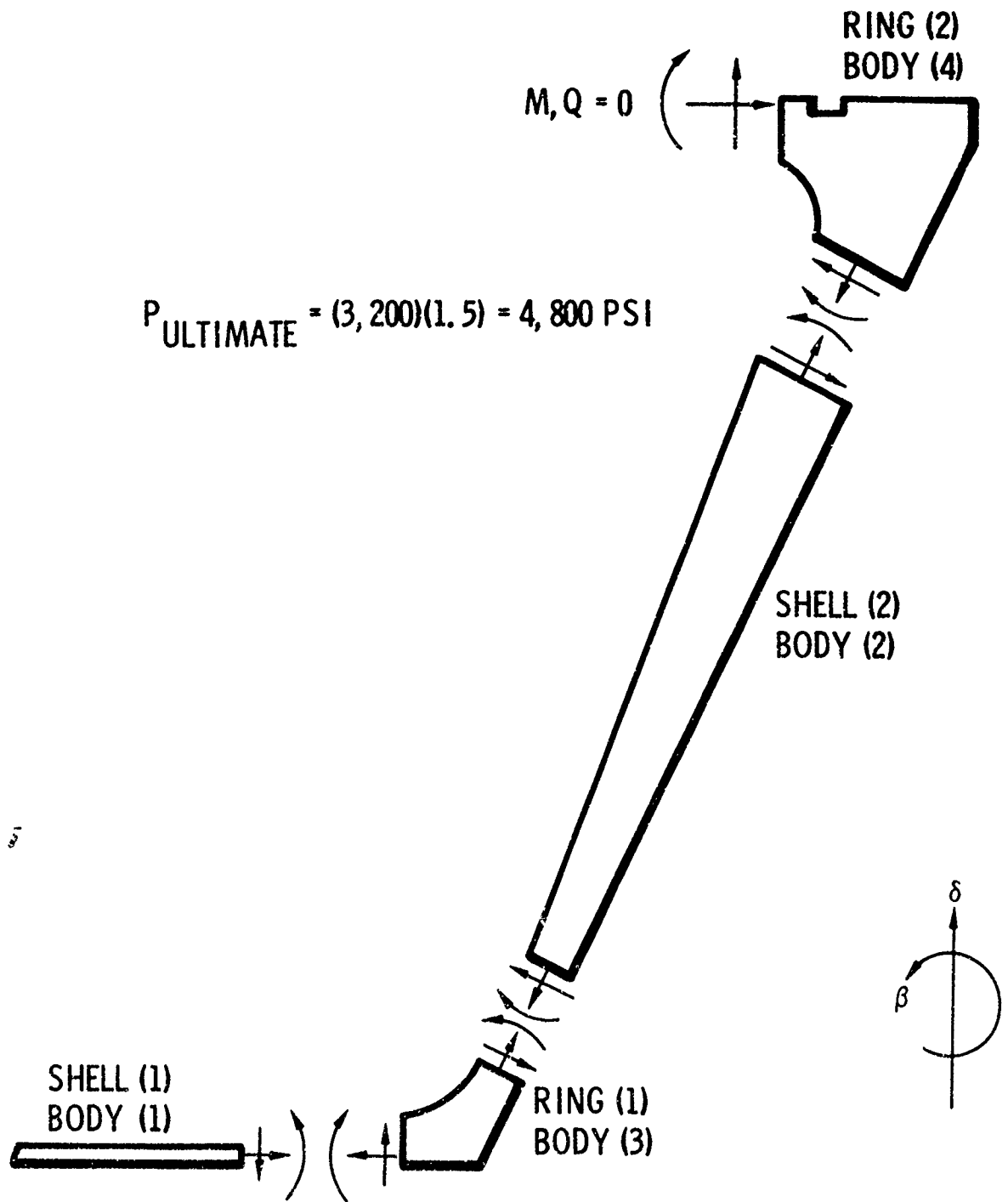


Figure 2. Free-Body Diagram of Aft Closure

At maximum radius

$$\sigma_{\theta} = \frac{PR}{t \cos \alpha} = \frac{(3600) (1.5) (9)}{(0.73) (0.5)}$$

$$\sigma_{\theta} = 133,200 \text{ psi}$$

Material is 4340 steel:  $F_{TU} = 200 \text{ ksi}$

$$MS = \frac{200,000}{133,200} - 1 = 0.50$$

(2) Aft Closure to Nozzle Shell Joint

Thread shear

$$F_{EJ} = \pi R^2 P_c = (\pi) (3)^2 (1.5) (3,600)$$

$$F_{EJ} = 152,700 \text{ lb}$$

The thread shear area in the aft closure is

$$A_S = A_i \ell = (14.1028) (0.78)$$

$$A_S = 11.00 \text{ in.}^2$$

The shear stress in the thread is

$$f_S = \frac{152,700}{11.00} = 13,900 \text{ psi}$$

$$MS = \frac{120,000}{13,900} - 1 = 7.63$$

(3) The thread shear area in the nozzle shell is

$$A_S = A_e \ell = (12.016) (0.78)$$

$$A_S = 9.37 \text{ in.}^2$$

The shear stress in the thread is

$$f_S = \frac{152,700}{7.37} = 20,700 \text{ psi}$$

$$MS = \frac{108,000}{20,700} - 1 = 4.22$$

(4) Nozzle Shell - Membrane Stress

$$\sigma_{\theta} = \frac{PR}{t} = \frac{3600 (1.5) (2.813 + 0.25)}{0.25}$$

$$\sigma_{\theta} = 66,200 \text{ psi}$$

$$MS = \frac{90,000}{66,200} - 1 = 0.36$$

The following summary of factors of safety resulted from an analysis of the throat retention for the higher MEOP of 3,600 psia. The factors are based on each method of retention being independent of the other factors.

<u>Failure Mode</u>	<u>Factors of Safety (Qualification)</u>
Steel ring bonding	1.34 (for total ejection force of 43,500 lb)
Steel ring retention failure by shearing screws	1.89 (for total ejection force of 43,500 lb)
Steel ring retention failure of bond	1.90 (for 75% bond and ejection force of 43,500 lb)
Phenolic bearing	2.66 (for ejection force of 43,500 lb)
Exit cone retention shear failure of screws	3.86 (for exit cone extension load of 6,750 lb)
Exit cone retention failure of screws	12.4 (for 75% bond efficiency and exit cone extension load of 6,750 lb)

Calculations for the throat ejection load and details for their factors of safety follow.

The throat ejection force on the exit cone was 3,600 psi MEOP. Assuming force acts on the face of the aft entrance cap,

$$\epsilon \text{ at 2.50-in. diameter: } \frac{2.50^2}{1.72^2} = 2.11, P/P_c = .115$$

$$\epsilon \text{ at 2.43-in. diameter: } \frac{2.43^2}{1.72^2} = 1.996, P/P_c = 0.94$$

$$F = P_c \pi/4 \left\{ [0.94(4.70^2 - 2.43^2)] + \frac{0.94 + .568}{2} \right.$$

$$\left. (2.43^2 - 1.72^2) \right\} - \left[ \left( \frac{.568 + .115}{2} \right) (2.50^2 - 1.72^2) \right.$$

$$\left. + (4.60^2 - 2.50^2) \right\} \left( \frac{.115 + 0}{2} \right)$$

$$F = P_c \pi/4 [(15.2 + 2.2 - 1.1 - 0.9)]$$

$$F = P_c \pi/4 (15.4)$$

$$F = 12.1 P_c$$

$$F = 43,500 \text{ lb.}$$

### Redesign of Exit Cone

#### A. Steel Ring Retention

12 5/16 - 24 unf ss set screws

$$F_{tu} = 170 \text{ ksi}$$

$$F_s = (9800) (.70)$$

$$F_s = 6860 \text{ lb/screw (Ref: Allen handbook)}$$

The total shear capacity of the screws is

$$(F_s)_{tot} = (6860) (12)$$

$$(F_s)_{tot} = 82,320 \text{ lb}$$

for a total throat ejection force of 43,500 (MEOP = 3600 psi), the factor of safety is

$$FS = \frac{82,320}{43,500} = 1.89$$

#### B. Ring Section Props

<u>Node</u>	<u>X</u>	<u>Y</u>
1	0	0
2	0	.45
3	.75	.25
4	.75	0
5	0	0

#### Section Properties of an Area

$$\text{Area} = 0.26250$$

$$X\text{-bar} = 0.33929$$

$$Y\text{-bar} = 0.17976$$

$$I_{XX} = 0.00311$$

$$I_{YY} = 0.01197$$

C. Ring Bending Stresses

$$f_B = \frac{Mc}{I} = \frac{(43,500)(.045)(.41)}{(11.97 \times 10^{-3})}$$

$$f_B = 67,000 \text{ psi}$$

Allowable ultimate = 90,000 psi

$$FS = \frac{90,000}{67,000} = 1.34$$

D. Bondline Stress

For the throat insert retaining steel ring assuming 75% bond efficiency, the shear area is

$$\begin{aligned} A_s &= \pi D \ell \\ &= (\pi)(5)(3.5)(.75) \end{aligned}$$

$$A_s = 41.3 \text{ in.}^2$$

The bondline shear stress is

$$\tau_s = \frac{43,500}{41.3} = 1050 \text{ psi}$$

assuming a 2000 psi bond

$$FS = \frac{2000}{1050} = 1.90$$

Bearing stress on exit cone

$$\begin{aligned} A_B &= \pi(R_o^2 - R_i^2) \\ &= \pi(2.61^2 - 2.38^2) \end{aligned}$$

$$A_B = 3.606 \text{ in.}^2$$

$$f_B = \frac{43,500}{3.606} = 12,060 \text{ psi.}$$

Allowable bearing stress = 32,000 psi

$$FS = \frac{32,000}{12,060} = 2.66$$

The force on the exit cone candidate materials was 3600 psi MEOP.

$$e \text{ at 2.50-in. diameter: } \frac{2.50^2}{1.72^2} = 2.11, P/P_c = .115$$

$$F = P_c \pi/4 [5.2^2 - 2.50^2] (.115)$$

$$F = 3600 (16.3) (.115) = 6750 \text{ lb}$$

E. Candidate Material Retention

6 1/4 in. - 28 unf ss set screws

$$E_{tu} = 170 \text{ ksi}$$

$$F_s = (6200)(.70)$$

$$F_s = 4340 \text{ lb/screw (Ref: Allen handbook)}$$

The total shear capacity of the screws is

$$(F_s)_{tot} = (4340)(6)$$

$$(F_s)_{tot} = 26,040 \text{ lb.}$$

For the exit cone extension load of 6,750 lb, the factor of safety is

$$FS = \frac{26,040}{6,750} = 3.86$$

The exit cone material bondline is

$$A_s = \pi D \ell$$

$$= (\pi)(5.50)(3.25)(.75)$$

$$A_s = 42 \text{ in.}^2$$

$$\tau_s = \frac{6,750}{42} = 161 \text{ psi}$$

$$FS = \frac{2000}{161} = 12.4$$